

Meterwavelength Single-pulse Polarimetric Emission Survey III: The Phenomenon of Nulling in Pulsars.

Rahul Basu^{1,*}, Dipanjan Mitra^{2,3,1}, George I. Melikidze^{1,4}
rahulbasu.astro@gmail.com

ABSTRACT

A detailed analysis of nulling was conducted for the pulsars studied in the Meterwavelength Single-pulse Polarimetric Emission Survey. We characterized nulling in 36 pulsars including 17 pulsars where the phenomena were reported for the first time. The most dominant nulls lasted for a short duration, less than five periods. The longer duration nulls extending to hundreds of periods were also seen in some cases. A careful analysis showed the presence of periodicities in the transition from the null to the burst states in 11 pulsars. In our earlier work fluctuation spectrum analysis showed multiple periodicities in 6 of these 11 pulsars. We demonstrate that the longer periodicity in each case was associated with nulling. The shorter periodicities usually originate due to subpulse drifting. The nulling periodicities were more aligned with the periodic amplitude modulation indicating a possible common origin for both. Most prevalent nulling lasts for a single period and can be potentially explained using random variations affecting the plasma processes in the pulsar magnetosphere. On the other hand, the longer duration nulls require changes in the pair production processes that need an external triggering mechanism for the change. The presence of periodic nulling puts an added constrain on the triggering mechanism which also needs to be periodic.

Subject headings: pulsars: general — pulsars:

1. Introduction

The radio emission from pulsars show variability over multiple timescales. These variations can either be due to intrinsic changes in the emission process or result of external effects like interaction of the emission with the intervening medium. The presence of nulling was first reported by Backer (1970) where the emission ceased within one rotation period. Nulling can manifest over multiple timescales ranging from a few periods to hours

at a time and in the case of intermittent pulsars from weeks to months. The nulling fractions also show wide variations ranging from less than a few percent to more than seventy percent of time when the emission nulls. There are studies which show that pulsars with similar nulling fractions sometimes exhibit very different nulling patterns (Gajjar *et al.* 2014a).

There are around 75 pulsars where nulling has been reported (Ritchings 1976; Rankin 1986; Biggs 1992; Wang *et al.* 2007; Gajjar *et al.* 2012). The physical processes responsible for the transitions between the null to the burst states are still unclear. The long duration nulls in the intermittent pulsar B1931+24 have been identified with large changes in the spin down energy loss (Kramer *et al.* 2006). This has motivated the idea of nulling being associated with large scale magnetospheric changes in pulsars (Cordes 2013; Gajjar *et al.* 2014a,b). However,

¹Janusz Gil Institute of Astronomy, University of Zielona Góra, ul. Szafrana 2, 65-516 Zielona Góra, Poland

²National Centre for Radio Astrophysics, Ganeshkhind, Pune 411 007, India

³Physics Department, University of Vermont, Burlington VT 05405

⁴Abastumani Astrophysical Observatory, Ilia State University, 3-5 Cholokashvili Ave., Tbilisi, 0160, Georgia

*Present address: Inter-University Centre for Astronomy and Astrophysics, Pune 411007, India

it is not clear if the short and the intermediate nulls lasting few periods (seconds) to hundreds of periods (hours) have the same physical origin as nulling in the intermittent pulsars which last for days at a time. Nulling is largely considered to be a stochastic process switching between two states. But, in some cases the transition from the null to the burst states have shown periodicity (Herfindal & Rankin 2007, 2009).

The sparking discharges in the Inner Acceleration Region (IAR) of pulsars are believed to generate the plasma necessary for radio emission (Ruderman & Sutherland 1975, hereafter RS75). RS75 considered a system where the rotation and magnetic axis were aligned in opposite directions. The sparks, also called subbeams, were postulated to rotate around the common axis in a steady pattern due to the $\mathbf{E} \times \mathbf{B}$ drifting. (Deshpande & Rankin 2001) expanded the RS75 model to the pulsar B0943+10 where the rotation axis is not aligned with the magnetic axis. They considered the sub-beam system to rotate around the magnetic axis in order to explain the subpulse drifting seen in this pulsar. This model has now been used in a large number of pulsars to explain the subpulse drifting phenomenon. The periodic nulls are associated with the line of sight passing between the empty regions of the sub-beam pattern. Although, in our recent work (Basu *et al.* 2016) we found the rotating sub-beam system around the magnetic axis to be physically inconsistent in non-aligned pulsars. The sparks are instead expected to move around the rotation axis.

The underlying physical processes responsible for nulling are still unresolved. The longer duration nulls allude to unknown physical phenomena which require constraints from observations as well as detailed modelling. In this work we have looked for additional observational clues to characterize nulling. We have carried out detailed analysis of nulling properties in the Meterwavelength Single-pulse Polarimetric Emission Survey (MSPES, Mitra *et al.* 2016). The paper is organized as follows: in section 2 we present the observing details and the analysis schemes used; section 3 gives the results of our analysis; in sections 4 and 5 we discuss the implications of our results on the physical processes in pulsars and finally a summary is presented in section 6.

2. Observation and Analysis

The observing procedure and initial data processing are detailed in Mitra *et al.* (2016); Basu *et al.* (2016). We have searched for nulling in 123 pulsars observed at 333 and 618 MHz for roughly 2100 pulses in each case. The pulse energy distributions are represented as two histograms corresponding to the on and off pulse energies (see figure 1, bottom left panel). The off pulse distributions are centered around zero and reflect the noise characteristics of the baseline level. The off pulse distributions are expected to exhibit noise like characteristics resembling a gaussian function. However, in some cases low level wings are seen due to the presence of systematics which smear the statistical boundary between null and burst pulses.

2.1. Determining Nulling behavior

The nulling was identified when a bimodal shape was seen in the on pulse distribution. The null pulses resembled a scaled down version of the off pulse distribution and were separated from the burst distribution (see figure 1, bottom left panel). In a number of pulsars the detection sensitivities of the single pulses were insufficient to separate out the two. However, in a few cases averaging 3-5 pulses helped to identify the presence of nulling. The nulling behavior is usually characterized by the nulling fraction which signifies the fraction of time the pulsar is in the null state. We have determined the nulling fraction as follows. A gaussian functional fit was estimated for the off pulse distribution which was then scaled appropriately to the nulling part of the on pulse distribution. The ratio of the two gaussian peaks gave the measured value of the nulling fraction. In a few cases the entire nulling durations were too small to form well constrained distributions. The nulling fraction in these cases were estimated by counting the individual null pulses.

2.2. Resolved Nulls: Estimating Periodicity

We carried out additional analysis when the null and the burst pulses were well separated. The 3σ noise level of the off-pulse window was initially considered the boundary between the two states. Each single pulse was identified either as the null

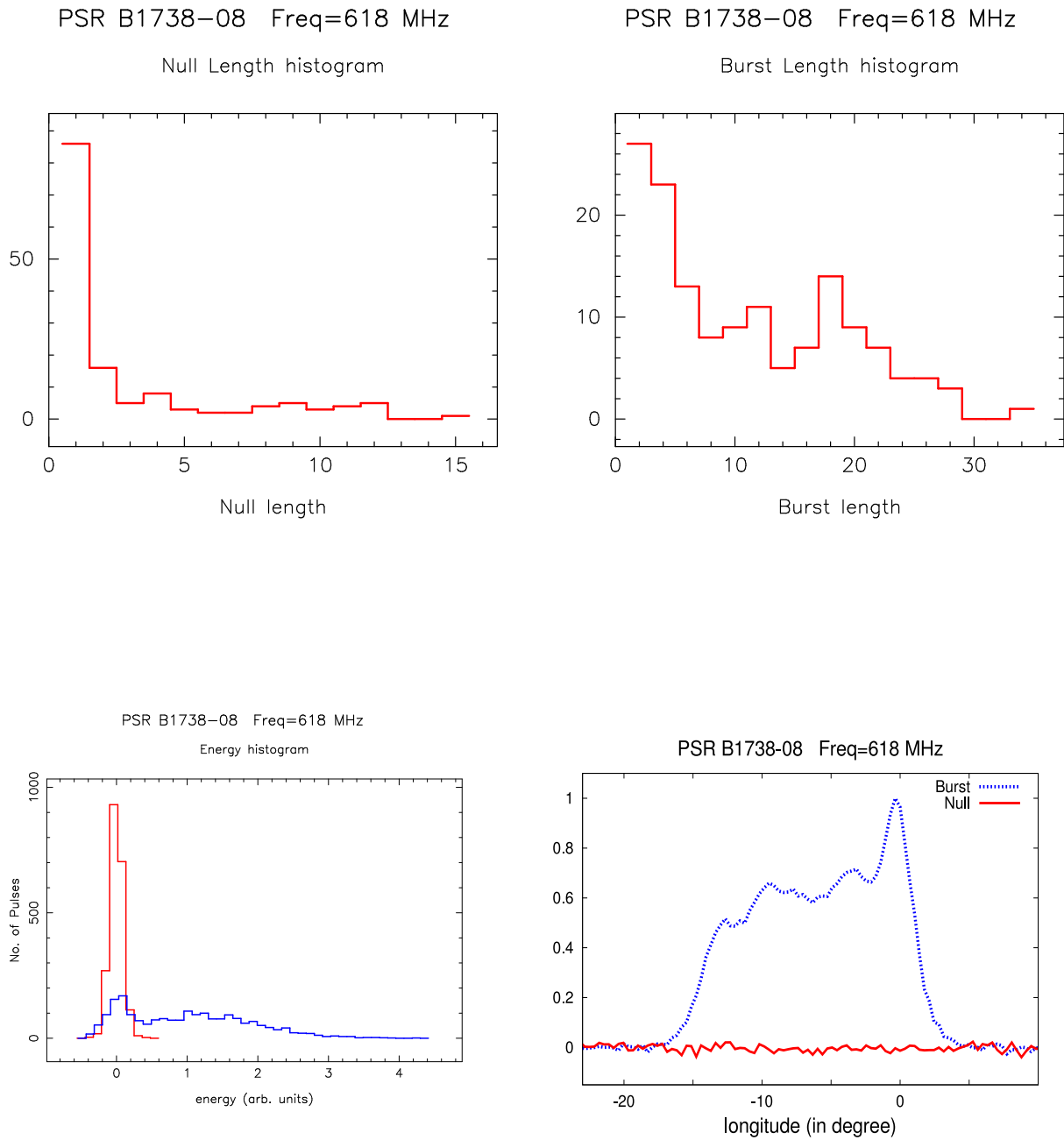


Fig. 1.— The nulling with well resolved null and burst pulses: Null length histogram (top left); Burst length histogram (top right); the average energy distribution (bottom left) for on-pulse (blue histogram) and off-pulse (red histogram); the folded profile (bottom right) for the null pulses (red line, noise like characteristics) and burst pulses (blue line).

or the burst pulse based on the above boundary. In the next phase all single pulses around the boundary were inspected to correct any weak emission identified as nulls. At this stage the null and the burst pulses were separately averaged to form respective profiles (see figure 1, bottom right panel). Further analysis was carried out if no significant emission was detected in the null profile. The null and burst lengths were determined during each transition along with the total number of transitions between the states. Finally, the null and burst length histograms were estimated (see figure 1, top panels).

Additionally, given the sequence of null and burst pulses we examined the presence of periodicity in the transitions between the states. The time series data of 0's and 1's were setup corresponding to the null and the burst pulses respectively. This ensured that all subpulse information was washed away and the only possible periodicity was contained in the transition between the two states. One dimensional discrete Fourier transform (DFT) was carried out on the time series data. In general we used 256 consecutive points for carrying out the DFT. If the peak frequency was too close to the edge the number of points used for the DFT were increased accordingly to resolve the periodicity. The starting position was shifted by 10 pulses and the process was repeated till the end. Finally, all the individual DFTs were averaged to produce a more sensitive spectra. This also enabled us to examine any time variations in the periodicity (see figure 2). In Herfindal & Rankin (2007, 2009) the pulse modulation quelling (PMQ) method was used to estimate the periodicity in nulling. One primary difference in this method was that these authors used the pulses that exhibited the 'partial nulls'. For example, PSR B1133+16 has a two component profile where at certain times the emission corresponding to one of the components is missing. This case is called the partial null. The PMQ used scaled down average profiles for every burst pulse and a similarly scaled half-average profile for the partial nulls (Herfindal & Rankin 2007). In our work we only considered the complete nulls and the partial nulls were identified as burst emission.

3. Results

We have detected nulling in thirty six pulsars including seventeen pulsars where it was reported for the first time. Table 1 lists the measured nulling fraction at the two observing frequencies. In some cases nulling was found to be broadband in nature (Smits *et al.* 2005; Gajjar *et al.* 2014b) while other studies have reported excess nulls at certain frequencies (Bhat *et al.* 2007). Our observations were not simultaneous at the two frequencies to investigate this effect but we found the nulling behavior to be similar at both frequencies. In three pulsars B1114–41, B1524–39 and B1918+19 nulling could only be measured at 333 MHz but not at 618 MHz due to lower sensitivity.

In nineteen pulsars the null and burst pulses were well separated and we determined the null length as well as the burst length histograms. The histograms were dominated by the short nulls with duration of a few periods. In five pulsars B0031–07, B0301+19, B1706–16, J1727–2739 and B1944+17 the average null lengths exceeded five periods. In eleven pulsars we detected periodicity in the transition between the two states. The average null lengths of the pulsars with periodic nulling were higher than the non periodic cases.

3.1. Statistical Study

A number of statistical studies exist in the literature to examine randomness in the null/burst sequence. One of the more widely used techniques is the 'Wald-Wolfowitz runs test' applied to a two state system (Redman & Rankin 2009; Gajjar *et al.* 2012). It is assumed that the transition from a null to a burst state is random resembling a coin toss experiment. The run (R) correspond to number of transitions between the two states with a total of n_1 nulls and n_2 bursts. The statistics pertaining to R are defined by the mean (μ), standard deviation (σ) and the factor Z which are calculated as:

$$\begin{aligned}\mu &= \frac{2n_1n_2}{n_1 + n_2} + 1, \\ \sigma &= \sqrt{\frac{2n_1n_2(2n_1n_2 - n_1 - n_2)}{(n_1 + n_2)^2(n_1 + n_2 - 1)}}, \\ Z &= \frac{R - \mu}{\sigma}.\end{aligned}\tag{1}$$

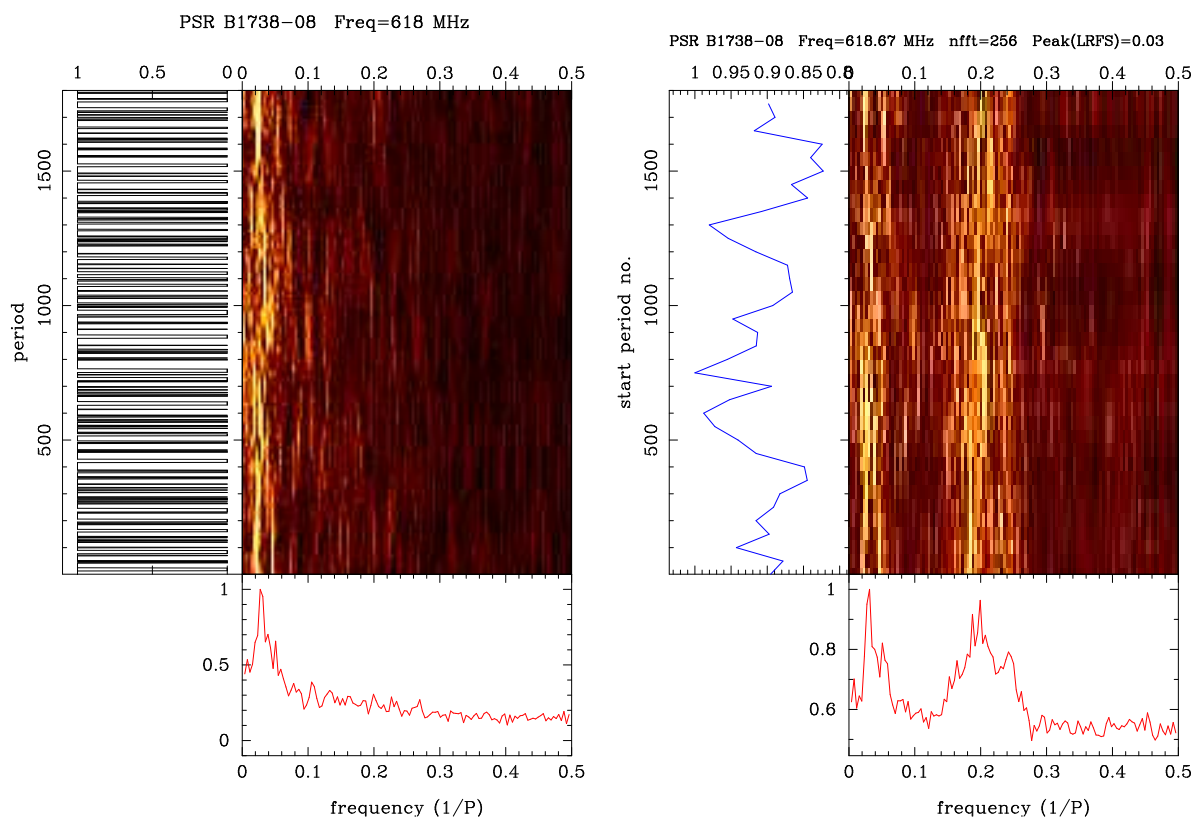


Fig. 2.— The figure shows the time varying Fourier transform of the null/burst (0/1) time series data for the pulsar B1738-08 observed at 618 MHz (left). The longitude resolved fluctuation spectra (LRFS, right panel) from Basu *et al.* (2016) is also shown for comparison. The LRFS shows a wide drifting feature at higher frequency and a narrower feature at low frequency. The low frequency feature is identically reflected in the null/burst spectra where the drifting feature is absent.

Table 1: The list of nulling pulsars is presented with the pulsar name in column 1 along with the period from the ATNF database in column 2. Column 3 and 4 quotes the number of single pulses and the nulling fraction at 333 MHz while column 5 and 6 presents the corresponding values at 610 MHz. In some cases our criterion for estimating nulling (see text) implied that nulling could be measured at only one frequency and the non detections are represented as ‘N’. In some cases nulling fraction could only be estimated by counting the number of pulses below a statistical threshold and no error is calculated for these cases with the numbers serving as an upper limit. Finally, column 7 lists the references for previous nulling studies.

	PSR	Period (sec)	333 MHz		618 MHz		References
			N_p	NF %	N_p	NF %	
1.	B0031-07	0.943	2096	31.3±2.3	1119	22.8±1.8	1,2,3,4,5,6
2.	B0301+19	1.388	2115	8.7±1.2	2115	6.1±0.6	7
3.	B0525+21	3.746	400	14.4±1.2	—	—	8
4.	B0628-28	1.244	2112	13.6±1.9	2111	N	8
5.	B0818-13	1.238	969	9.8±1.2	2122	0.8	9,10,11
6.	B0834+06	1.274	1052	3.9±0.3	2116	4.7±0.7	8,12
7.	B0906-17	0.402	2078	26.8±1.7	2234	25.7±1.3	—
8.	B0942-13	0.570	2100	14.4±0.9	2196	N	—
9.	B1114-41	0.943	2095	3.3±0.5	1918	N	—
10.	B1133+16	1.188	753	13.7±2.1	494	11.9±2.3	8,13,14
11.	B1237+25	1.382	1081	2.0±0.1	864	3.1±0.4	8
12.	B1325-49	1.479	2100	4.0	2100	4.4	—
13.	B1524-39	2.418	862	5.1±1.3	1233	N	—
14.	B1556-44	0.257	2293	N	2484	0.24	—
15.	B1700-32	1.212	1716	1.6	2125	0.4	—
16.	B1706-16	0.653	2106	3.7±1.3	2106	4.9±0.3	15
17.	J1727-2739	1.293	2126	57.0±2.3	2127	48.3±1.8	16,17
18.	B1730-37	0.338	—	—	2110	52.4±3.5	—
19.	B1738-08	2.043	1753	15.7±1.7	2052	15.8±1.4	—
20.	B1742-30	0.367	2120	40.2±1.9	2119	24.8±1.0	18
21.	B1747-46	0.742	2017	2.4±0.5	2084	2.4	—
22.	B1749-28	0.563	2129	0.2	2129	1.7±0.4	18
23.	B1758-03	0.921	2145	27.7±1.3	1944	26.1±2.6	—
24.	J1808-0813	0.876	2110	12.8±1.3	1557	8.2±1.0	—
25.	B1813-36	0.387	2158	16.7±0.7	—	—	—
26.	B1819-22	1.874	2106	4.7±0.9	1309	5.5±0.7	—
27.	B1857-26	0.612	2152	5.1±0.8	2152	8.1±0.5	8,19
28.	J1901-0906	1.782	2076	2.9	1068	5.6±0.7	—
29.	B1918+19	0.821	2105	2.0	2180	N	20
30.	B1944+17	0.441	5566	29.7±1.4	2174	37.9±2.3	8,21,22
31.	B2003-08	0.581	2157	15.6±1.0	2157	24.2±1.5	—
32.	B2045-16	1.962	924	8.3±1.4	1828	9.0±0.5	8
33.	B2303+30	1.576	1698	5.3±0.5	—	—	23
34.	B2310+42	0.349	2572	3.7±0.5	—	—	24
35.	B2327-20	1.644	1284	9.6±0.9	1500	13.1±1.5	18
36.	J2346-0609	1.181	2130	42.5±3.8	2128	28.7±1.8	—

References : 1-Huguenin *et al.* (1970), 2-Vivekanand (1995), 3-Vivekanand & Joshi (1997), 4-Joshi & Vivekanand (2000), 5-Smits *et al.* (2005), 6-Gajjar *et al.* (2014b), 7-Rankin (1986), 8-Ritchings (1976), 9-Lyne & Ashworth (1983), 10-Janssen & van Leeuwen (2004), 11-Gajjar *et al.* (2012), 12-Rankin & Wright (2007), 13-Bhat *et al.* (2007), 14-Herfindal & Rankin (2007), 15-Naidu *et al.* (2015), 16-Wang *et al.* (2007), 17-Wen *et al.* (2016), 18-Biggs (1992), 19-Mitra & Rankin (2008), 20-Rankin *et al.* (2013), 21-Kloumann & Rankin (2010), 22-Deich *et al.* (1986), 23-Redman *et al.* (2005), 24-Wright *et al.* (2012)

Here, Z is Gaussian distribution with zero mean and standard deviation unity. The randomness of the sequence with 95% confidence level correspond to $-1.96 < Z < 1.96$. Table 2 shows the Z factor calculated assuming that the two frequencies represent different segments of a larger time series configuration. The runs test indicates the null/burst sequence to be non-random in the majority of pulsars, with B0834+06 and B1747-46 being the notable exceptions.

The inherent assumption in the runs test is that the transition probabilities from one state to another are identical. In the cases where the transition probabilities differ the 2-state Markov process provides a more appropriate description. The transition probabilities are expressed in a 2×2 transition matrix \mathbf{Q} as :

$$\mathbf{Q} = \begin{pmatrix} q_{11} & q_{12} \\ q_{21} & q_{22} \end{pmatrix}$$

Here q_{11} and q_{22} are the probabilities of continuing in the null and burst states respectively, while q_{12} and q_{21} signify the transition probabilities from the null to burst states and vice versa. These quantities are estimated as (Cordes 2013):

$$\begin{aligned} \langle NL \rangle &= 1/q_{12}, \\ \langle BL \rangle &= 1/q_{21} \end{aligned} \quad (2)$$

along with the normalization condition $\sum_j q_{ij} = 1$. Here $\langle NL \rangle$ and $\langle BL \rangle$ are the average null lengths and burst lengths respectively. The expected nulling fraction is calculated as:

$$NF = \frac{q_{21}}{q_{12} + q_{21}} \quad (3)$$

The estimated transition probabilities are shown in Table 2 along with the expected nulling fractions. We have once again combined the sequences from the two frequencies for these calculations. The expected nulling fractions from a 2-state Markov process, particularly with periodic nulling, were larger than the measured values. This implies that the 2-state Markov process is not an appropriate explanation for the transition from the null to the burst state and vice versa.

3.2. The Nulling Periodicity

As mentioned earlier we have measured periodic nulling in eleven pulsars. In six pulsars B0031-07, B0301+19, J1727-2739, B1738-08, B1944+17

and B2045-16 both nulling and subpulse drifting were seen in the same system as evidenced by the multiple peaks in their fluctuation spectra (see Basu *et al.* 2016, for a detailed analysis). The nulling periodicities coincided with the low frequency peaks (see figure 2) while the high frequency structures were identified with subpulse drifting. The nulling periodicities, ranging from $20 P$ to $600 P$, were larger than typical subpulse drifting periodicities.

3.3. Individual pulsars

In this section we describe the single pulse behavior in individual pulsars. In some cases nulling was affected by signal to noise issues. In others we noticed peculiar mode changing. The single pulse plots are available in Mitra *et al.* (2016)¹.

B0628-28 was studied in Ritchings (1976) who did not find any significant nulling. The single pulse behavior were different at the two frequencies. Nulling was seen only at 333 MHz with bursts of emission interspersed by longer duration nulls or very low level emission. The 618 MHz data showed a continuous but steadily decreasing burst state. Nulling appeared to be periodic or quasi periodic in nature. The periodicity study could not be conducted due to the presence of weaker burst pulses particularly around the nulls.

B0942-13 exhibited two types of nulling at 333 MHz within our short window of 2000 pulses. In the beginning the nulls were of short duration interspersed with the burst state. The mean intensity of the emission started decreasing gradually around the 1000th pulse and completely switched off around the 1500th pulse. A short burst of emission with much lower intensity was seen between the 1800th and 1900th pulse. The 618 MHz emission had weaker signal and nulling could not be identified in the energy histograms.

B1556-44 did not show much variation in intensity for the majority of the observations. At the very end of the 618 MHz data the intensity dropped for 5-10 pulses leading to possible nulls. The pulsar profile is dominated by a core compo-

¹The single pulse time series plots can also be accessed from <http://mspes.ia.uz.zgora.pl/>

Table 2: The nulling statistics of pulsars where the null and burst periods were resolved. Columns 2, 3 and 4 represents the number of transitions between the null and burst states, N_T , the average burst length, $\langle \text{BL} \rangle$, and the average null length, $\langle \text{NL} \rangle$, respectively at 333 MHz, while column 5, 6 and 7 present the corresponding values at 618 MHz. Column 8 presents the periodicity (P_N) in the transition from the null to the burst states, while column 9 presents the Z statistics for the runs test. Columns 10 and 11 show the estimated transition probability from the null to burst state and vice versa for a 2-state Markov process with the estimated nulling fraction from these transition probabilities, $\text{NF}(\text{E})$, is shown in column 12.

PSR	333 MHz			618 MHz			P_N (P)	Z	q_{12}	q_{21}	NF(E) (%)
	N_T	$\langle \text{BL} \rangle$ (P)	$\langle \text{NL} \rangle$ (P)	N_T	$\langle \text{BL} \rangle$ (P)	$\langle \text{NL} \rangle$ (P)					
1. B0031-07	45	26.0	19.3	14	42.3	34.1	75±14	-52.0	0.044	0.034	43.4
2. B0301+19	43	41.9	6.3	30	61.2	6.6	103±34	-52.9	0.155	0.020	11.4
3. B0525+21	17	16.8	4.9	—	—	—	—	-14.4	0.202	0.059	22.7
4. B0818-13	58	14.6	2.1	15	111.5	1.0	—	-22.6	0.537	0.029	5.1
5. B0834+06	64	15.5	1.0	156	12.4	1.0	—	-1.3	0.905	0.075	7.7
6. B1133+16	—	—	—	57	6.9	1.5	29±2	-4.0	0.679	0.145	17.6
7. B1237+25	41	24.0	1.6	24	33.1	1.5	—	-13.5	0.657	0.036	5.3
8. B1524-39	36	22.3	1.3	—	—	—	—	-5.9	0.766	0.045	5.5
9. B1700-32	13	127.5	2.1	5	348.4	1.0	—	-29.2	0.514	0.005	1.0
10. B1706-16	52	36.9	3.3	48	37.8	5.9	130±70	-48.9	0.220	0.027	10.9
11. J1727-2739	—	—	—	43	12.5	35.9	206±33	-41.1	0.028	0.080	74.1
12. B1738-08	152	8.1	3.4	144	10.5	3.6	34±8	-37.4	0.287	0.108	27.3
13. B1747-46	75	25.2	1.0	46	42.2	1.0	—	-1.2	0.953	0.032	3.2
14. B1749-28	2	820.0	2.0	14	147.6	3.6	—	-44.0	0.291	0.004	1.5
15. B1944+17	255	7.2	14.5	78	10.4	17.5	600±52	-71.0	0.066	0.126	65.7
16. B2045-16	57	13.2	2.3	109	14.3	2.4	51±20	-26.8	0.417	0.072	14.7
17. B2303+30	88	17.3	1.9	—	—	—	43±8	-17.6	0.518	0.058	10.0
18. B2310+42	44	51.6	3.6	—	—	—	32±11	-35.2	0.274	0.019	6.6
19. B2327-20	87	12.0	2.5	117	10.3	2.4	19±1	-26.1	0.412	0.091	18.0

ment which makes the presence of nulling interesting.

B1706–16 showed periodic nulling as reported in table 2. Naidu *et al.* (2015) also reported longer duration nulls lasting several thousand periods. The pulsar belongs to a small group which show extreme nulling.

J1808–0813 showed the likely presence of periodic or quasi periodic nulling at both frequencies. Due to lower sensitivity of the emission we were not able to separate the null and the burst pulses and carry out a more detailed study of the nulling periodicity.

B1819–22 exhibits phase modulated drifting as reported in Basu *et al.* (2016). The nulling appeared to exhibit a periodic or quasi periodic nature. We were not able to estimate the nulling periodicity due to weaker signal. However, a low frequency feature was seen in the LRFS in addition to subpulse drifting which may be indicative of nulling periodicity.

B2003–08 has a multi component profile with a likely core emission. The pulsar exhibits amplitude modulated drifting as reported in Basu *et al.* (2016). Multiple peaks were seen in the LRFS with the possibility of periodicity due to nulling. The single pulses were once again of lower sensitivity to carry out a more detailed analysis.

J2346–0609 showed relatively high nulling fractions with bursts of emission. The 333 MHz data were affected by radio frequency interference (RFI). The 618 MHz data had lower sensitivity for carrying out the nulling periodicity studies.

3.4. Non Detections

We were not able to carry out measurements in ten pulsars where nulling was previously reported. In seven pulsars B0148–06, B0450–18, B0656+14, B0736–40, B1907+03, B1929+10 and B2315+21 the energy histogram analysis were unable to separate the two states due to lower sensitivity of signals. Three pulsars B0740–28, B1727–47 and B1818–04 did not show any nulling despite high

sensitivity. In all three cases the previously reported nulling fractions were upper limits with low values (< 0.1 percent, Biggs 1992). They are relatively high energetic with spin down energy loss greater than 10^{33} erg s $^{-1}$. It is likely that nulling is not present, however, one cannot rule out the possibility of shorter duration less frequent nulls.

4. Comparing Nulling Periodicity and Subpulse Drifting

The nulling periodicities detected in our studies correspond to complete nulls, i.e. no partial nulls have been included, with periodicities similar to certain drifting cases. However, in contrast to particularly the phase modulated subpulse drifting the periodicities associated with nulling show relative spread as evidenced by the null length and burst length histograms. In an attempt to connect these two phenomena the periodic nulls have been termed as ‘pseudo-nulls’ and interpreted by Herfindal & Rankin (2007, 2009); Rankin & Wright (2008); Rankin *et al.* (2013) using the rotating subbeam ‘carousel’ system (Deshpande & Rankin 2001). The pulsar emission beam is believed to consist of a central core component with concentric conal subbeams rotating around the core (Rankin 1990, 1993a). The core components are phase stationary and do not participate in the carousel rotation. If the line of sight cuts the emission beam tangentially this model predicts that there should be the phase modulated subpulse drifting. In the other case when the line of sight traverses the beam, the amplitude modulation of conal components (without any phase variations) are expected. The periodic nulling can manifest the carousel model in two possible ways. In the first case nulling occurs for short durations of few periods when the line of sight passes between two conal subbeams during their rotation cycle. This can also explain the partial nulls where the sight-line nulls only appear on one side of the subbeam system. A typical example of this phenomenon was reported in the pulsar B1133+16 by Herfindal & Rankin (2007). In the second scenario parts of the rotating subbeam system are postulated to be missing. The longer duration periodic nulls lasting several tens of periods are seen when the line of sight passes through these empty regions. The longer duration nulls in PSR J1819+1305 were reported to exhibit this

Table 3: The details of Pulsars with Periodic Nulling. The period and spin down energy loss is listed in column 3 and 4 respectively. Column 5 lists the nulling periodicity while column 6 describes the classification of each pulsar.

	PSR	Period (sec)	\dot{E} (10^{30} erg s $^{-1}$)	P_N (P)	Class.
1.	B0031-07	0.943	19.2	75±14	S_d
2.	B0301+19	1.388	19.1	103±34	D
3.	B0525+21	3.746	30.1	46±4	D
4.	B0751+32	1.442	14.2	73±10	D
5.	B0834+06	1.274	130	16±4	D
6.	B1133+16	1.188	87.9	29±2	D
7.	J1649+2533	1.015	21.1	27±2	—
8.	B1706-16	0.653	894	130±70	S_t
9.	J1727-2739	1.293	20.1	206±33	—
10.	B1738-08	2.043	10.5	34±8	${}_cQ?$
11.	J1819+1305	1.060	11.9	64±8	—
12.	B1839+09	0.381	776	37±3	S_t
13.	B1918+19	0.821	63.9	85±14	${}_cT$
14.	B1944+17	0.441	11.1	600±52	${}_cT$
15.	B2034+19	2.074	9.02	57±6	—
16.	B2045-16	1.962	57.3	51±20	T
17.	B2303+30	1.576	29.2	43±8	S_d
18.	B2310+42	0.349	104	32±11	M?
19.	B2327-20	1.644	41.2	19±1	T

Classifications from Rankin (1990, 1993b).

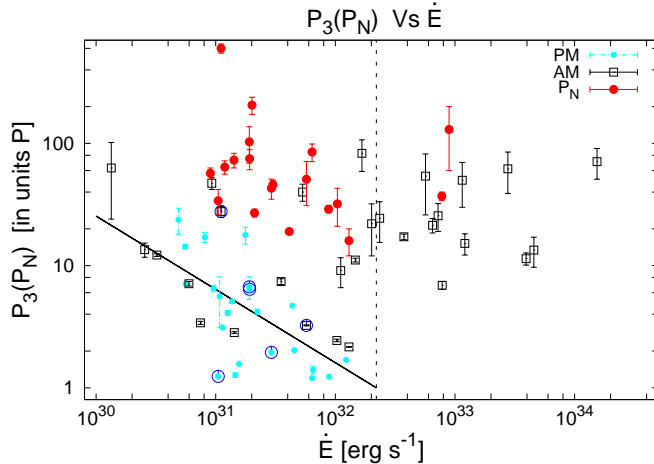


Fig. 3.— The figure shows the Nulling periodicity (P_N as well as the drifting periodicity (P_3) as a function of spin-down energy loss (\dot{E}). The drifting phenomenon can be categorized into the phase modulated drifting (PM, light blue dots) and the periodic amplitude modulation (AM, black open squares). The PM periodicities are anti-correlated with \dot{E} (black line) and restricted to a narrow window (black dashed line). The majority of AM periodicities are spread out over a large \dot{E} range and generally have large periodicities. The nulling periodicities (red dots) have properties similar to the AM cases. In some pulsars the P_N coexist with P_3 (open blue circles identify drifting pulsars with P_N) and are larger than the corresponding drifting periodicities.

phenomenon by Rankin & Wright (2008). The periodic nulling in the carousel model are associated with conal components (Herfindal & Rankin 2009) and provide an immediate prediction that these should not be manifested in the stationary core components. To test this prediction we have collected the nineteen pulsars with reported nulling periodicity in table 3 along with their profile classification. The table shows that in addition to conal components (S_d , D, ${}_cT$ and ${}_cQ$ profile classes) the pulsars with prominent core emission (S_t , T and M classes) also show periodic nulling. The nulling periodicity in the core components is difficult to understand using the carousel model. It seems more likely that the complete nulls correspond to the conditions when the emission is completely ceased. Additionally, Basu *et al.* (2016) reports the presence of periodic amplitude modulation in many pulsars which are core dominated. In a recent work by Mitra & Rankin (2017) highly periodic amplitude modulation was seen in the core component of the pulsar B1946+35. This also could not be explained using the carousel model and was considered as a newly emergent

phenomenon.

Basu *et al.* (2016) showed from theoretical perspectives that there are difficulties in explaining the subpulse drifting phenomenon using a carousel system rotating around the magnetic axis. However, an interesting correlation was seen between the spin-down energy loss (\dot{E}) and the drifting periodicity (P_3). The drifting population can be broadly separated into two groups. The first corresponding to phase modulated drifting showed significant subpulse motion across the pulse window. The periodicities were anti-correlated with \dot{E} ($P_3 \propto \dot{E}^{-0.6}$) and restricted to a narrow \dot{E} range ($< 2 \times 10^{32}$ erg s $^{-1}$). The second group showed periodic amplitude modulation with very little subpulse motion across the pulse window. They were spread out over a wider \dot{E} range and generally had large P_3 values. In a few cases the periodic amplitude modulation had smaller periodicities which could be anti-correlated with \dot{E} . They were possibly phase modulated drifters with specialized geometries resulting in small phase variations. At the lower \dot{E} range ($\sim 10^{30}$ erg s $^{-1}$) the two classes had comparable P_3 values.

We have explored the dependence of the nulling periodicities (P_N) on \dot{E} in order to explore if a connection exists with subpulse drifting. The P_3 versus \dot{E} plot in Basu *et al.* (2016) is reproduced in figure 3 where the P_N values have also been added. The periodic nulling seems to form a homologous group with the periodic amplitude modulation class. As reported earlier, in many pulsars both periodic nulling and phase modulated drifting appear. We propose the idea that there are two distinct periodic phenomenon connected with the radio emission in pulsars. The $\mathbf{E} \times \mathbf{B}$ drift in the IAR gives rise to the phase modulated drifting. This phenomenon is correlated with \dot{E} and discussed in more details by Basu *et al.* (2016). On the other hand the periodic amplitude modulation and periodic nulling, which can be considered as an extreme form of amplitude modulation, are related to an unexplored periodic phenomenon in pulsars.

5. Physical implications of Nulling

The duration of the most widespread nulling is short, just one or two pulse periods. This is evidenced by the null length histograms which generally peak at the lowest bin. In some cases the nulling also lasts for hundreds of periods at a time with a small but significant population of such pulsars now known (Lewandowski *et al.* 2004; Wang *et al.* 2007; Gajjar *et al.* 2012, 2014a; Kerr *et al.* 2014; Young *et al.* 2015). But, even in these cases the distribution is dominated by the short duration nulls. It has been argued that the processes that cause nulling at different timescales have a different physical origin. The short duration nulls are associated with stochasticity in the emission process while the longer duration nulls are large scale changes in the magnetosphere (see Cordes 2013, and references therein). One obvious way for nulling to occur is the pulsar emission beam moving in and out of the observers' line of sight. Effects like precession or the emission being blocked by an external object orbiting around the neutron star are some likely scenarios for this to happen. This necessitates nulling to be highly periodic with exact null and burst length intervals. However, as evident in the single pulses there is no repetitive pattern in the nulling phenomenon even in the cases that show an underlying periodicity. This is also represented in the null length

and the burst length histograms which show a distribution and rules out these mechanisms as the only possible source of nulling². It is more likely that nulling is related to disruptions in the radio emission process.

The radio emission can be disrupted if the distribution of particles flowing along the dipolar magnetic field lines changes. Goldreich & Julian (1969) demonstrated that the region around a fast spinning neutron star of surface magnetic field 10^{12} G cannot remain as vacuum. They determined a charge separated force-free magnetosphere with density $n_{GJ} = \Omega \cdot B / 2\pi c e$. It has been reported (e.g. most recently by Philippov *et al.* 2015; Pétri 2016, and references therein) that a sufficient supply of charges from the neutron star surface as well as from the pair production results in transition from a charge separated magnetosphere to a force-free magnetosphere. The charge separated magnetosphere corresponds to the case where charged particles are trapped in charge separated zones which co-rotate with the star. On the other hand the force-free magnetosphere is associated with the electromagnetically dominated pulsar wind and separated into the closed field line region in which charges corotate with the star and the open field line region in which charges can flow radially outwards. The coherent radio emission is excited due to some instabilities in the relativistic plasma outflowing along the open dipolar magnetic field lines. If the fluctuations in the pair production process are such that the pulsar exists in the transition region between an electrosphere and a force-free magnetosphere, nulling is expected in its electrosphere state when the particle flow is halted. The timescale for which the particle flow can stop is comparable to the return current generation time, which is a few hundred milliseconds for a typical one second pulsar. This provides an explanation for the single period nulls. However, it requires detailed investigation to see if the electrosphere can survive for longer durations and the transition between the magnetospheric states can support long period nulls.

Next we examine the conditions which may lead to disruption of the radio emission in the presence

²incidentally the carousel model of rotating sub-beams discussed in the previous section is also a form of geometric nulling

of particle flow. Several observational evidences suggest that the radio emission arises around 500 kilometers above the neutron star due to coherent curvature radiation (Mitra & Rankin 2002; Kijak & Gil 2003; Mitra & Li 2004; Krzeszowski *et al.* 2009; Mitra *et al.* 2009). These basic observational features can be best explained by the so called steady state polar cap models (e.g., Sturrock 1971; Ruderman & Sutherland 1975). In pulsars where $\mathbf{\Omega} \cdot \mathbf{B} < 0$, the positive ions cannot be extracted from the stellar surface due to high binding energy. This results in the formation of a vacuum gap or inner acceleration region (IAR) above the magnetic poles. Once the IAR is formed the radio emission process can be broadly divided into three stages occurring at distinct locations. The first stage consists of breakdown of the IAR by isolated discharges on the polar cap due to magnetic e^-e^+ pair production. High energy gamma-rays (> 1.02 MeV) can form pairs in the presence of strong magnetic fields (Shukre & Radhakrishnan 1982). The large electric fields separate out the pairs with the back streaming electrons heating the surface to very high temperatures (upto million degree kelvin). They further emit soft X-rays due to thermal radiation. The positrons, also called primary particles, accelerate to high Lorentz factors and stream away from the stellar surface. The second stage consists of the primary particles producing further higher energy photons via curvature radiation or inverse Compton scattering leading to more pairs. This eventually results in a cascade giving rise to a more dense but less energetic secondary pair plasma outside the IAR. The outflowing streams of secondary plasma clouds with the specific energy distribution function are formed at the end of this stage. At the final stage, around heights of ~ 500 kilometers, the two stream instability develops due to the overlapping of fast and slow moving particles of adjacent secondary plasma clouds (Asseo & Melikidze 1998) along a particular set of field lines. This leads to the generation of strong electrostatic Langmuir wave turbulence. The Langmuir waves are modulationally unstable and their nonlinear evolution produces the charged solitons that can excite the radio waves via the curvature radiation mechanism (Melikidze *et al.* 2000; Gil *et al.* 2004). The radiation finally emerges as ordinary and

extraordinary modes from the secondary plasma (Melikidze *et al.* 2014; Mitra *et al.* 2016b).

The emission mechanism is extremely sensitive to the plasma parameters. Any random fluctuations in these parameters are likely to appear between timescales of 100 nanoseconds (time to empty the gap after sparking has stopped) to 5 microseconds (spark formation time) which are much shorter than the typical nulling timescales. The only possibilities that can change the plasma parameters are additional physical processes which alter the nature of the IAR. There are two different mechanisms in the literature which can be used in this context. The first proposed by Timokhin (2010) suggests changes in the magnetospheric state leading to variations in the spin-down rates. This is brought about by the changes in the current flow and the size of the open field line region which might be effective in altering the parameters of the outflowing plasma. The second method leads to modifications in the potential drop across the IAR by introducing the concept of a partially screened gap (PSG, Gil *et al.* 2003; Szary *et al.* 2015). The surface temperature is considered to be at the critical level for the ions to be emitted and in the process reducing the gap potential. This results in altering the energy of the primary particle which can further change the process of secondary particle production. The secondary pair production process can switch from being dominated by curvature radiation mechanism to inverse Compton scattering resulting in a modified energy distribution function. However, the transition between different states would still require an additional triggering mechanism which are not addressed at present. This triggering mechanism would likely involve an additional source of high energy photons from outside the IAR. Additionally, the processes generating these photons should be self regulating to switch from the null to the burst states and vice versa. The underlying mechanisms which can lead to such high energy photons outside the IAR need to be developed with detailed modelling. However, one of our results provide some constraints on this process. The presence of nulling periodicity seen in a number of pulsars suggest that the additional mechanism should be periodic in certain cases.

6. Summary

A detailed study of the nulling was conducted for the 123 pulsars observed in the Meterwavelength Single-pulse Polarimetric Emission Survey. Nulling was observed in thirty six pulsars including eleven pulsars showing the presence of nulling periodicity. The nulling periodicity was demonstrated to be different and of longer duration than the phase modulated subpulse drifting. The presence of nulling require a triggering mechanism to change the pair production process within the magnetosphere. The triggering mechanism is not yet known but should be periodic in some pulsars with periodic nulling.

Acknowledgments: We thank the referee for the valuable comments which helped to improve this paper. This work was supported by grant DEC-2013/09/B/ST9/02177 of the Polish National Science Centre. We would like to thank the staff of Giant Meterwave Radio Telescope and National Center for Radio Astrophysics for providing valuable support in carrying out this project. GMRT is run by the National Centre for Radio Astrophysics of the Tata Institute of Fundamental Research.

REFERENCES

- Asseo, E.; Melikidze, G.I. 1998, MNRAS, 301, 59
- Backer, D.C. 1970, Nature, 228, 42
- Basu, R.; Mitra, D.; Melikidze, G.I.; Maciesiak, K.; Skrzypczak, A.; Szary, A. 2016, ApJ, 833, 29
- Bhat, N. D. R.; Gupta, Y.; Kramer, M.; Karastergiou, A.; Lyne, A. G.; Johnston, S. 2007, A&A, 462, 257
- Biggs, J.D. 1992, ApJ, 394, 574
- Deich, W. T. S.; Cordes, J. M.; Hankins, T. H.; Rankin, J. M. 1986, ApJ, 300, 540
- Cordes, J.M. 2013 ApJ, 775, 47
- Deshpande, A.A.; Rankin, J.M. 2001 MNRAS, 322, 438
- Gajjar, V.; Joshi, B.C.; Kramer, M. 2012, MNRAS, 424, 1197
- Gajjar, V.; Joshi, B.C.; Wright, G. 2014a, MNRAS, 439, 221
- Gajjar, V.; Joshi, B.C.; Kramer, M.; Karuppusamy, R.; Smits, R. 2014b, ApJ, 797, 18
- Gil, J.A.; Sendyk, M. 2000, ApJ, 541, 351
- Gil, J.; Melikidze, G.I.; Geppert, U. 2003, A&A, 407, 315
- Gil, J.; Lyubarsky, Y.; Melikidze, G.I. 2004, ApJ, 600, 872
- Goldreich, P; Julian, W.H. 1969, ApJ, 157, 869
- Hankins, T. H.; Wolszczan, A. 1987, ApJ, 318, 410
- Herfindal, J.L.; Rankin, J.M. 2007, MNRAS, 380, 430
- Herfindal, J.L.; Rankin, J.M. 2009, MNRAS, 393, 1391
- Huguenin, G. R.; Taylor, J. H.; Troland, T. H. 1970, ApJ, 162, 727
- Janssen, G. H.; van Leeuwen, J. 2004, A&A, 425, 255
- Joshi, B. C.; Vivekanand, M. 2000, MNRAS, 316, 716
- Kerr, M.; Hobbs, G.; Shannon, R.M.; Kiczynski, M.; Hollow, R.; Johnston, S. 2014, MNRAS, 445, 320
- Kijak, J.; Gil, J. 2003, A&A, 397, 969
- Kloumann, Isabel M.; Rankin, Joanna M. 2010, MNRAS, 408, 40
- Krzyszowski, K.; Mitra, D.; Gupta, Y.; Kijak, J.; Gil, J.; Acharyya, A. 2009, MNRAS, 393, 1617
- Kramer, M.; Lyne, A.G.; O'Brien, J.T.; Jordan, C.A.; Lorimer, D.R. 2006, Science, 312, 549
- Lewandowski, W.; Wolszczan, A.; Feiler, G.; Konacki, M.; Soltysinski, T. 2004, ApJ, 600, 905
- Lyne, A. G.; Ashworth, M. 1983, MNRAS, 204, 519
- Melikidze, G.I.; Gil, J.A.; Pataraya, A.D. 2000, ApJ, 544, 1081
- Melikidze, G.I.; Mitra, D.; Gil, J.A. 2014, ApJ, 794, 105
- Mitra, D.; Rankin, J.M. 2002, ApJ, 577, 322
- Mitra, D.; Li, X.H. 2004, A&A, 421, 215
- Mitra, D.; Rankin, J.M. 2008, MNRAS, 385, 606
- Mitra, D.; Gil, J.; Melikidze, G.I. 2009, ApJ, 696, L141
- Mitra, D.; Basu, R.; Maciesiak, K.; Skrzypczak, A.; Melikidze, G.I.; Szary, A.; Krzyszowski, K. 2016, ApJ, 833, 28

- Mitra, D.; Rankin, J.M.; Arjunwadkar, M. 2016, MNRAS, 460, 3063
- Mitra, D.; Rankin, J.M. 2017, MNRAS, 468, 4601
- Naidu, A.; Joshi, B.C.; Manoharan, P.K.; Krishnakumar, M.A. 2015, ExA, 39, 319
- Pétri, J. 2016, JPIPh, 82, 6302
- Philippov, A.A.; Spitkovsky, A.; Cerutti, B. 2015, ApJ, 801, 19
- Rankin, J.M. 1986, ApJ, 301, 901
- Rankin, J.M. 1990, ApJ, 352, 247
- Rankin, J.M. 1993, ApJ, 405, 285
- Rankin, J.M. 1993, ApJS, 85, 145
- Rankin, J. M.; Wright, G. A. E. 2007, MNRAS, 379, 507
- Rankin, J. M.; Wright, G. A. E. 2008, MNRAS, 385, 1923
- Rankin, J. M.; Wright, G.A.E.; Brown, A.M. 2013, MNRAS, 433, 445
- Redman, S.L.; Wright, G. A. E.; Rankin, J.M. 2005, MNRAS, 357, 859
- Redman, S.L.; Rankin, J.M. 2009, MNRAS, 393, 1391
- Ritchings, R. T. 1976, MNRAS, 176, 249
- Ruderman, M.A.; Sutherland, P.G. 1975, ApJ, 196, 51
- Shukre, C.S.; Radhakrishnan, V. ApJ, 258, 121
- Smits, J.M.; Mitra, D.; Kuijpers, J. 2005, A&A, 440, 683
- Sturrock, P.A. 1971, ApJ, 164, 529
- Szary, A., Melikidze, G.I., Gil, J. 2015, MNRAS, 447, 2295
- Timokhin, A.N. 2010, MNRAS, 408, L41
- Vivekanand, M. 1995, MNRAS, 274, 785
- Vivekanand, M.; Joshi, B. C. 1997, ApJ, 477, 431
- Wang, N.; Manchester, R. N.; Johnston, S. 2007, MNRAS, 377, 1383
- Weltevrede, P.; Edwards, R. T.; Stappers, B. W. 2006, A&A, 445, 243
- Wen, Z. G.; Wang, N.; Yuan, J. P.; Yan, W. M.; Manchester, R. N.; Yuen, R.; Gajjar, V. 2016, A&A, 592, 127
- Wright, G.; Weltevrede, P.; Rankin, J.; Herfindal, J. 2012, ASPC, 466, 87
- Young, S.A.E.; Rankin J. 2012, MNRAS, 424, 2477
- Young, N.J.; Weltevrede, P.; Stappers, B.W.; Lyne, A.G.; Kramer, M. 2015, MNRAS, 449, 1495

This 2-column preprint was prepared with the AAS L^AT_EX macros v5.2.

A. Individual Pulsars in our Sample

We discuss the previously reported nulling studies for the pulsars, particularly the cases where nulling periodicities are reported, and compare them with our results.

B0031–07 is a conal single profile which exhibits the phase modulated subpulse drifting as well as nulling. The drifting is seen in three different modes A, B and C with P_3 values of roughly $12 P$, $7 P$ and $4 P$ respectively (Huguenin *et al.* 1970). Smits *et al.* (2005); Gajjar *et al.* (2014b) showed the nulling to be broadband in this pulsar. We find the nulling to exhibit a longer periodicity of $75 \pm 14 P$ which cannot be connected harmonically with any of the three modes.

B0301+19 is a conal double profile which also shows both nulling and subpulse drifting. The LRFS of this pulsar show two features, one associated with drifting with P_3 roughly $6 P$ and another corresponding to nulling at $103 \pm 34 P$. Herfindal & Rankin (2009) also identified the low frequency feature in their PMQ analysis. Interestingly Young & Rankin (2012) showed that the bridge emission between the conal components has a hidden core emission. We find that both the bridge and the conal components vanish during the periodic nulls and it is unlikely to be a result of carousel rotation.

B0525+21 is a conal double profile where the PMQ analysis of Herfindal & Rankin (2009) showed the presence of a low frequency double peaked structure which they identified with nulling. Young & Rankin (2012) reports the bridge emission to contain a hidden core component. We recorded only 400 pulses for this pulsar and the periodicity was not clear in our analysis. However, we found nulling to extend to all the components which make the carousel interpretation unlikely.

B0818–13 is a conal single profile which shows the presence of two distinct emission states (Lyne & Ashworth 1983; Janssen & van Leeuwen 2004). In the brighter phase the pulsar shows the presence of prominent drift bands with occasional single period nulls. The weaker emission state shows longer nulling while the drifting continues to exist during the weaker burst states. There is no detectable periodicity in the null to burst transition during either of the two states.

B0834+06 is a conal double profile which shows the presence of drifting as well as nulling. The LRFS in this pulsar shows the presence of a periodicity corresponding to $2.2 P$ (Weltevrede *et al.* 2006; Basu *et al.* 2016). This feature corresponds to the amplitude modulation. The PMQ analysis of Herfindal & Rankin (2009) found the same feature in a weaker way as well as a low frequency feature. The periodicity was interpreted as corresponding to non random partial nulls (Rankin & Wright 2007). In our analysis with only the complete nulls we did not see any periodicity for the null to burst transitions. Nulling is seen for short durations in this pulsar lasting for few periods. We have argued that complete nulls are not geometrical in nature but arise due to changes in the pulsar magnetosphere over short timescales. In section 5 we discuss possible conditions, such as transition from a charge separated magnetosphere to a force free magnetosphere, etc., where physical mechanism can change over such short timescales.

B1133+16 is a conal double profile similar to B0301+19 and B0525+21 with the bridge likely once again exhibiting core emission (Young & Rankin 2012). The LRFS show the presence of a low frequency feature as reported in (Backer 1970; Weltevrede *et al.* 2006). The feature becomes more prominent in both the PMQ and our analysis and is clearly related to periodic nulls. Herfindal & Rankin (2007) identified the periodicity as the longer circulation time of the rotating carousel model with sparse and occasional beamlets. They interpreted the shorter nulls as empty sight-line traverse between subbeams. Our analysis uses only the complete nulls and the presence of a hidden core component makes it unlikely to be a result of carousel circulation. Nulling is supposed to be a broadband phenomenon (Smits *et al.* 2005; Gajjar *et al.* 2014b) but simultaneous observations by Bhat *et al.* (2007) report the presence of excess nulls below 1.4 GHz for

this pulsar. However, more observations are needed to show if the periodicity persists across the frequencies.

J1727–2739 is a conal double profile with both nulling and drifting. Wang *et al.* (2007) reported frequent short bursts separated by null intervals in this pulsar. A more detailed study by Wen *et al.* (2016) showed the presence of three distinct modes during the burst state with modes A and B showing different drifting properties while in mode C no subpulse drifting is detected. We have additionally found nulling to exhibit periodicity.

B1918+19 shows a three component conal profile with nulling as well as subpulse drifting. Hankins & Wolszczan (1987) showed the presence of three different drift modes A, B, C with periodicities $\sim 6P$, $\sim 4P$ and $\sim 3P$ respectively, along with a disordered mode (N) without any drifting. Rankin *et al.* (2013) found the nulls to be confined mainly in the B and N modes with the modes exhibiting specific modal sequences. The three different drift modes have been interpreted in the framework of the carousel model as the number of sparks or subbeams changing in each mode. The PMQ analysis of Herfindal & Rankin (2009) show the presence of two harmonically connected peaks at $85 \pm 14P$ and $43 \pm 4P$ in addition to a wide structure at $12P$. The $12P$ periodicity was taken as a confirmation of the carousel circulation time, the longer periodicities has been associated with the mode sequences. The single pulse data were not sensitive for us to carry out a detailed null periodicity study.

B1944+17 is a conal profile with long null intervals as well as subpulse drifting. Deich *et al.* (1986) identified 4 distinct modes in the pulsar with modes A and B associated with subpulse drifting having periodicities $\sim 14P$ and $\sim 6P$ respectively while mode C and D do not show any drifting periodicity. Kloumann & Rankin (2010) divided the nulling behavior into two groups, the short duration nulls were assumed to be pseudo-nulls resulting from carousel rotation while the longer duration nulls were expected to be true nulls without any periodicity. But the results of our periodicity studies show contrasting nulling behavior for this pulsar. The null periodicity 600 ± 52 is the longest known case and correspond to the longer duration nulls. No corresponding periodicity was detected for the shorter null lengths.

B2303+30 shows the presence of nulling as well as subpulse drifting. The pulsar shows two emission modes with the B mode having a near $2P$ periodicity while the Q mode show a $3P$ periodicity (Redman *et al.* 2005). Nulling is reported to be mainly seen in the Q mode. The PMQ analysis of Herfindal & Rankin (2009) showed the presence of low frequency structure which is verified in our nulling periodicity studies.

B. The plots detailing the nulling phenomenon with well resolved null and burst pulses.

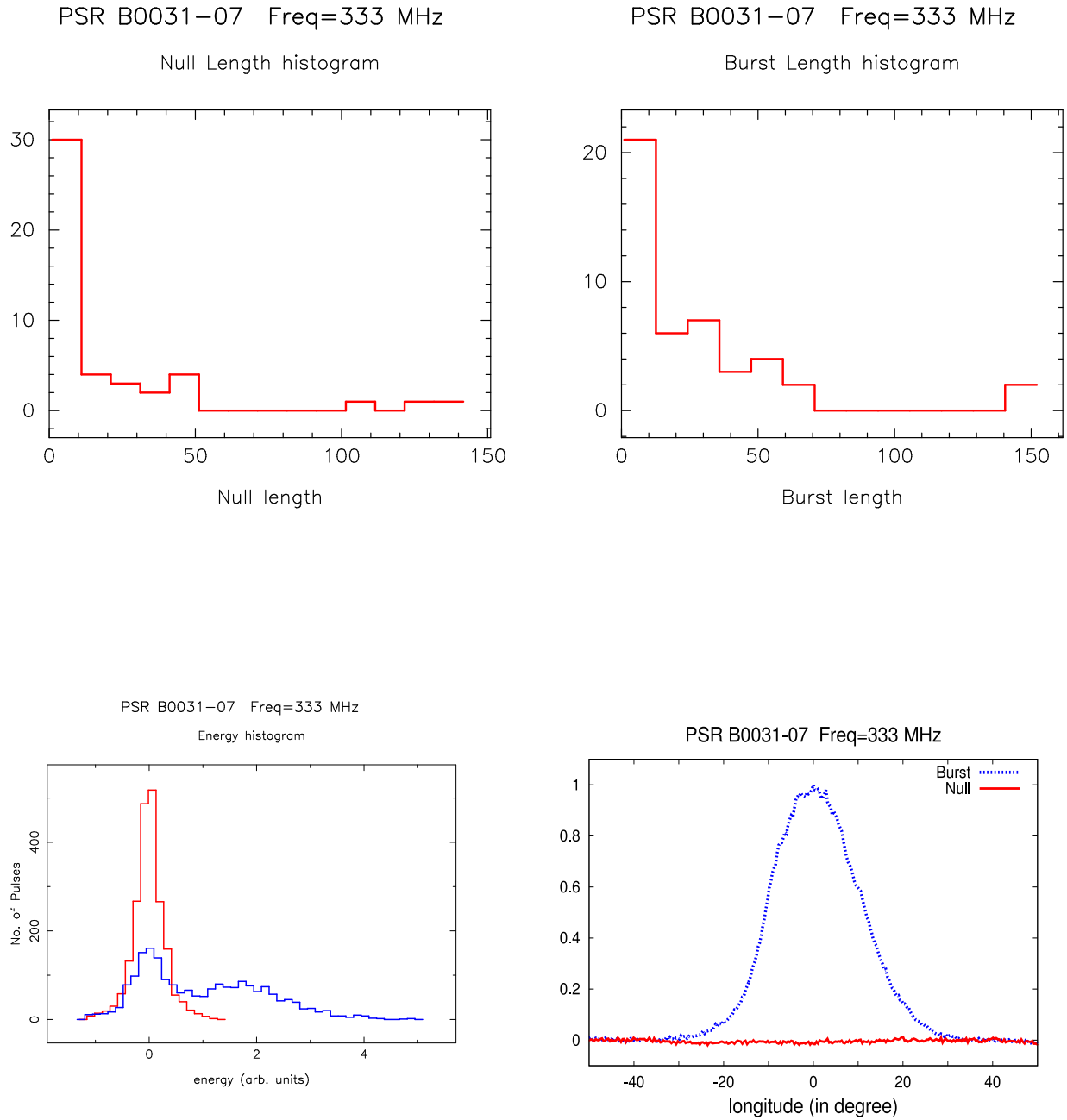


Fig. 4.— Null length histogram (top left); Burst length histogram (top right); the average energy distribution (bottom left) for on-pulse window (blue histogram) and off-pulse window (red histogram); the folded profile (bottom right) for the null pulses (red line, noise like characteristics) and burst pulses (blue line).

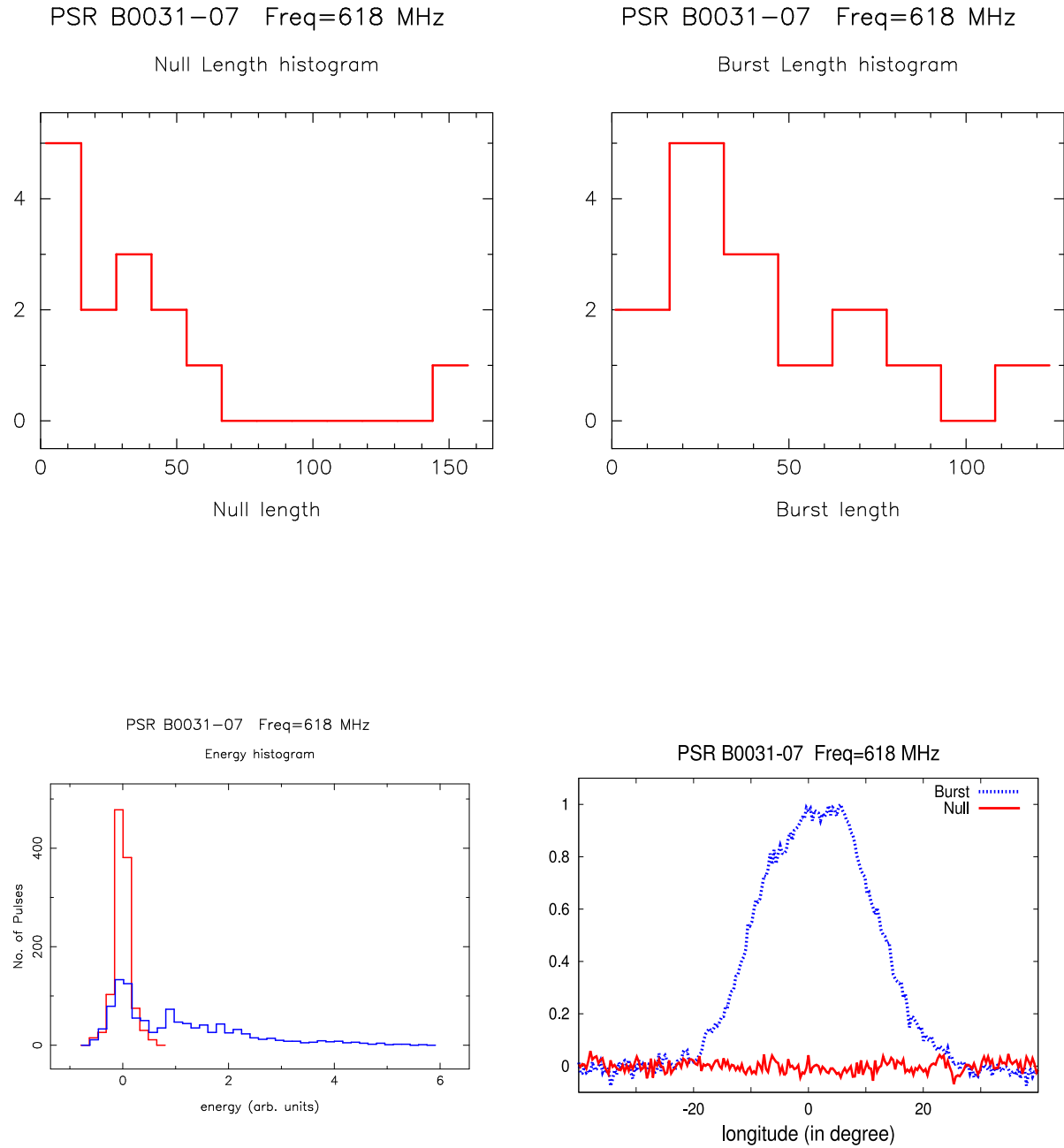


Fig. 5.— Null length histogram (top left); Burst length histogram (top right); the average energy distribution (bottom left) for on-pulse window (blue histogram) and off-pulse window (red histogram); the folded profile (bottom right) for the null pulses (red line, noise like characteristics) and burst pulses (blue line).

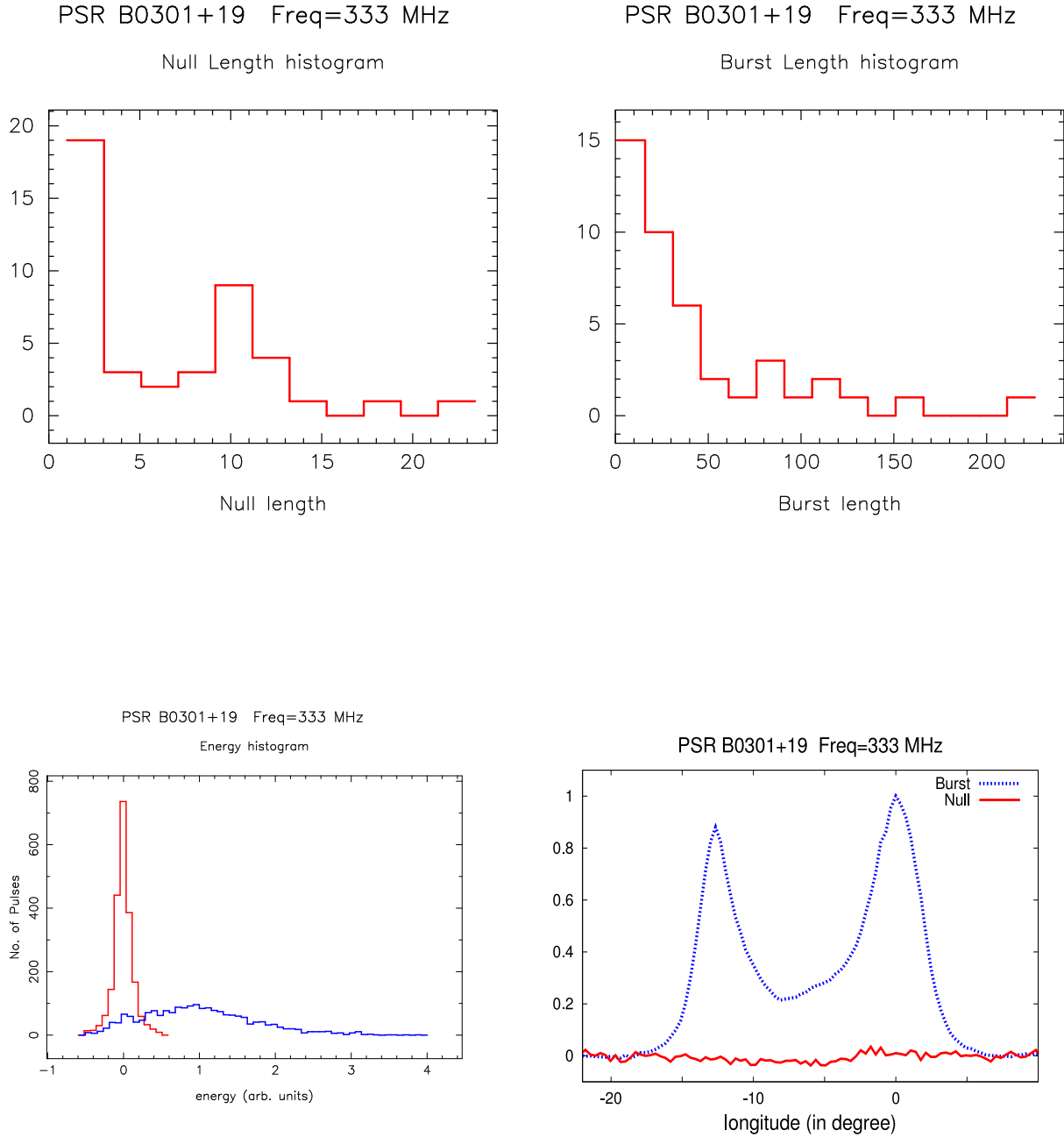


Fig. 6.— Null length histogram (top left); Burst length histogram (top right); the average energy distribution (bottom left) for on-pulse window (blue histogram) and off-pulse window (red histogram); the folded profile (bottom right) for the null pulses (red line, noise like characteristics) and burst pulses (blue line).

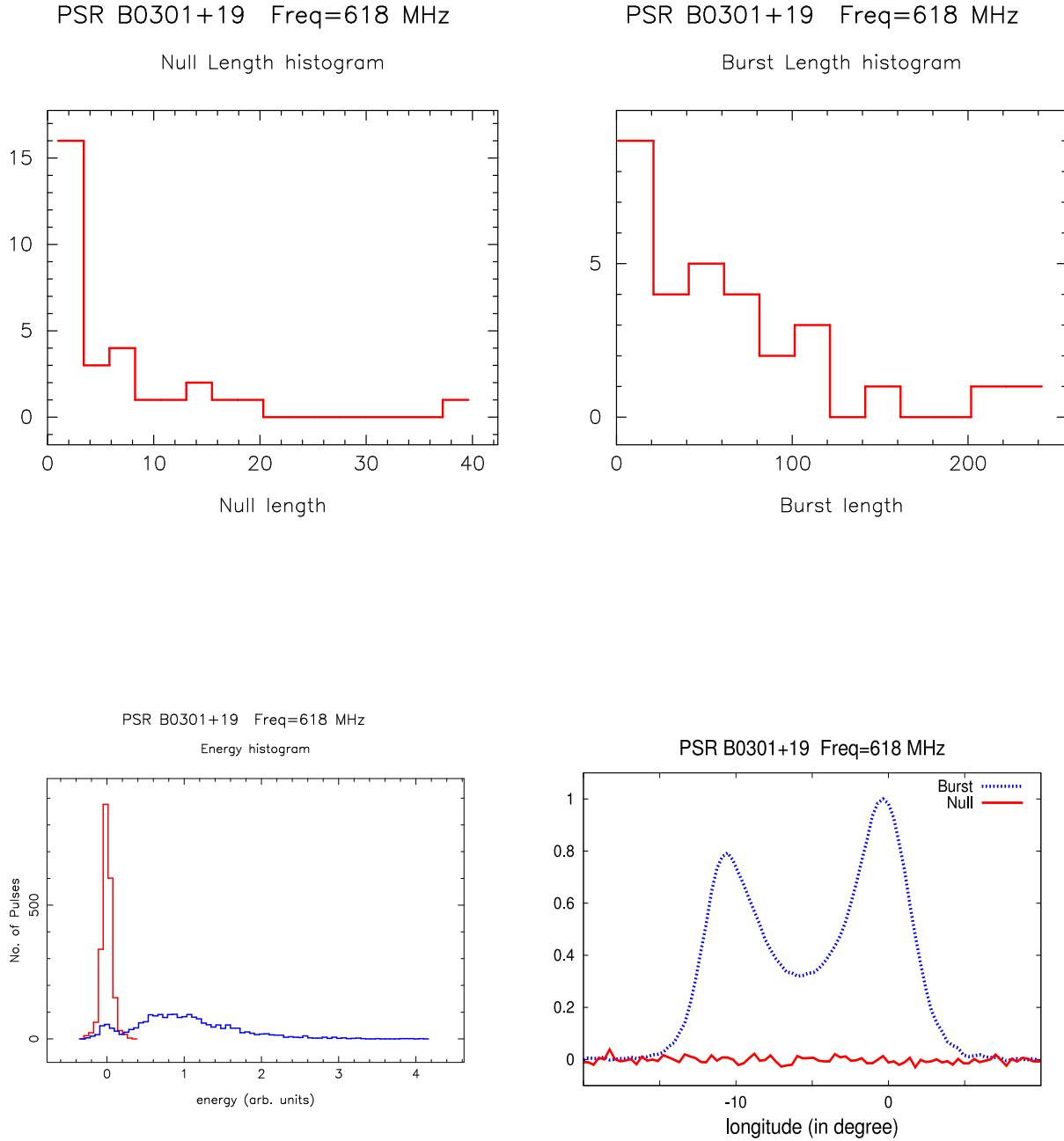


Fig. 7.— Null length histogram (top left); Burst length histogram (top right); the average energy distribution (bottom left) for on-pulse window (blue histogram) and off-pulse window (red histogram); the folded profile (bottom right) for the null pulses (red line, noise like characteristics) and burst pulses (blue line).

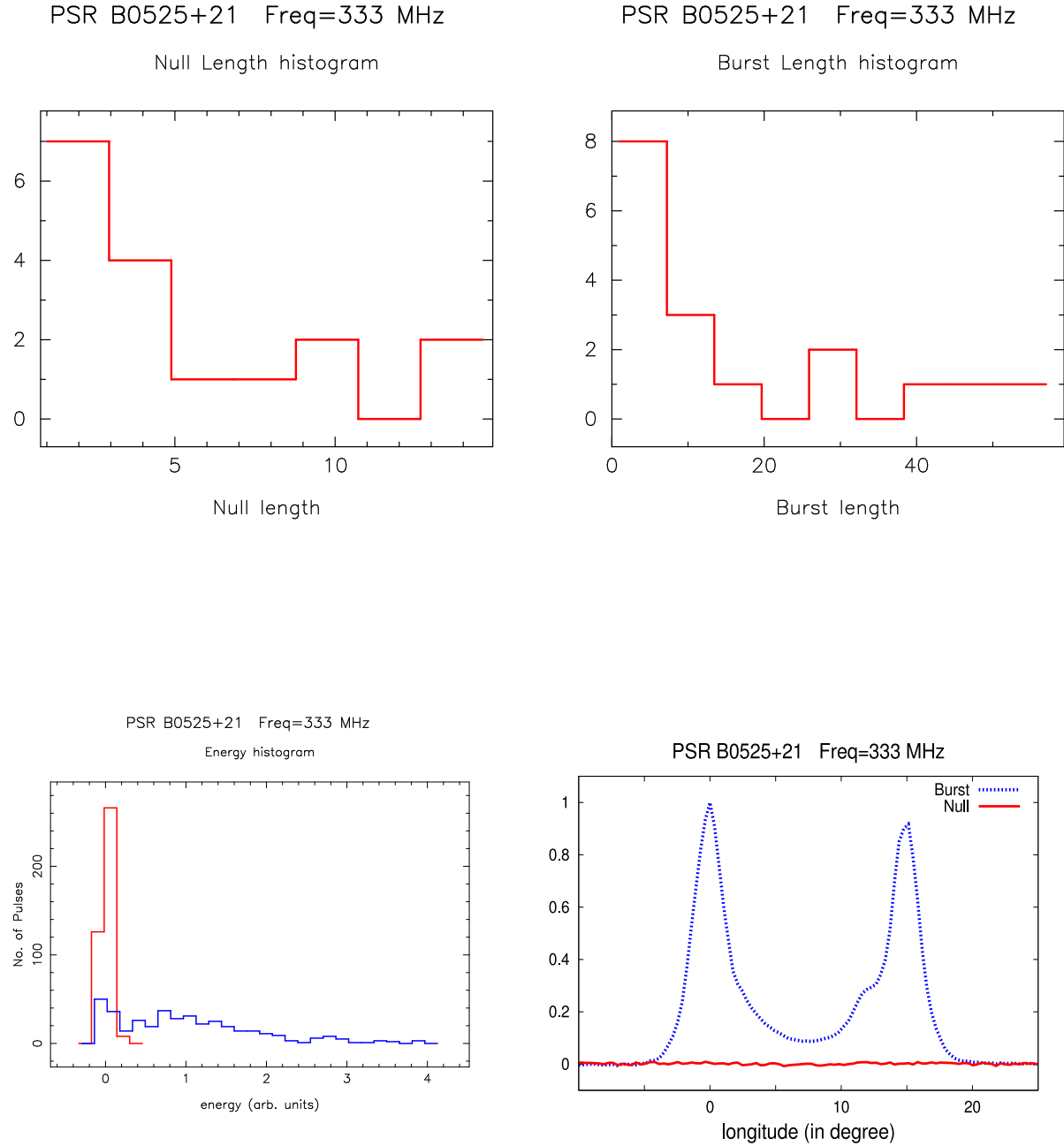


Fig. 8.— Null length histogram (top left); Burst length histogram (top right); the average energy distribution (bottom left) for on-pulse window (blue histogram) and off-pulse window (red histogram); the folded profile (bottom right) for the null pulses (red line, noise like characteristics) and burst pulses (blue line).

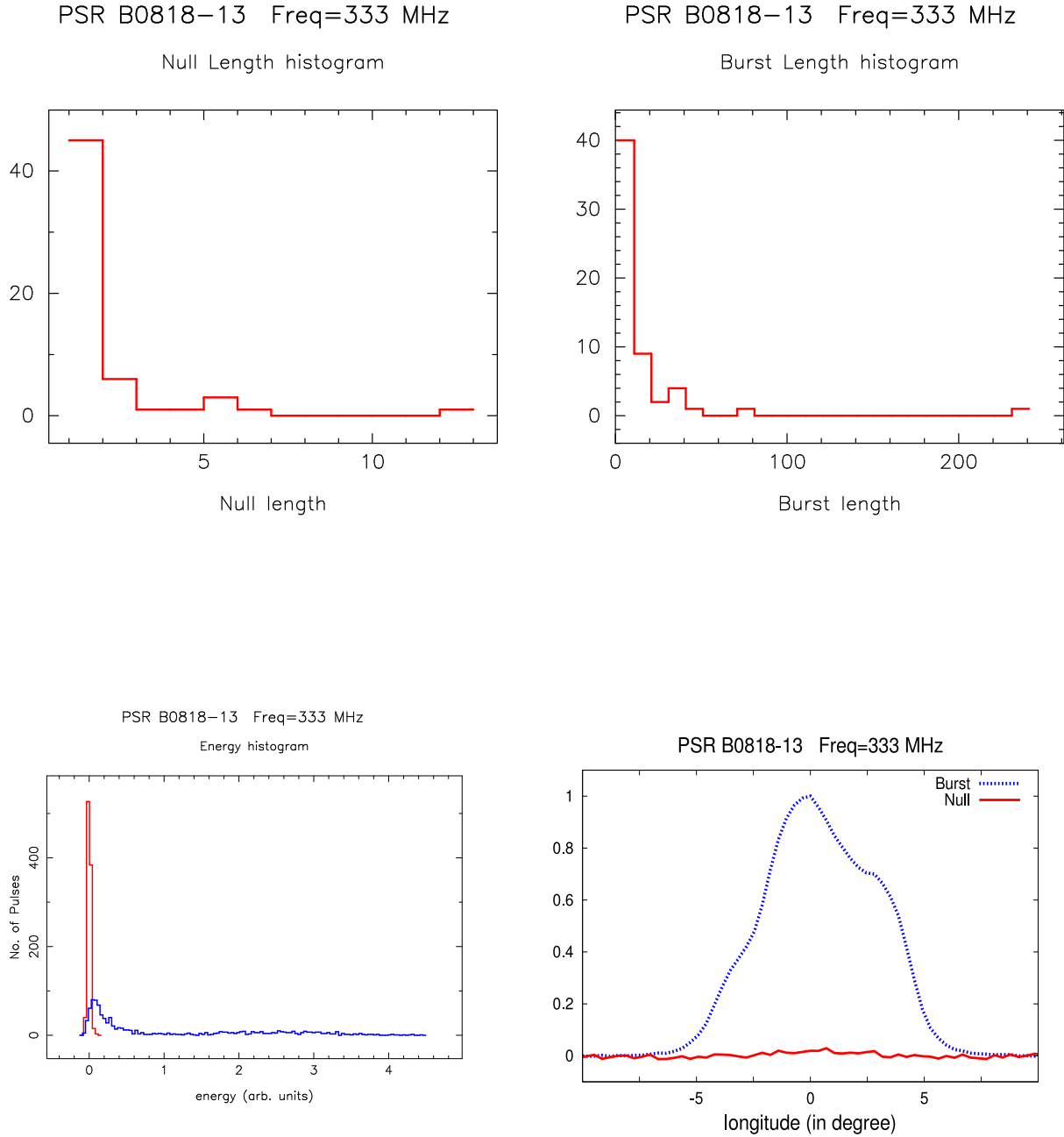
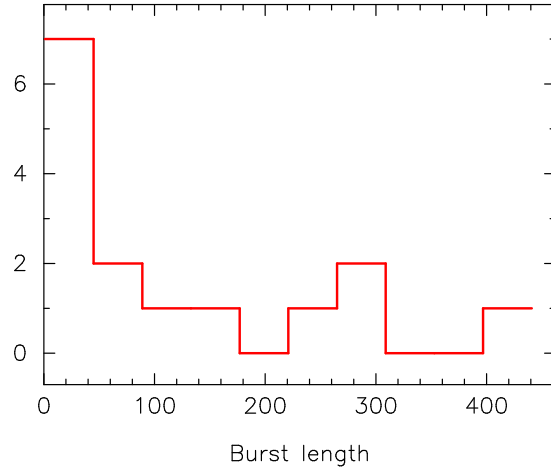


Fig. 9.— Null length histogram (top left); Burst length histogram (top right); the average energy distribution (bottom left) for on-pulse window (blue histogram) and off-pulse window (red histogram); the folded profile (bottom right) for the null pulses (red line, noise like characteristics) and burst pulses (blue line).

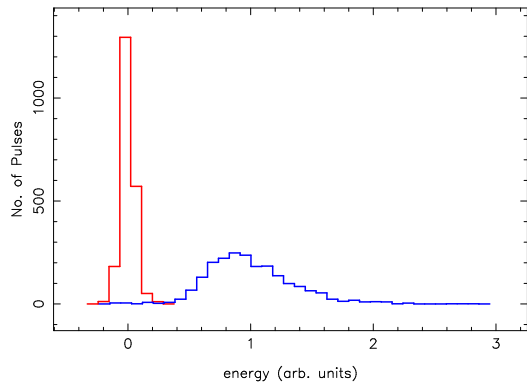
PSR B0818-13 Freq=618 MHz

Burst Length histogram



PSR B0818-13 Freq=618 MHz

Energy histogram



PSR B0818-13 Freq=618 MHz

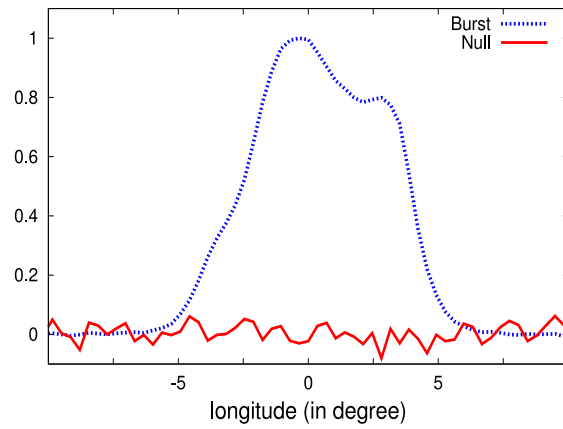
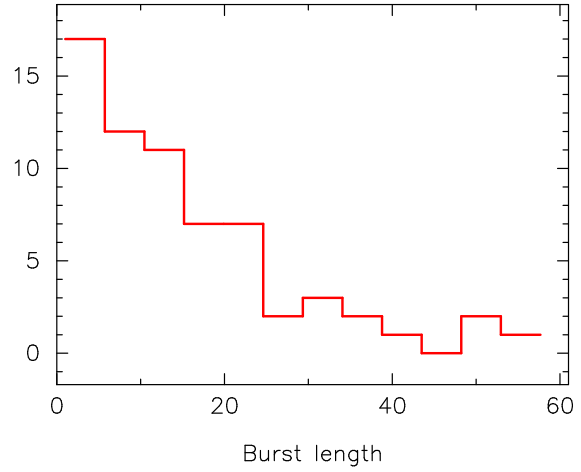


Fig. 10.— 15 single period nulls, no null length histogram; Burst length histogram (top right); the average energy distribution (bottom left) for on-pulse window (blue histogram) and off-pulse window (red histogram); the folded profile (bottom right) for the null pulses (red line, noise like characteristics) and burst pulses (blue line).

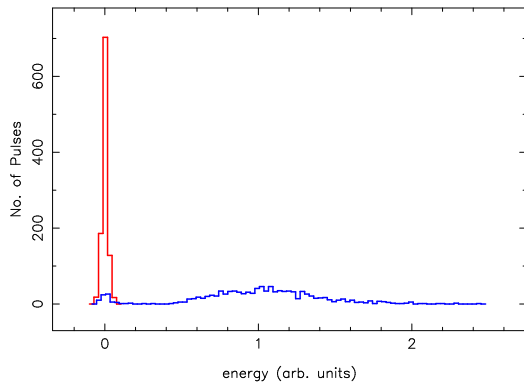
PSR B0834+06 Freq=333 MHz

Burst Length histogram



PSR B0834+06 Freq=333 MHz

Energy histogram



PSR B0834+06 Freq=333 MHz

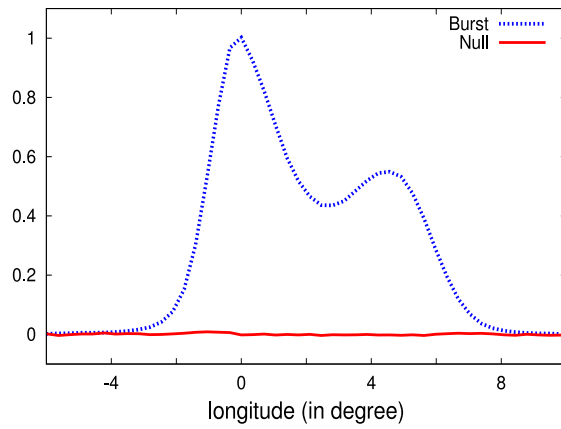


Fig. 11.— 64 single period nulls, no null length histogram; Burst length histogram (top right); the average energy distribution (bottom left) for on-pulse window (blue histogram) and off-pulse window (red histogram); the folded profile (bottom right) for the null pulses (red line, noise like characteristics) and burst pulses (blue line).

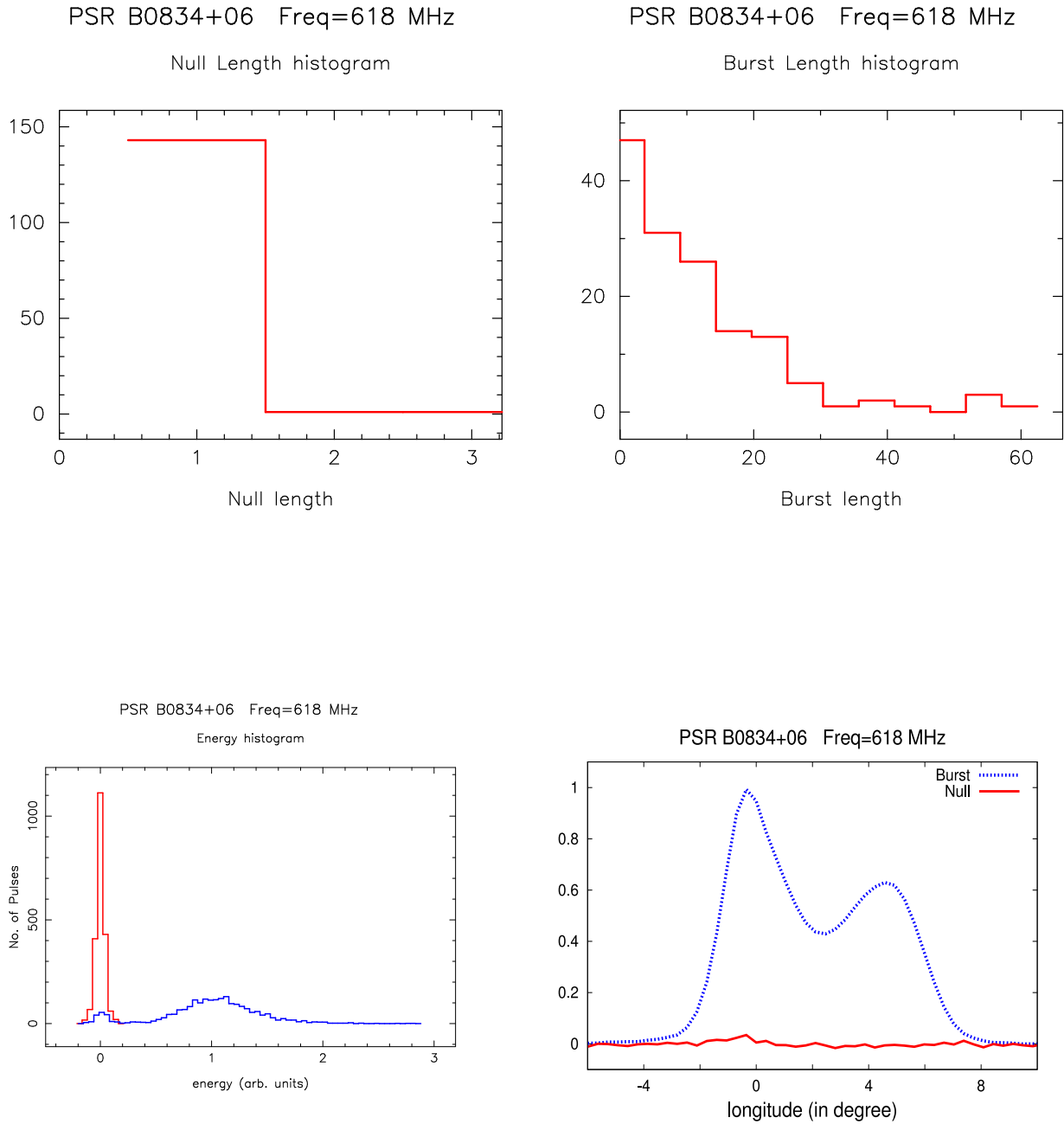


Fig. 12.— Null length histogram (top left); Burst length histogram (top right); the average energy distribution (bottom left) for on-pulse window (blue histogram) and off-pulse window (red histogram); the folded profile (bottom right) for the null pulses (red line, noise like characteristics) and burst pulses (blue line).

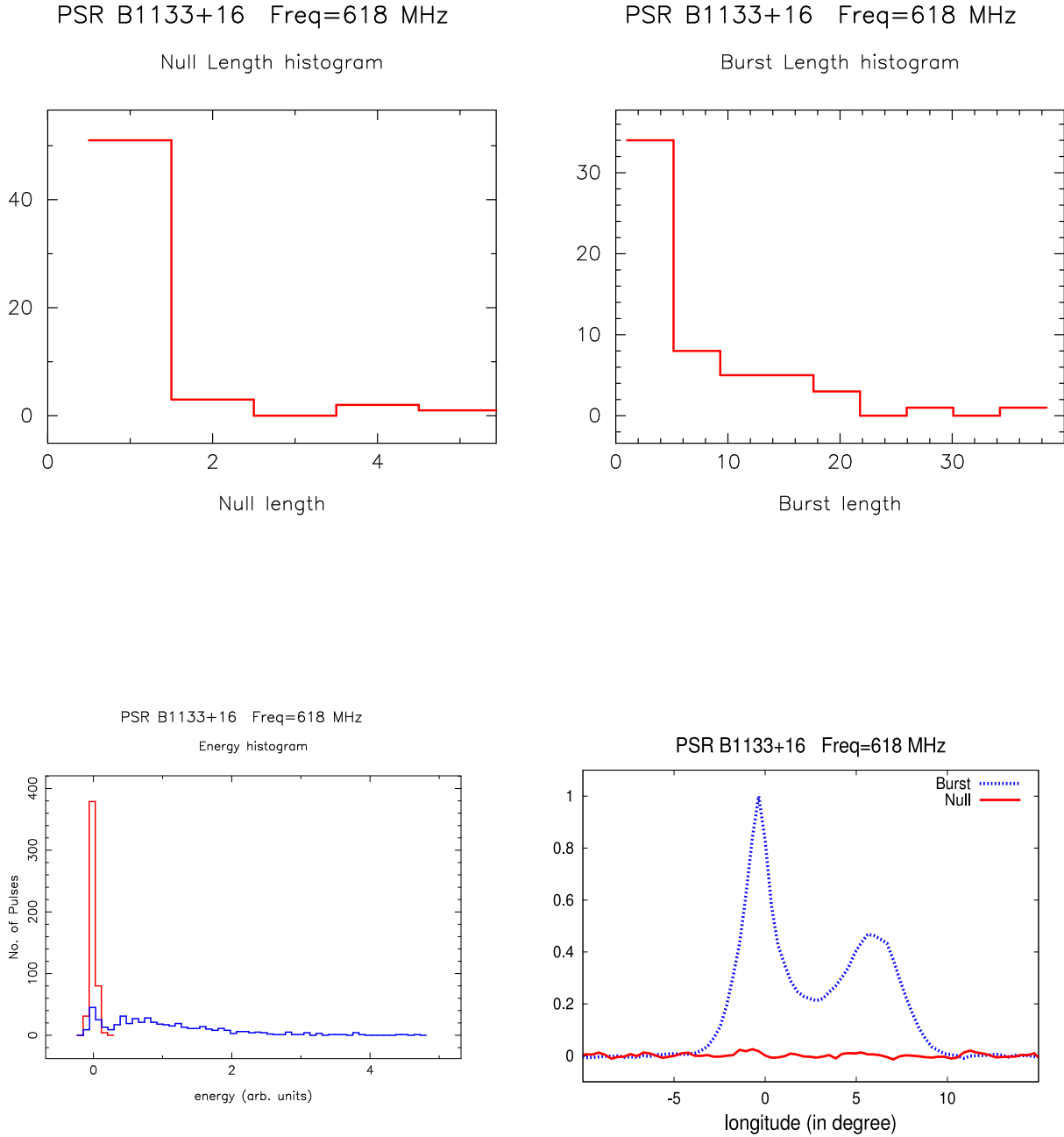


Fig. 13.— Null length histogram (top left); Burst length histogram (top right); the average energy distribution (bottom left) for on-pulse window (blue histogram) and off-pulse window (red histogram); the folded profile (bottom right) for the null pulses (red line, noise like characteristics) and burst pulses (blue line).

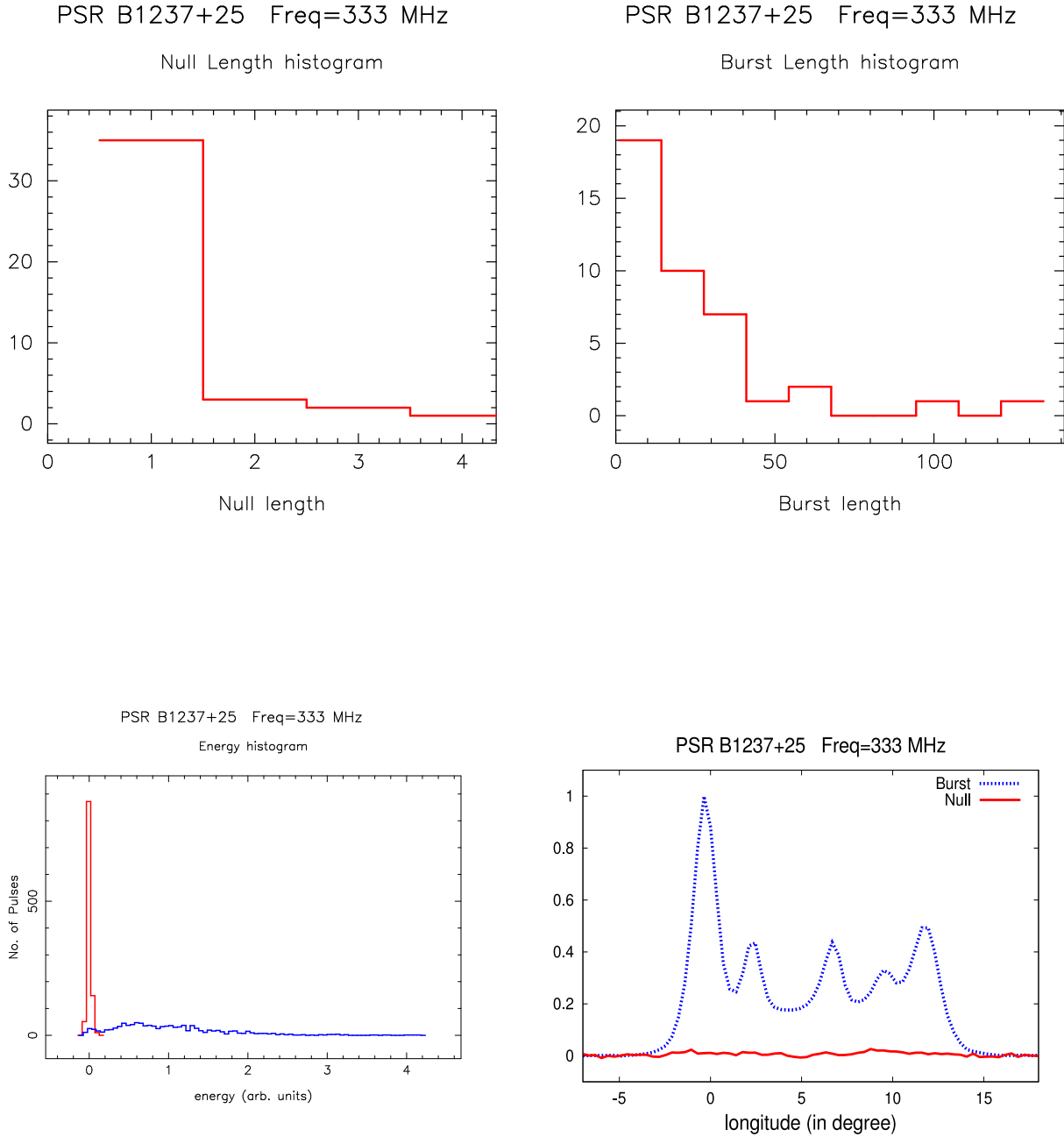


Fig. 14.— Null length histogram (top left); Burst length histogram (top right); the average energy distribution (bottom left) for on-pulse window (blue histogram) and off-pulse window (red histogram); the folded profile (bottom right) for the null pulses (red line, noise like characteristics) and burst pulses (blue line).

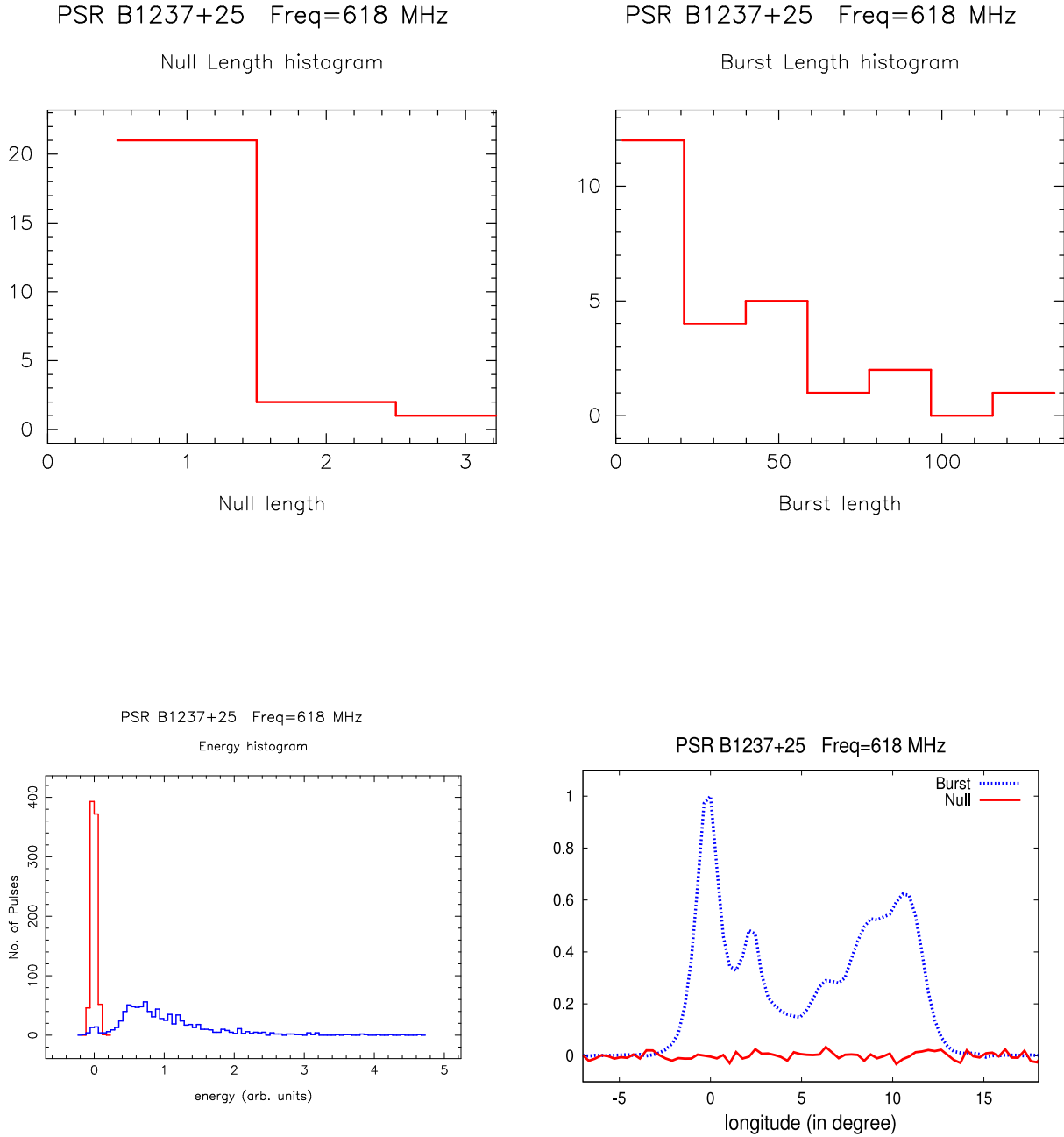


Fig. 15.— Null length histogram (top left); Burst length histogram (top right); the average energy distribution (bottom left) for on-pulse window (blue histogram) and off-pulse window (red histogram); the folded profile (bottom right) for the null pulses (red line, noise like characteristics) and burst pulses (blue line).

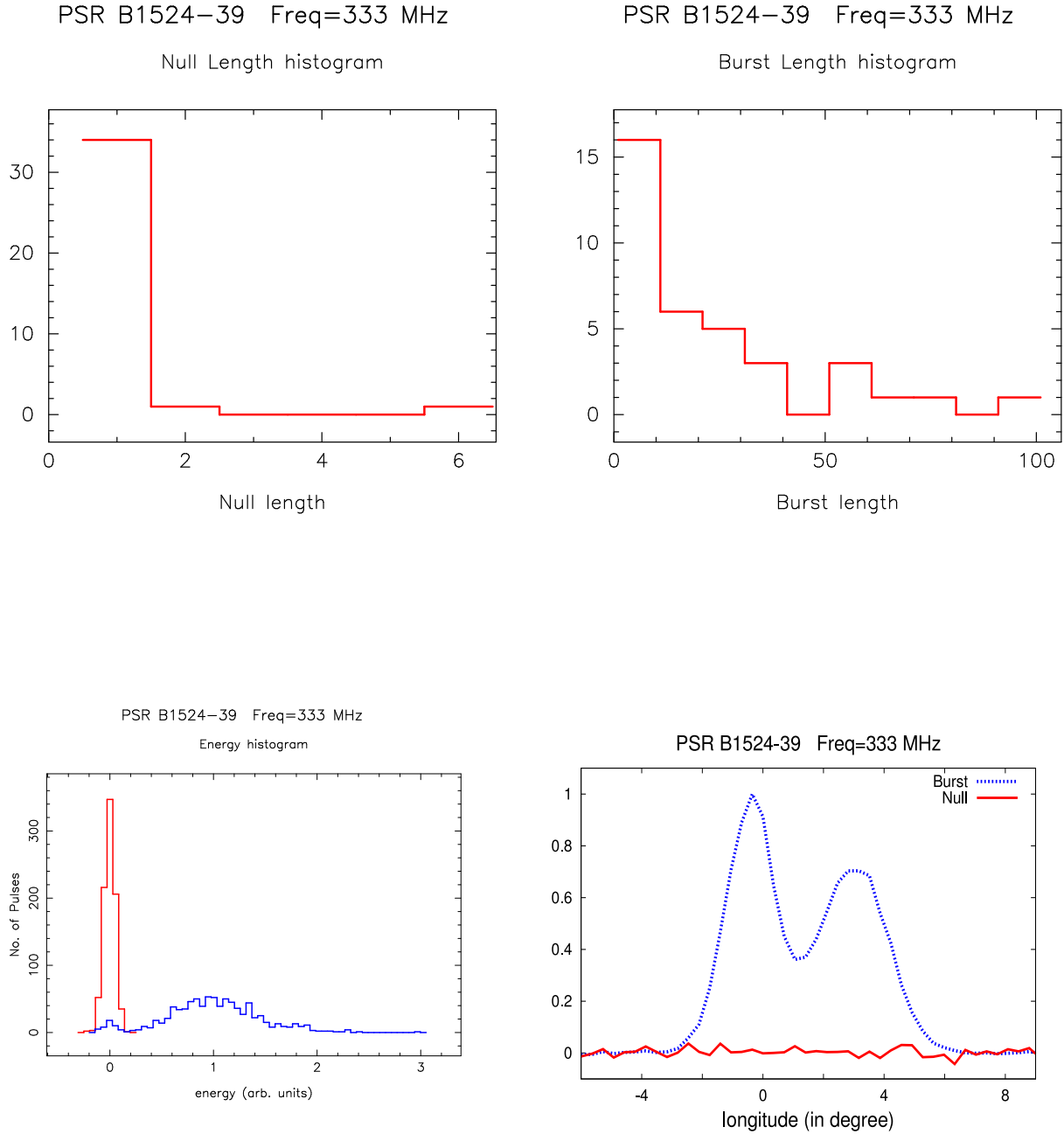


Fig. 16.— Null length histogram (top left); Burst length histogram (top right); the average energy distribution (bottom left) for on-pulse window (blue histogram) and off-pulse window (red histogram); the folded profile (bottom right) for the null pulses (red line, noise like characteristics) and burst pulses (blue line).

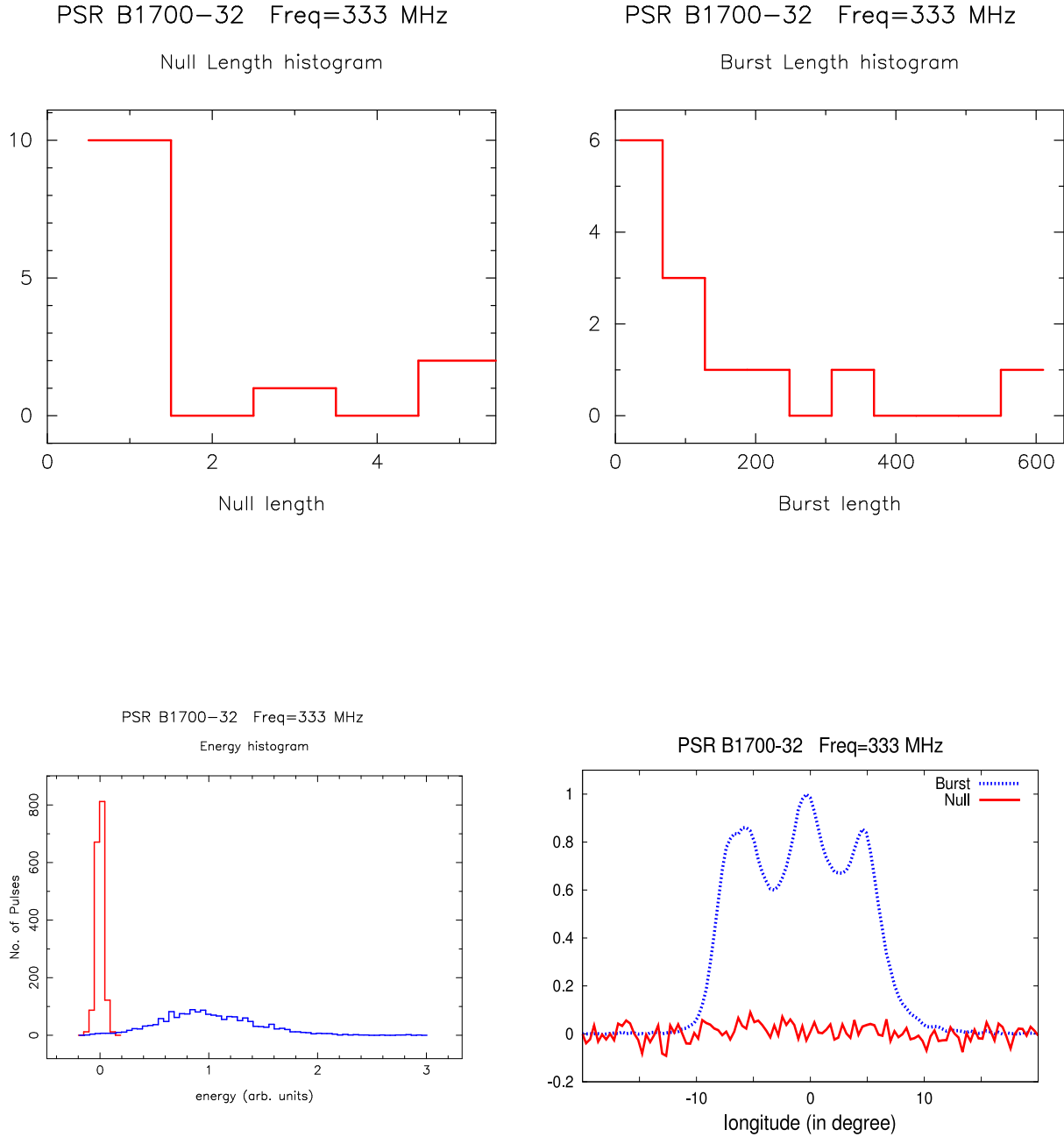


Fig. 17.— Null length histogram (top left); Burst length histogram (top right); the average energy distribution (bottom left) for on-pulse window (blue histogram) and off-pulse window (red histogram); the folded profile (bottom right) for the null pulses (red line, noise like characteristics) and burst pulses (blue line).

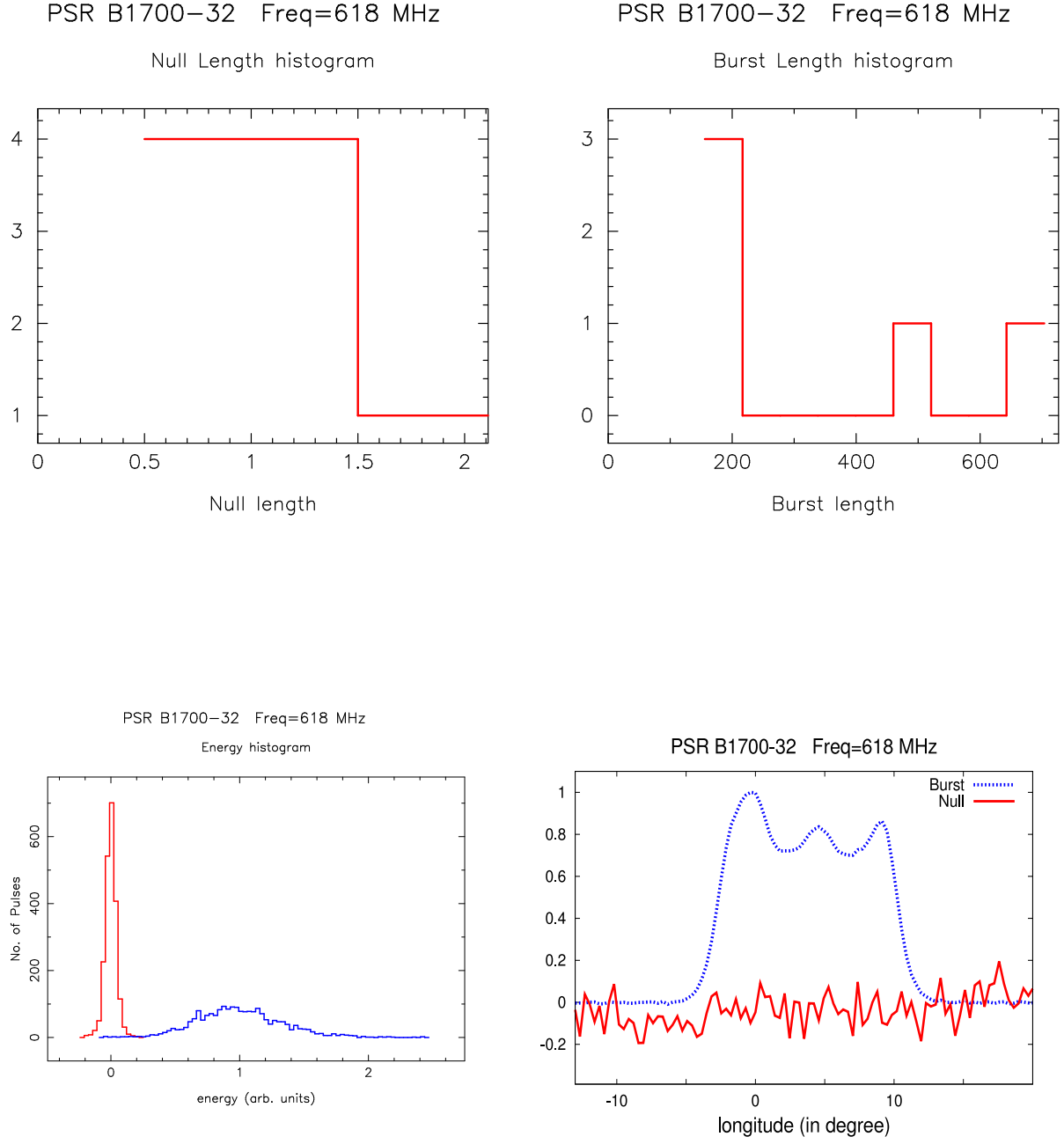


Fig. 18.— Null length histogram (top left); Burst length histogram (top right); the average energy distribution (bottom left) for on-pulse window (blue histogram) and off-pulse window (red histogram); the folded profile (bottom right) for the null pulses (red line, noise like characteristics) and burst pulses (blue line).

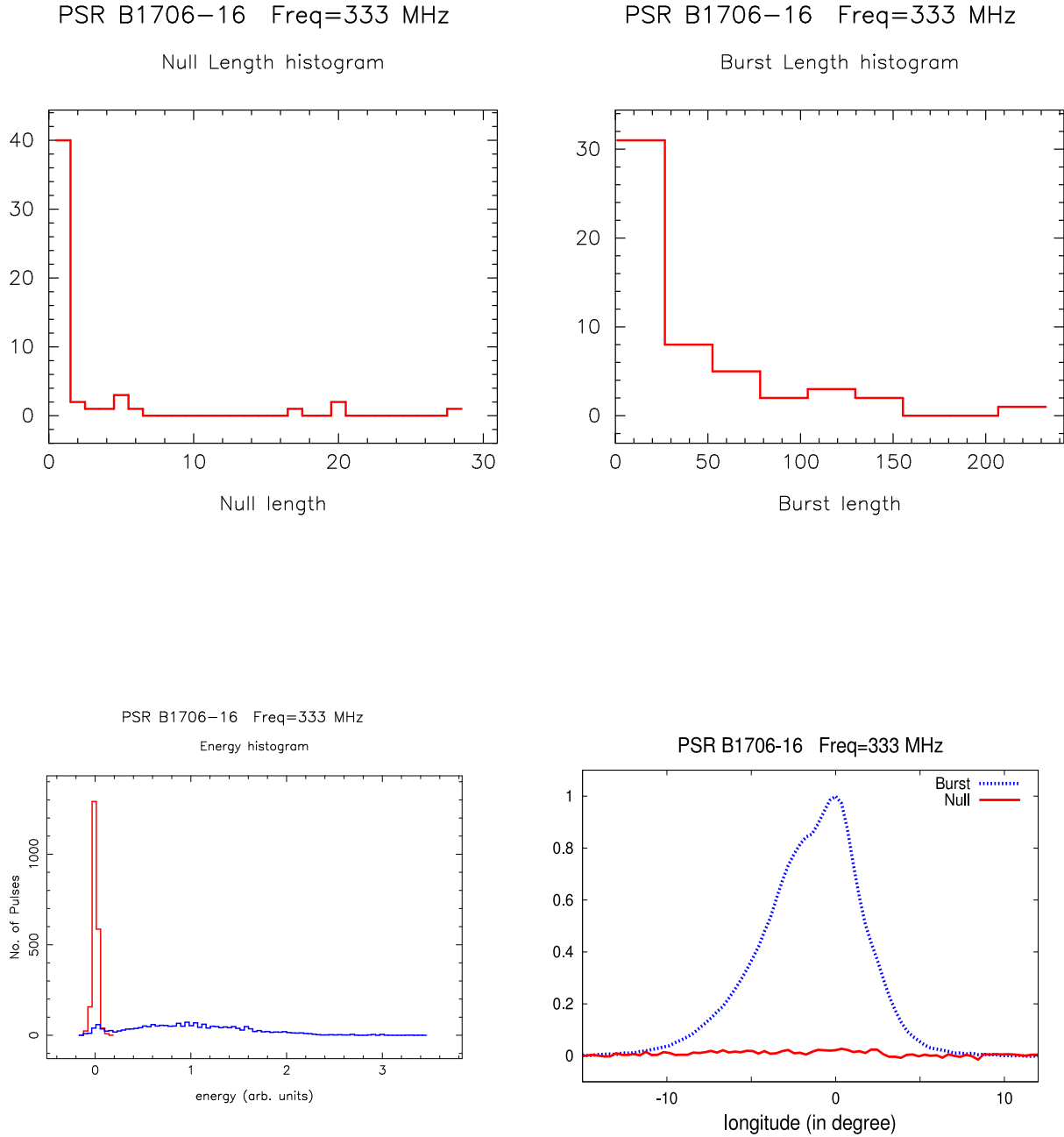


Fig. 19.— Null length histogram (top left); Burst length histogram (top right); the average energy distribution (bottom left) for on-pulse window (blue histogram) and off-pulse window (red histogram); the folded profile (bottom right) for the null pulses (red line, noise like characteristics) and burst pulses (blue line).

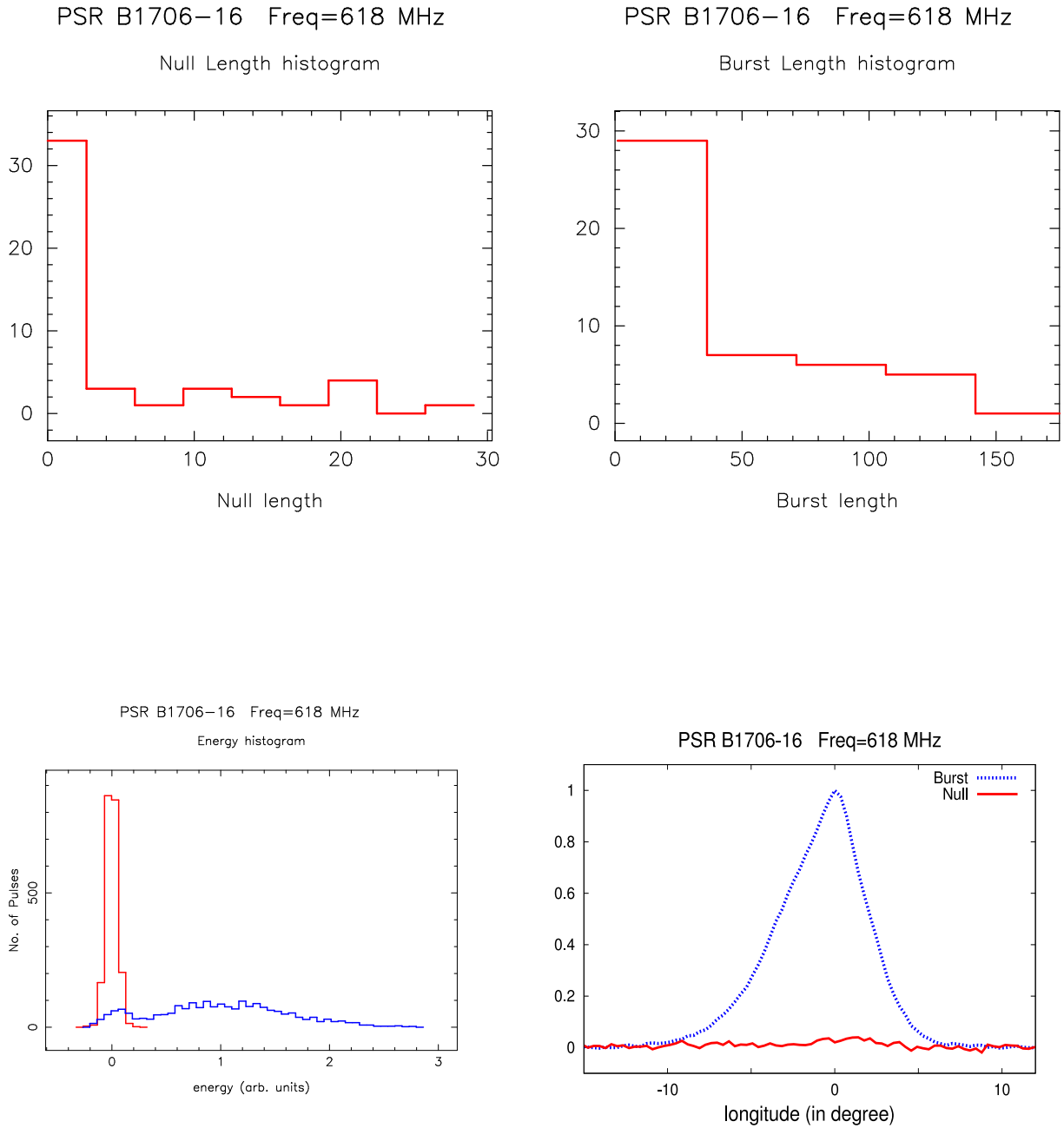


Fig. 20.— Null length histogram (top left); Burst length histogram (top right); the average energy distribution (bottom left) for on-pulse window (blue histogram) and off-pulse window (red histogram); the folded profile (bottom right) for the null pulses (red line, noise like characteristics) and burst pulses (blue line).

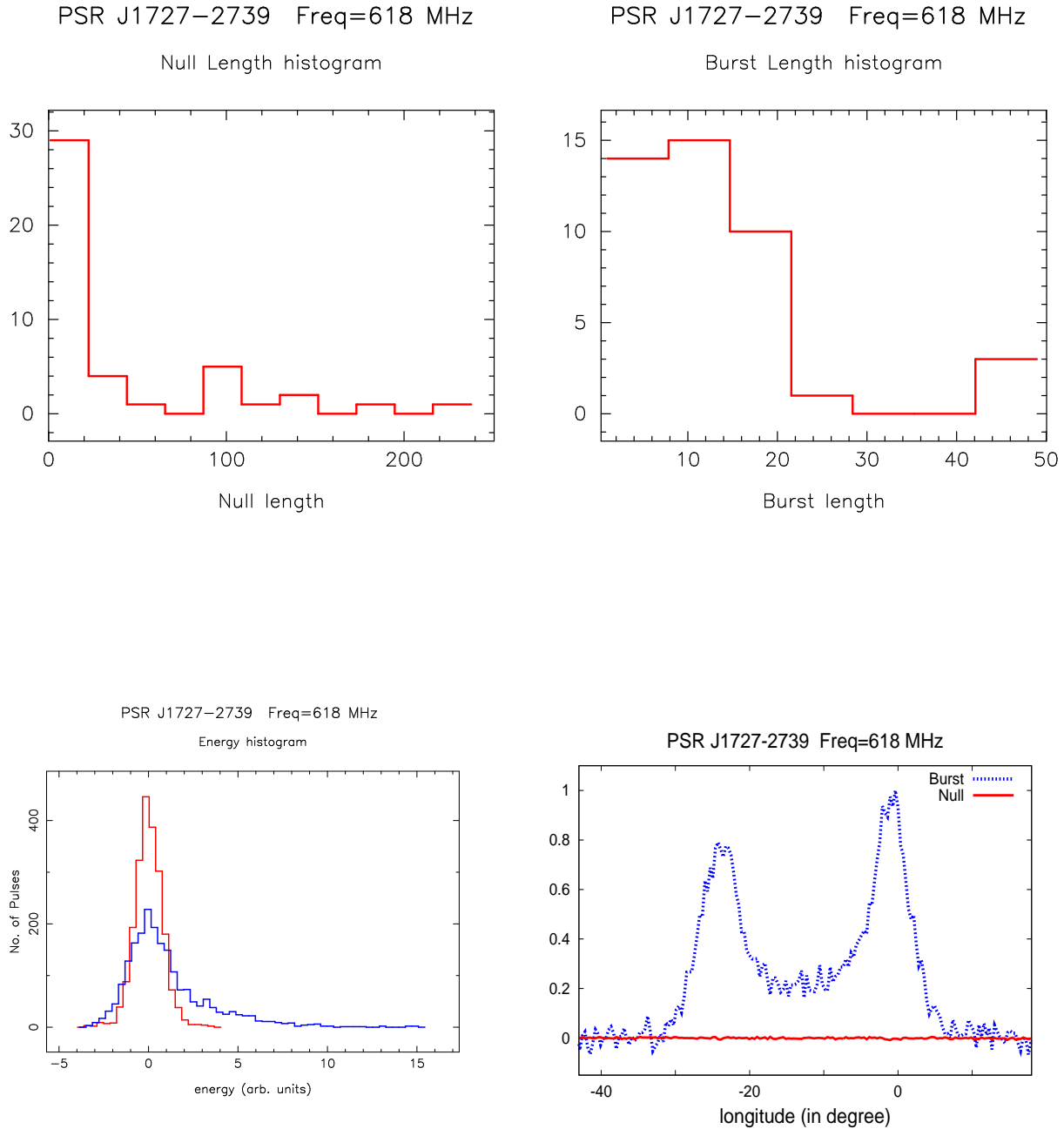


Fig. 21.— Null length histogram (top left); Burst length histogram (top right); the average energy distribution (bottom left) for on-pulse window (blue histogram) and off-pulse window (red histogram); the folded profile (bottom right) for the null pulses (red line, noise like characteristics) and burst pulses (blue line).

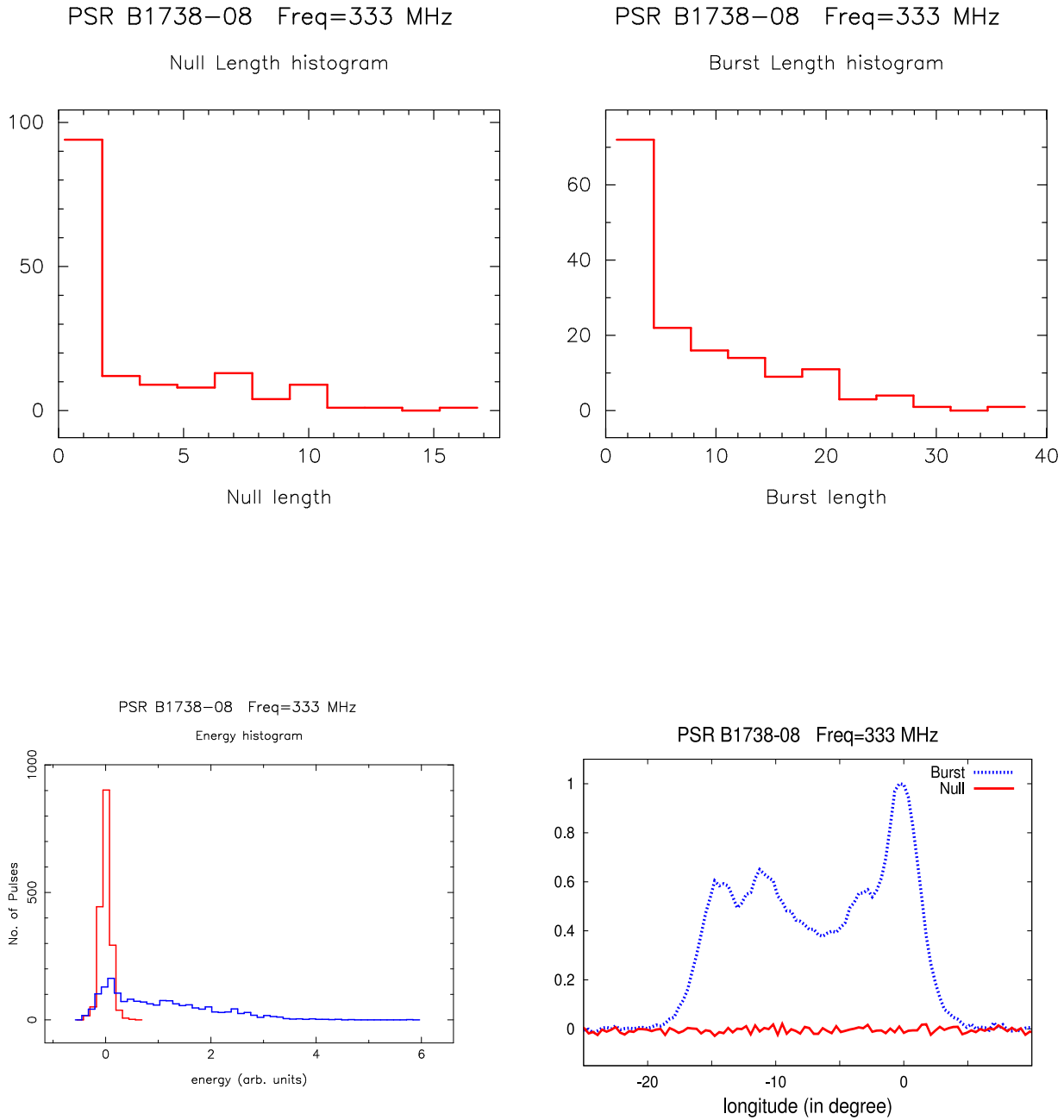


Fig. 22.— Null length histogram (top left); Burst length histogram (top right); the average energy distribution (bottom left) for on-pulse window (blue histogram) and off-pulse window (red histogram); the folded profile (bottom right) for the null pulses (red line, noise like characteristics) and burst pulses (blue line).

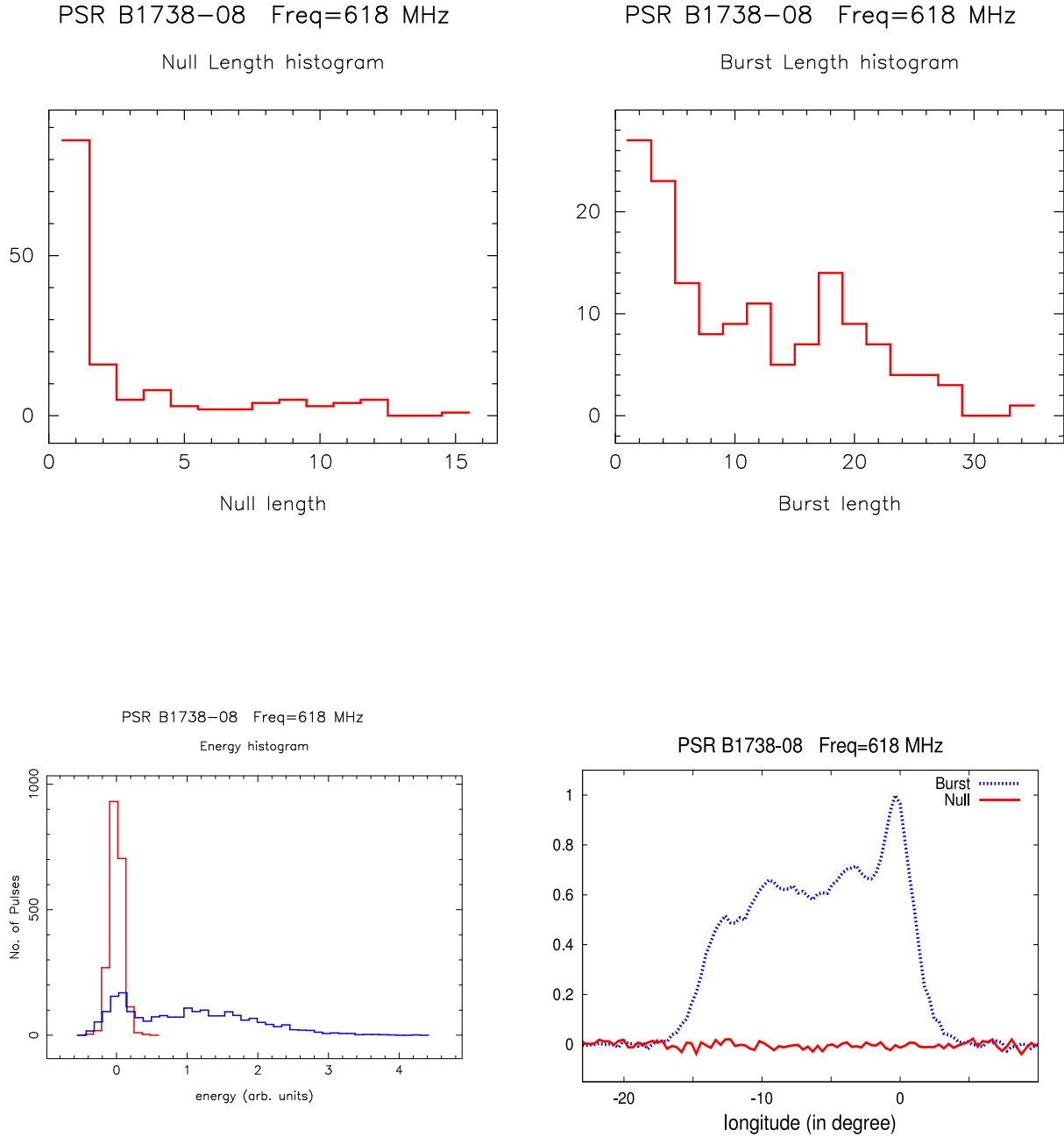
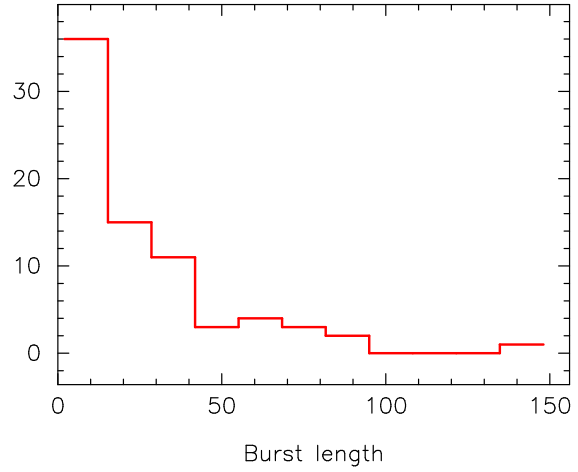


Fig. 23.— Null length histogram (top left); Burst length histogram (top right); the average energy distribution (bottom left) for on-pulse window (blue histogram) and off-pulse window (red histogram); the folded profile (bottom right) for the null pulses (red line, noise like characteristics) and burst pulses (blue line).

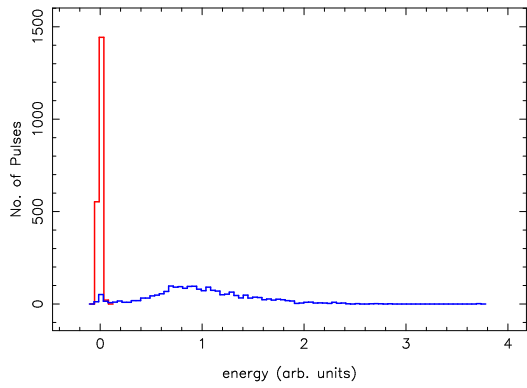
PSR B1747-46 Freq=333 MHz

Burst Length histogram



PSR B1747-46 Freq=333 MHz

Energy histogram



PSR B1747-46 Freq=333 MHz

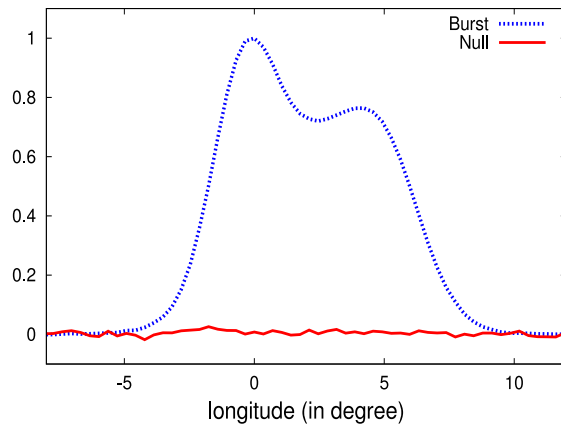
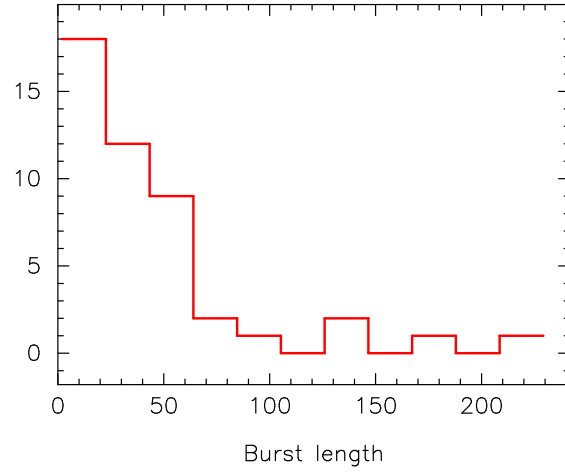


Fig. 24.— 75 single period nulls, no null length histogram; Burst length histogram (top right); the average energy distribution (bottom left) for on-pulse window (blue histogram) and off-pulse window (red histogram); the folded profile (bottom right) for the null pulses (red line, noise like characteristics) and burst pulses (blue line).

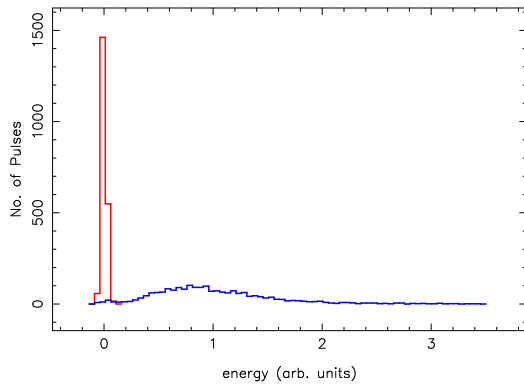
PSR B1747-46 Freq=618 MHz

Burst Length histogram



PSR B1747-46 Freq=618 MHz

Energy histogram



PSR B1747-46 Freq=618 MHz

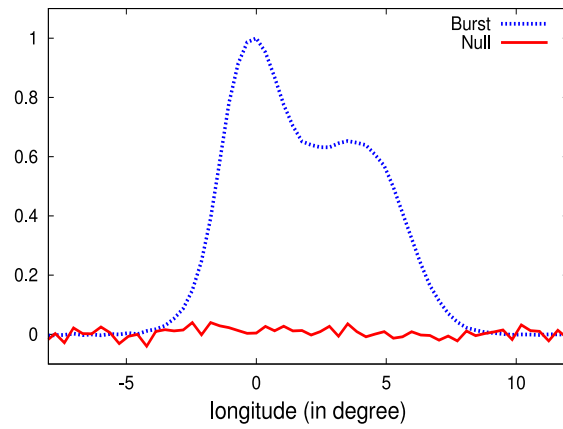
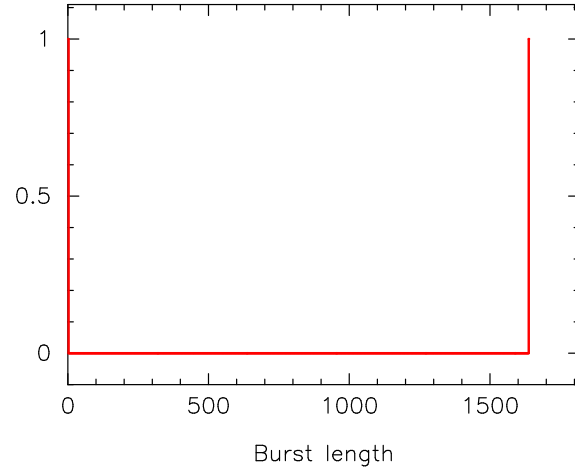


Fig. 25.— 46 single period nulls, no null length histogram; Burst length histogram (top right); the average energy distribution (bottom left) for on-pulse window (blue histogram) and off-pulse window (red histogram); the folded profile (bottom right) for the null pulses (red line, noise like characteristics) and burst pulses (blue line).

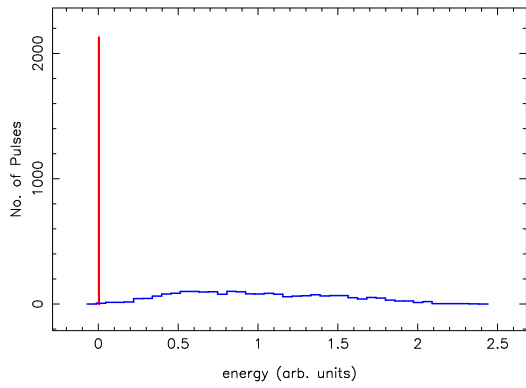
PSR B1749-28 Freq=333 MHz

Burst Length histogram



PSR B1749-28 Freq=333 MHz

Energy histogram



PSR B1749-28 Freq=333 MHz

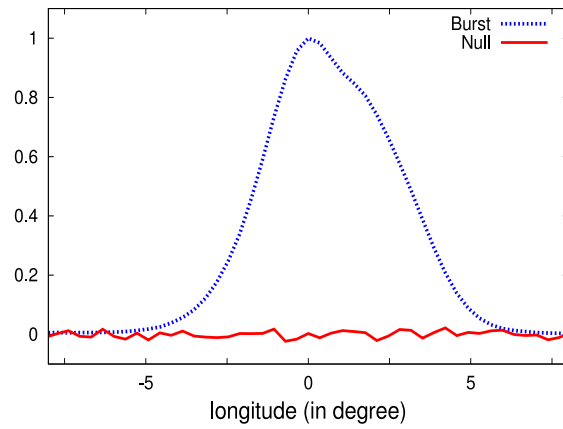


Fig. 26.— 2 two period nulls, no null length histogram; Burst length histogram (top right); the average energy distribution (bottom left) for on-pulse window (blue histogram) and off-pulse window (red histogram); the folded profile (bottom right) for the null pulses (red line, noise like characteristics) and burst pulses (blue line).

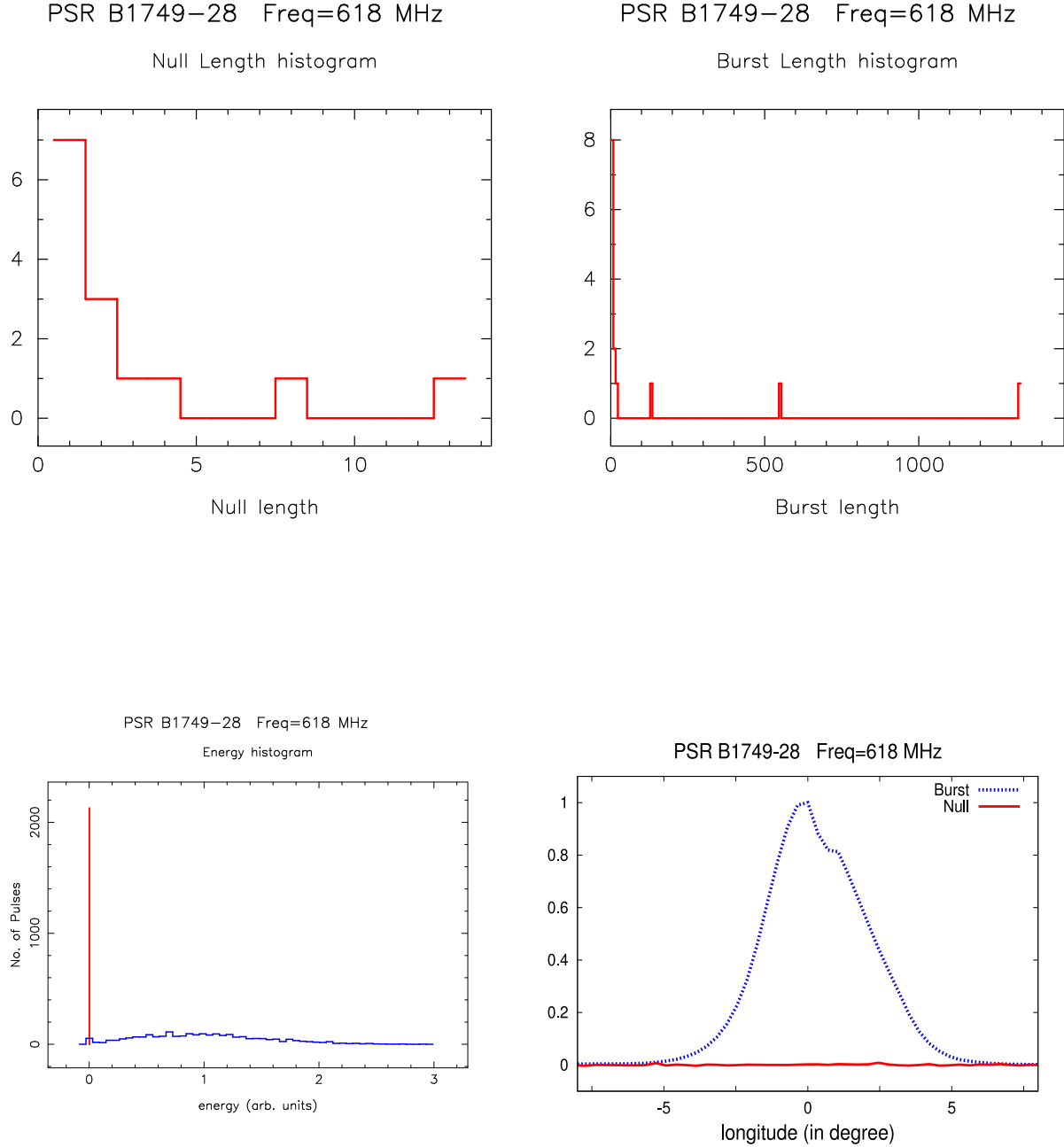
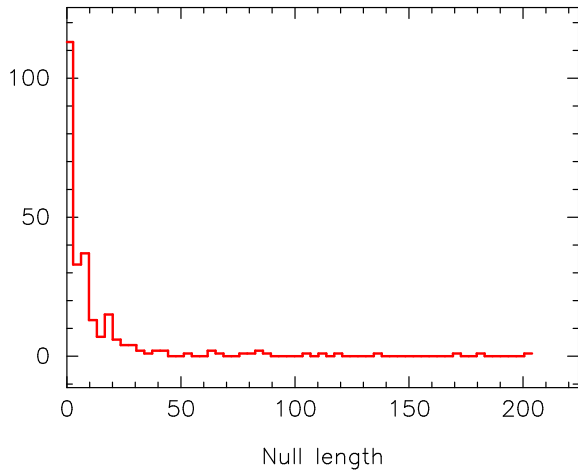


Fig. 27.— Null length histogram (top left); Burst length histogram (top right); the average energy distribution (bottom left) for on-pulse window (blue histogram) and off-pulse window (red histogram); the folded profile (bottom right) for the null pulses (red line, noise like characteristics) and burst pulses (blue line).

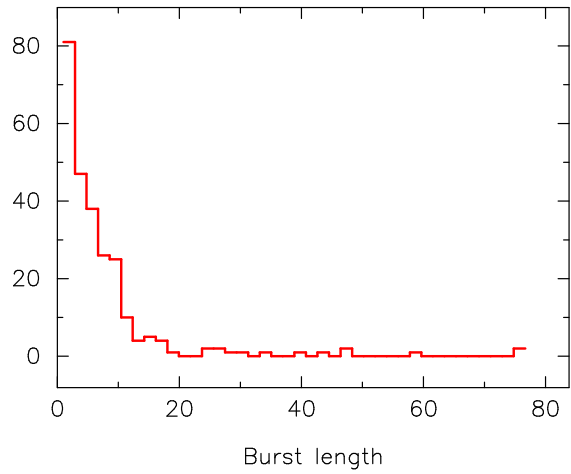
PSR B1944+17 Freq=333 MHz

Null Length histogram



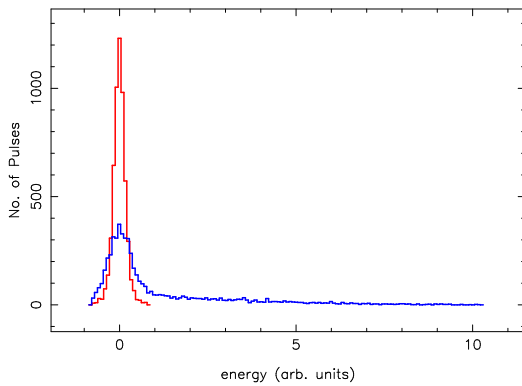
PSR B1944+17 Freq=333 MHz

Burst Length histogram



PSR B1944+17 Freq=333 MHz

Energy histogram



PSR B1944+17 Freq=333 MHz

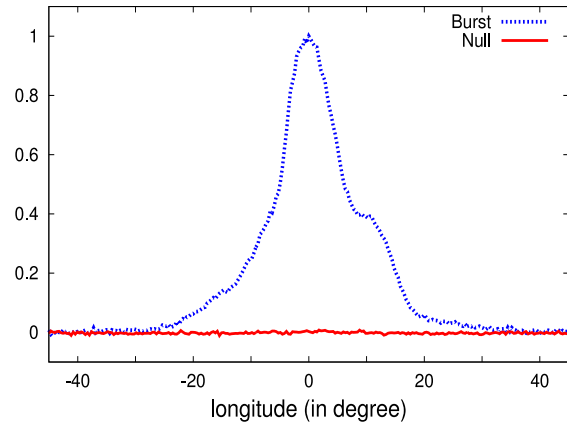


Fig. 28.— Null length histogram (top left); Burst length histogram (top right); the average energy distribution (bottom left) for on-pulse window (blue histogram) and off-pulse window (red histogram); the folded profile (bottom right) for the null pulses (red line, noise like characteristics) and burst pulses (blue line).

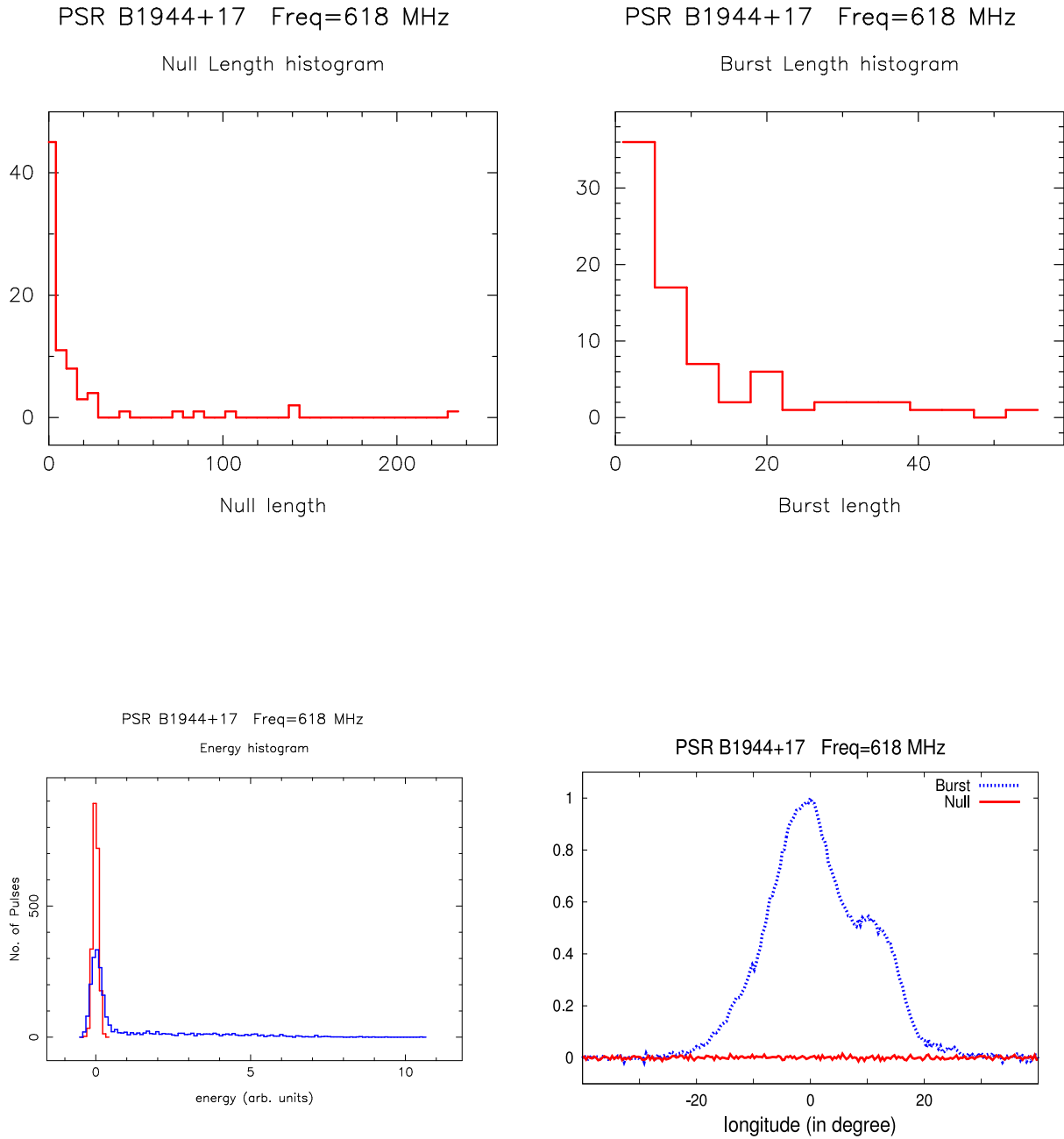


Fig. 29.— Null length histogram (top left); Burst length histogram (top right); the average energy distribution (bottom left) for on-pulse window (blue histogram) and off-pulse window (red histogram); the folded profile (bottom right) for the null pulses (red line, noise like characteristics) and burst pulses (blue line).

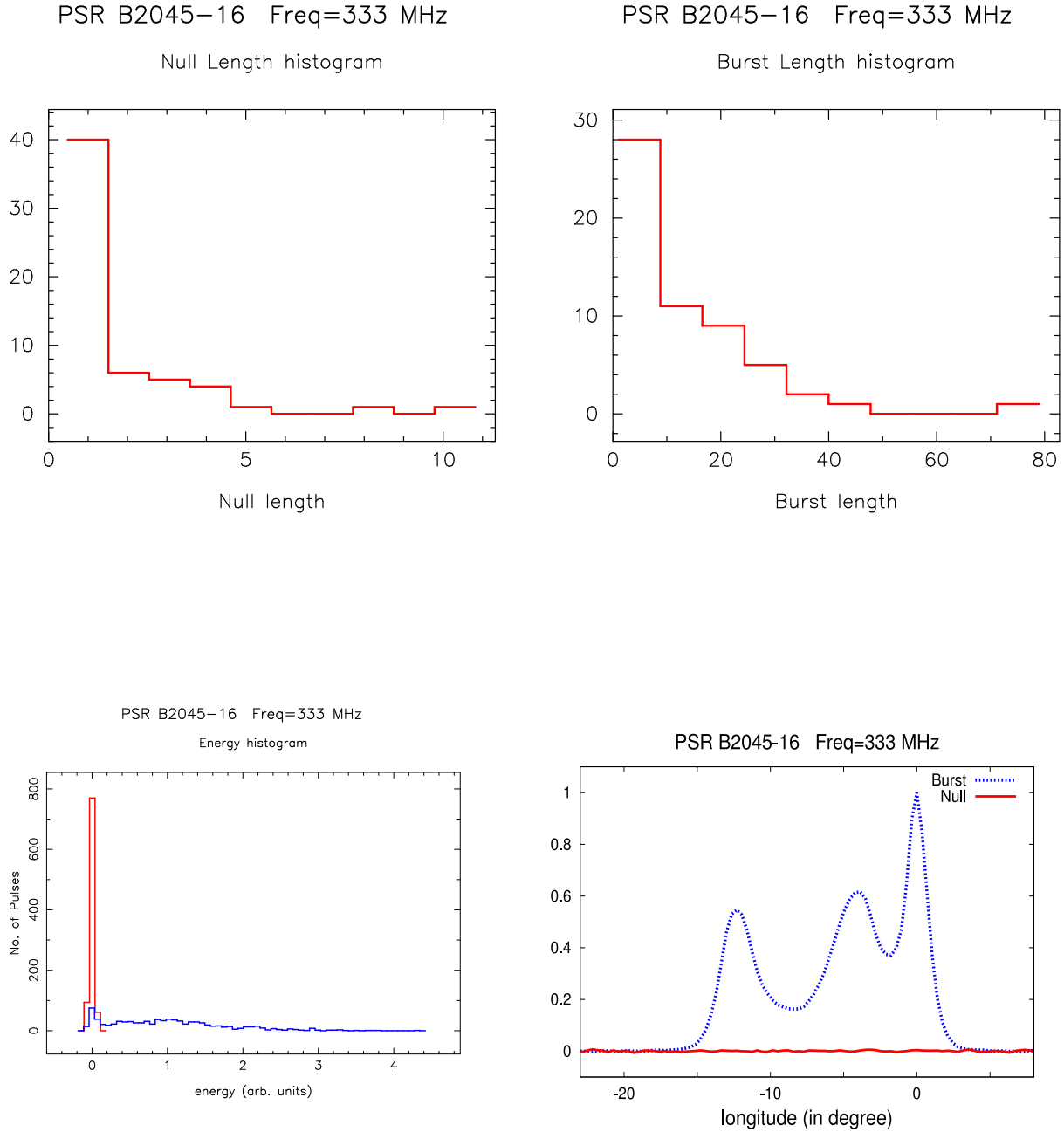


Fig. 30.— Null length histogram (top left); Burst length histogram (top right); the average energy distribution (bottom left) for on-pulse window (blue histogram) and off-pulse window (red histogram); the folded profile (bottom right) for the null pulses (red line, noise like characteristics) and burst pulses (blue line).

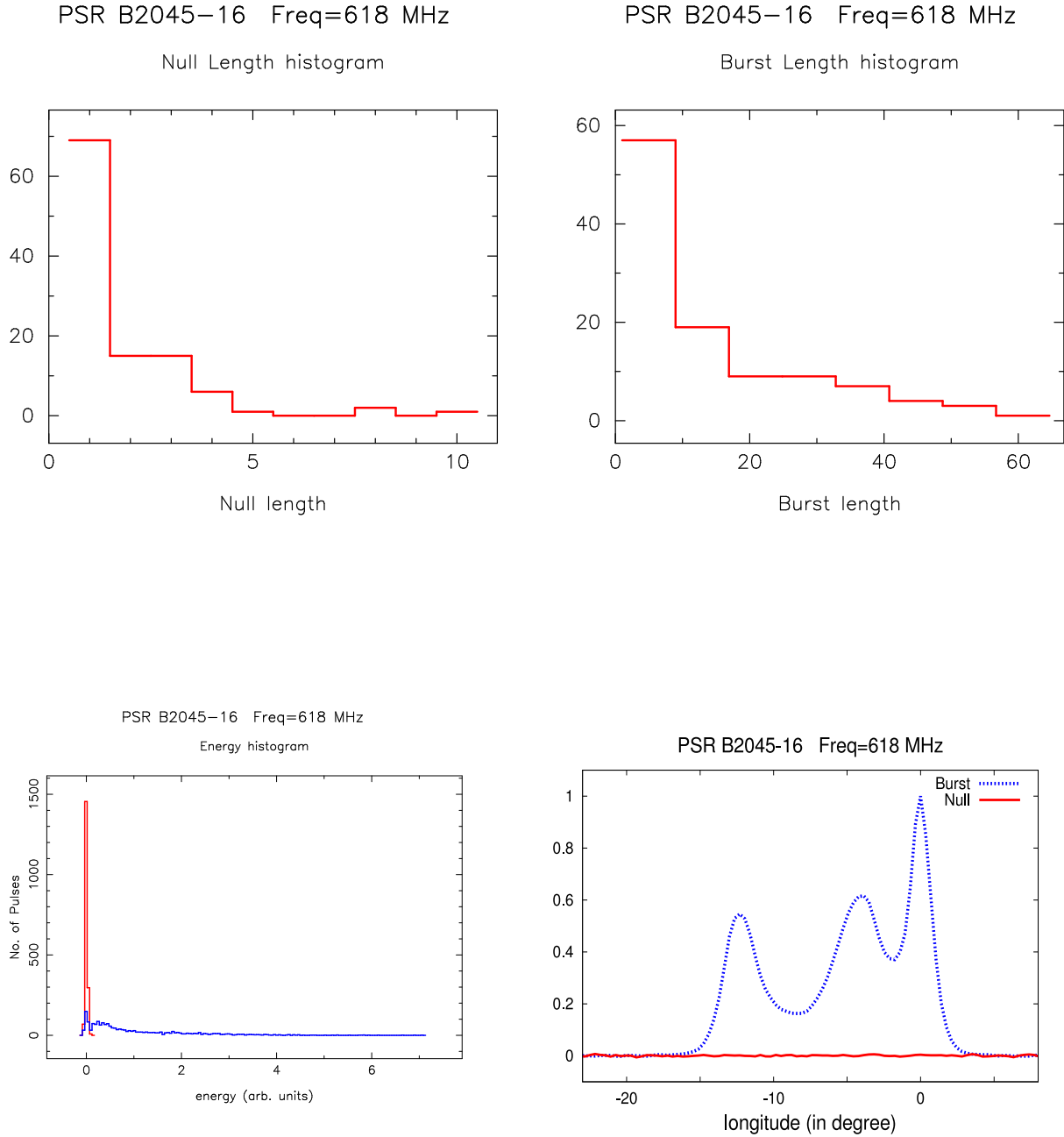


Fig. 31.— Null length histogram (top left); Burst length histogram (top right); the average energy distribution (bottom left) for on-pulse window (blue histogram) and off-pulse window (red histogram); the folded profile (bottom right) for the null pulses (red line, noise like characteristics) and burst pulses (blue line).

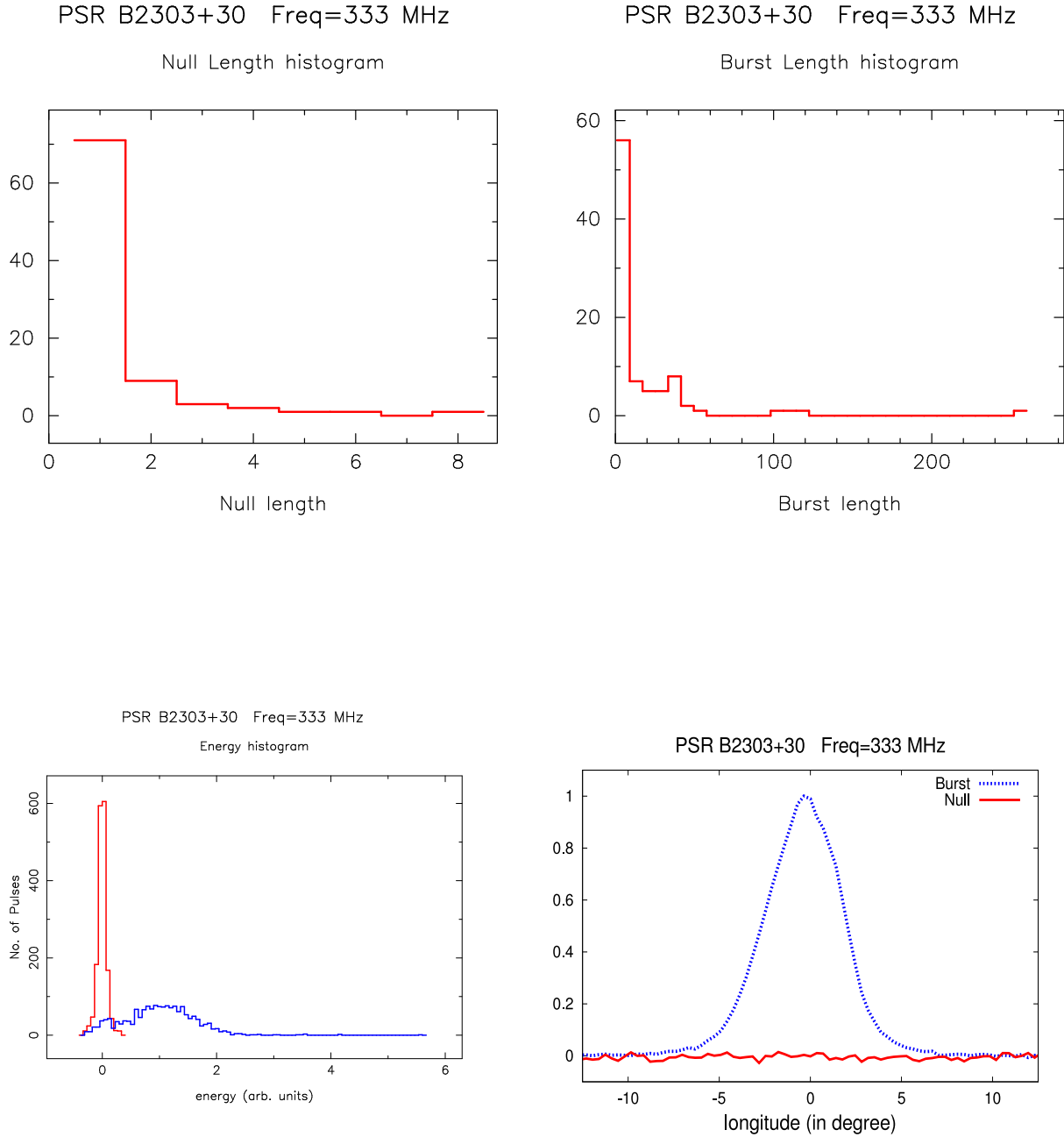


Fig. 32.— Null length histogram (top left); Burst length histogram (top right); the average energy distribution (bottom left) for on-pulse window (blue histogram) and off-pulse window (red histogram); the folded profile (bottom right) for the null pulses (red line, noise like characteristics) and burst pulses (blue line).

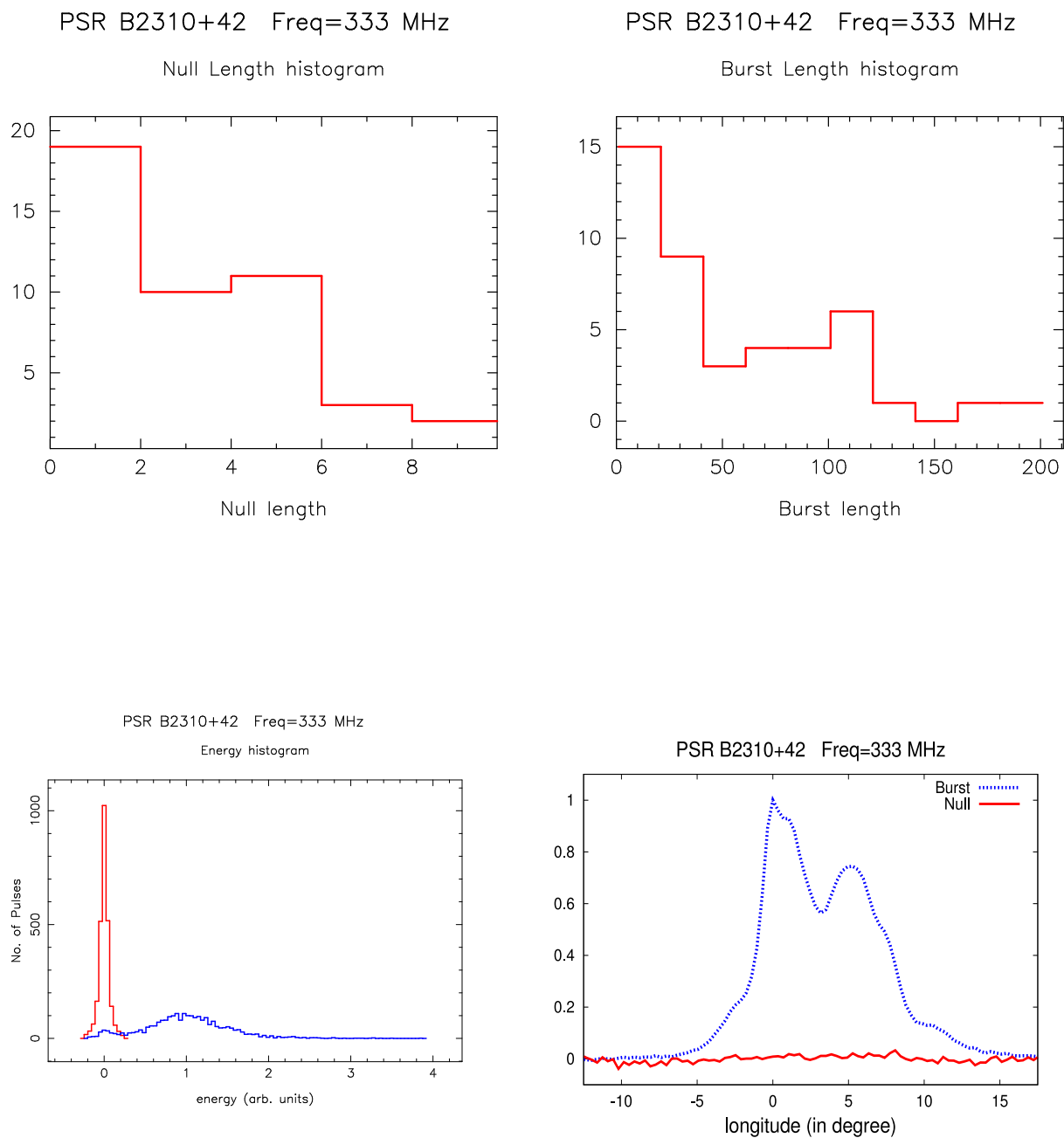


Fig. 33.— Null length histogram (top left); Burst length histogram (top right); the average energy distribution (bottom left) for on-pulse window (blue histogram) and off-pulse window (red histogram); the folded profile (bottom right) for the null pulses (red line, noise like characteristics) and burst pulses (blue line).

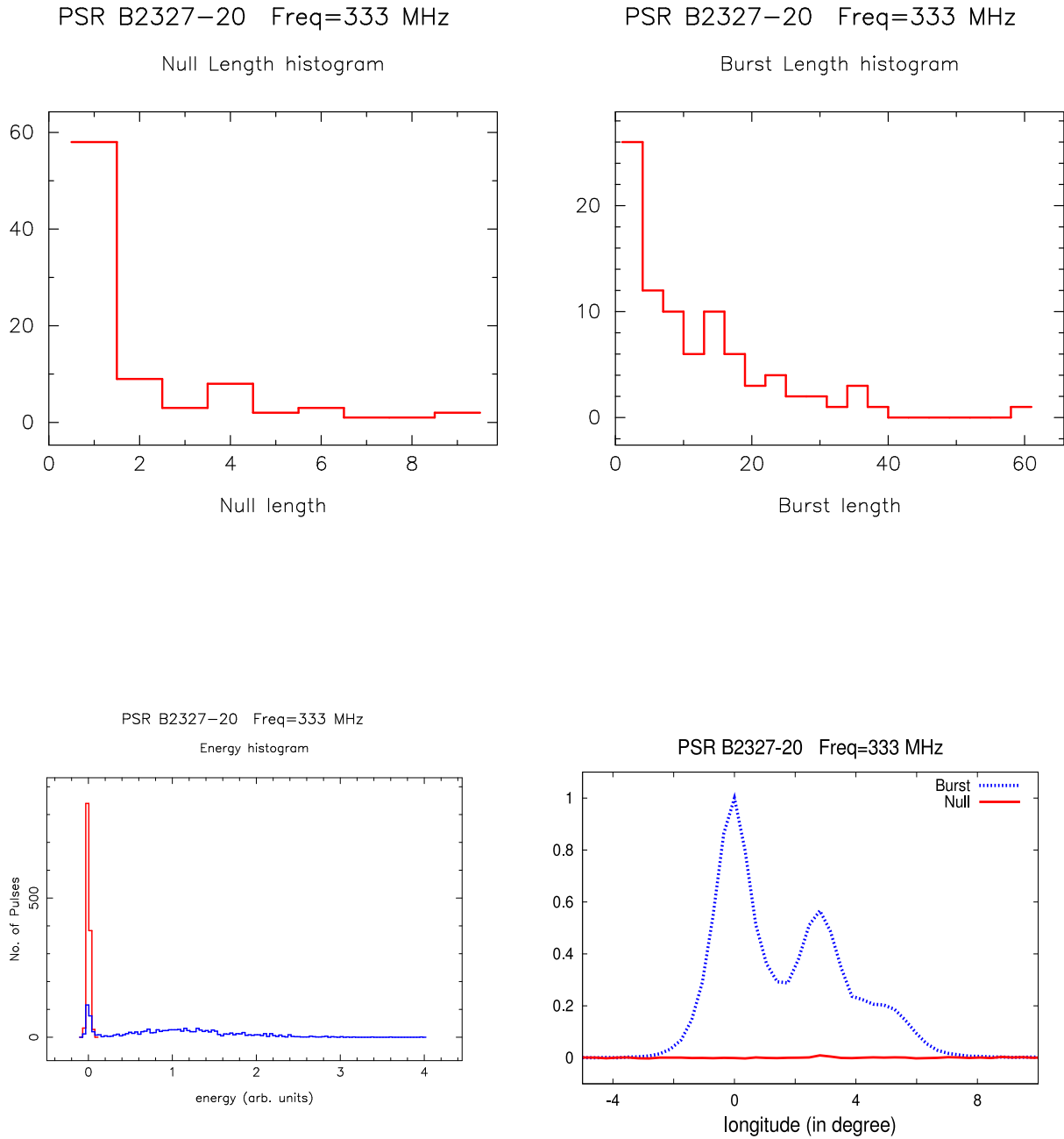


Fig. 34.— Null length histogram (top left); Burst length histogram (top right); the average energy distribution (bottom left) for on-pulse window (blue histogram) and off-pulse window (red histogram); the folded profile (bottom right) for the null pulses (red line, noise like characteristics) and burst pulses (blue line).

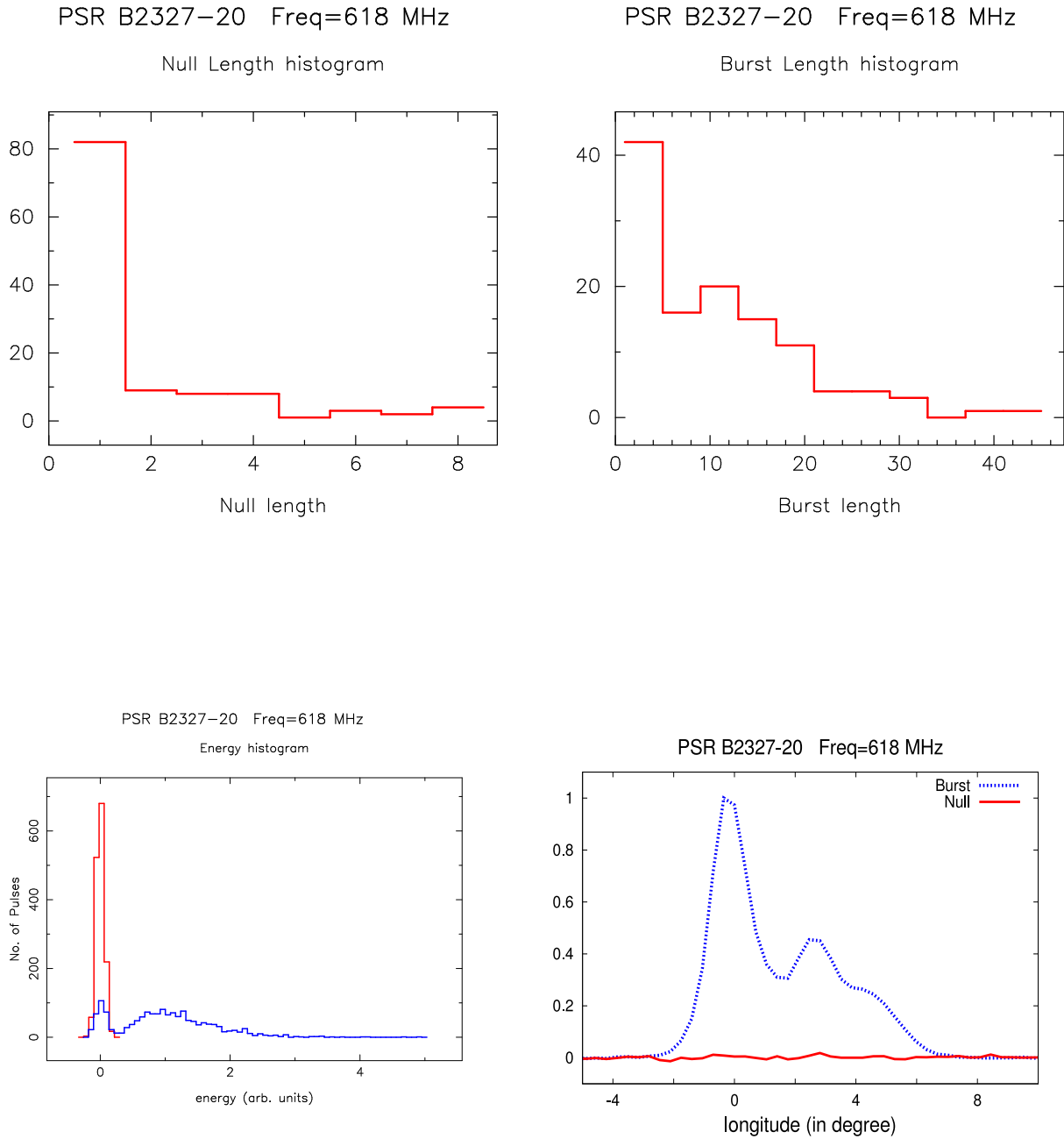


Fig. 35.— Null length histogram (top left); Burst length histogram (top right); the average energy distribution (bottom left) for on-pulse window (blue histogram) and off-pulse window (red histogram); the folded profile (bottom right) for the null pulses (red line, noise like characteristics) and burst pulses (blue line).

- C. The plots detailing the Fourier transform analysis to estimate the nulling periodicity.

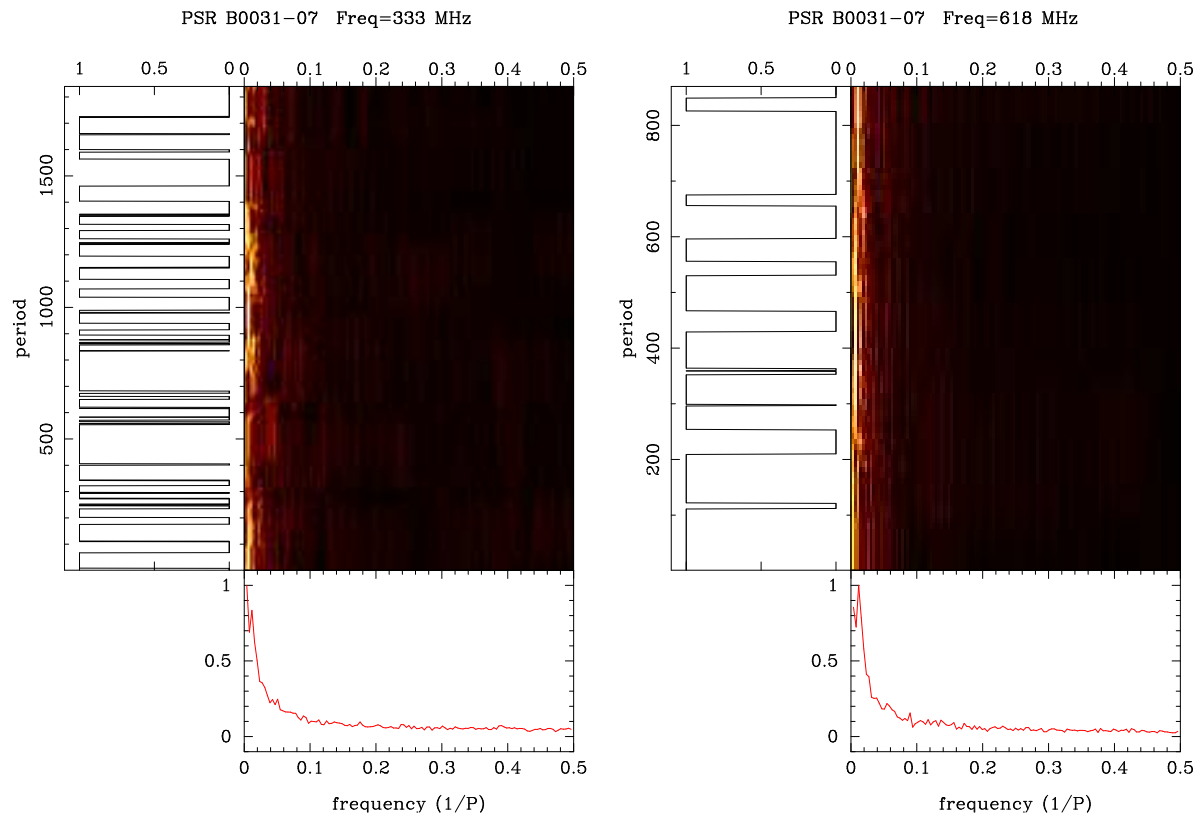


Fig. 36.— The figure shows the time varying Fourier transform of the null/burst time series data at 333 MHz (left panel) and 618 MHz (right panel).

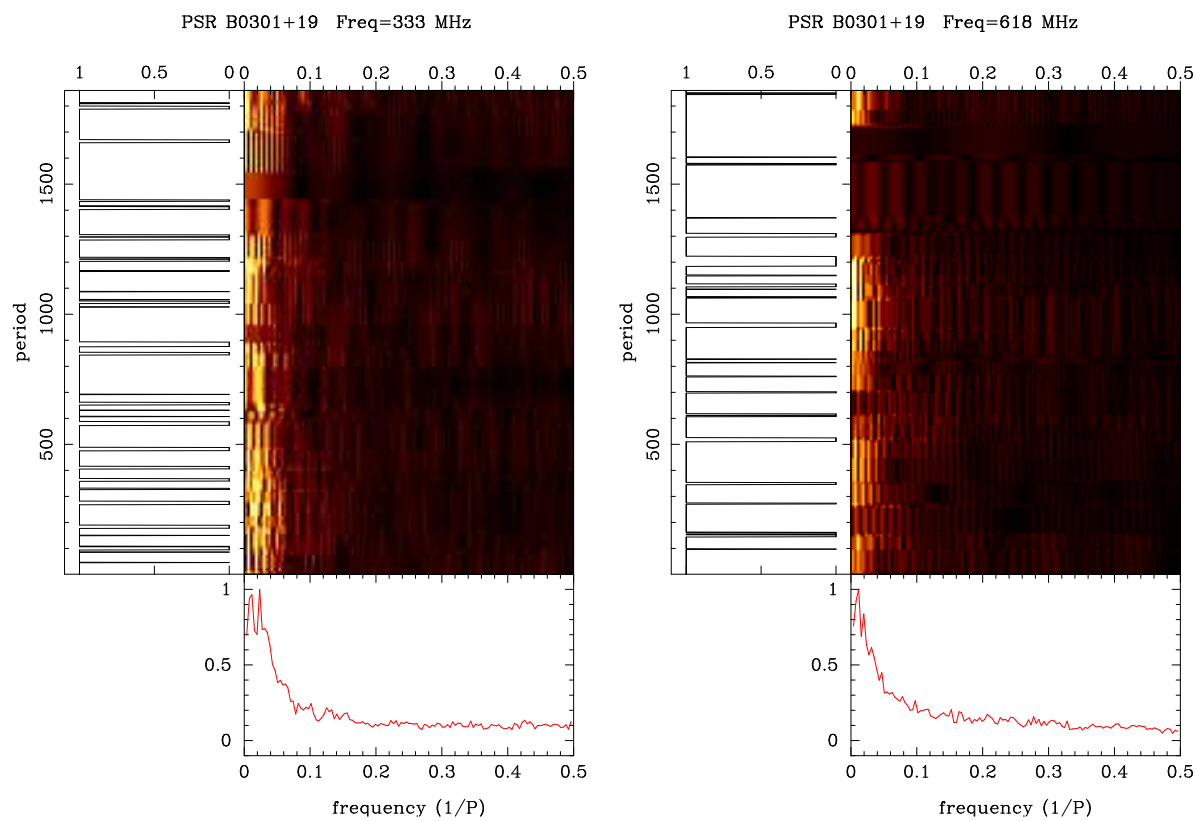


Fig. 37.— The figure shows the time varying Fourier transform of the null/burst time series data at 333 MHz (left panel) and 618 MHz (right panel).

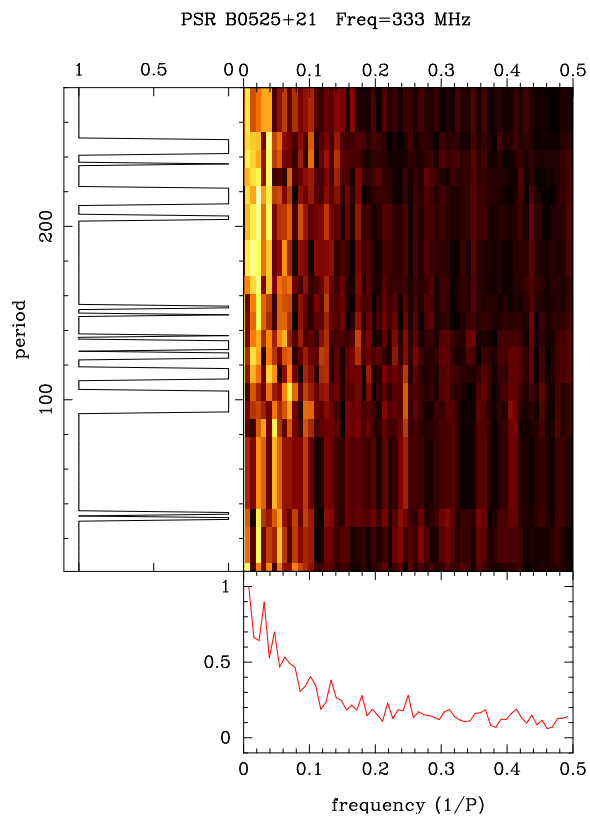


Fig. 38.— The figure shows the time varying Fourier transform of the null/burst time series data at 333 MHz.

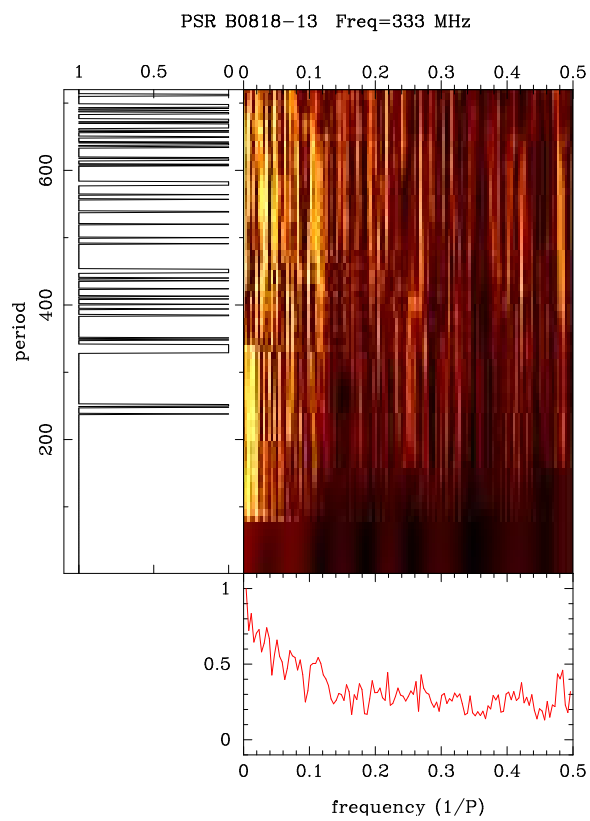


Fig. 39.— The figure shows the time varying Fourier transform of the null/burst time series data at 333 MHz.

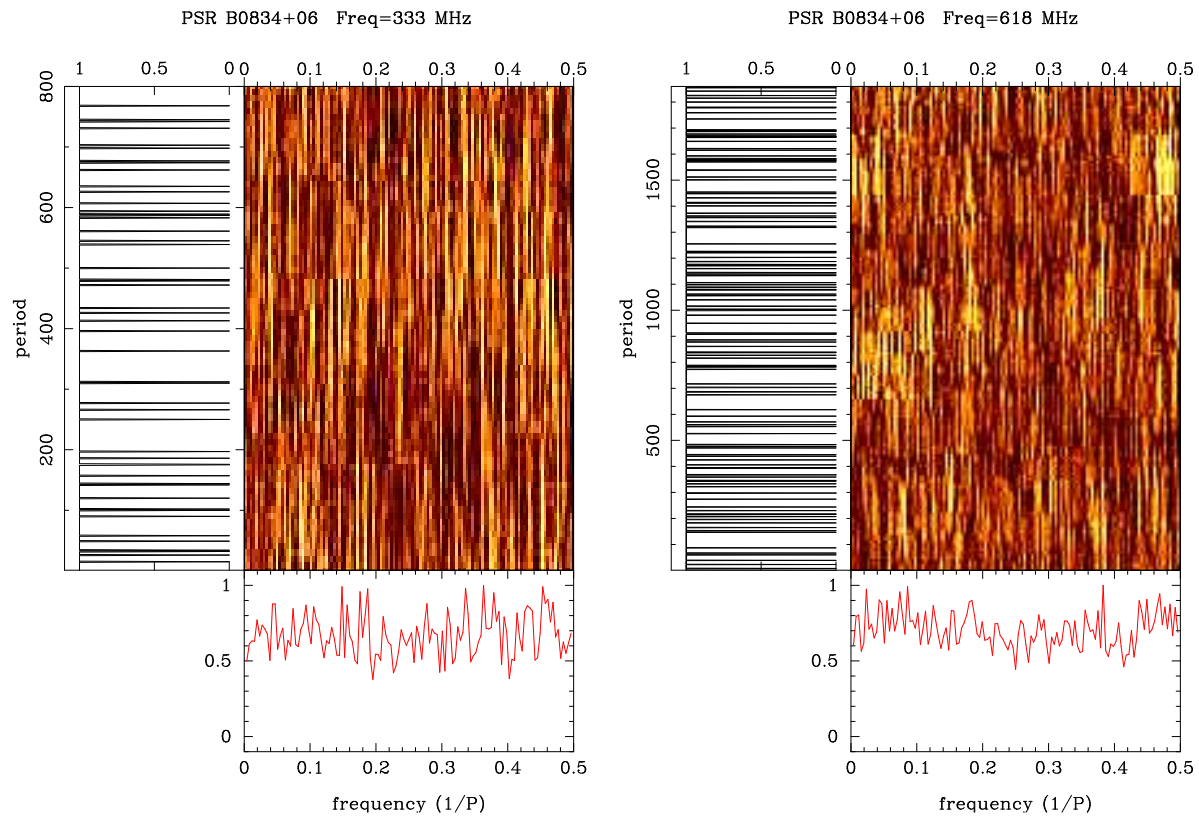


Fig. 40.— The figure shows the time varying Fourier transform of the null/burst time series data at 333 MHz (left panel) and 618 MHz (right panel).

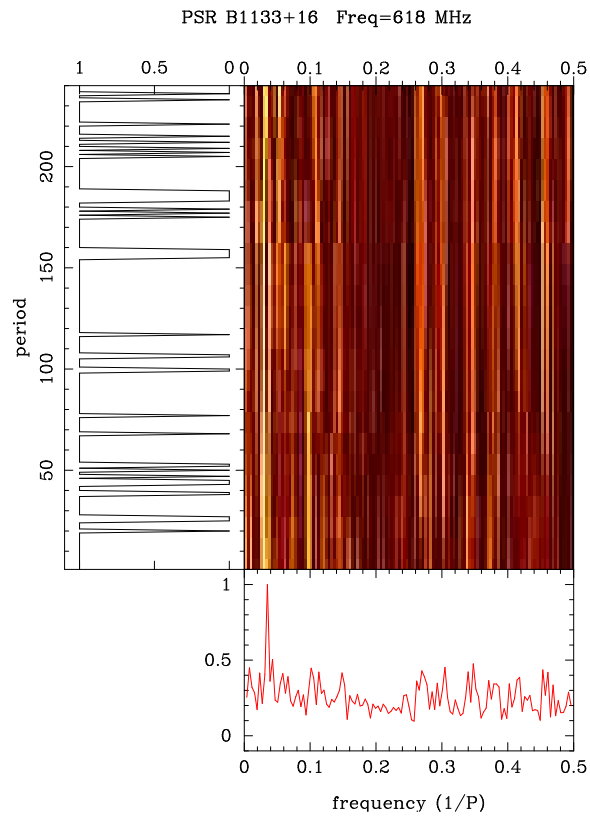


Fig. 41.— The figure shows the time varying Fourier transform of the null/burst time series data at 618 MHz.

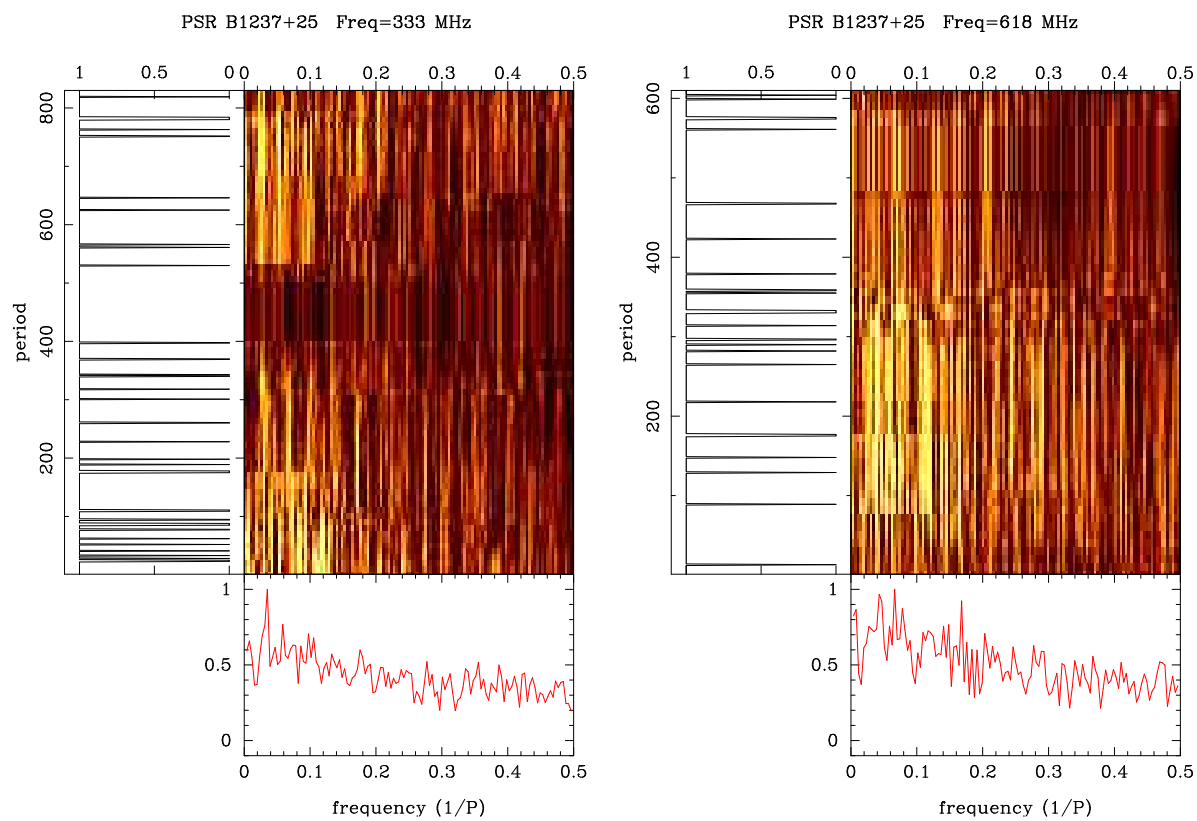


Fig. 42.— The figure shows the time varying Fourier transform of the null/burst time series data at 333 MHz (left panel) and 618 MHz (right panel).

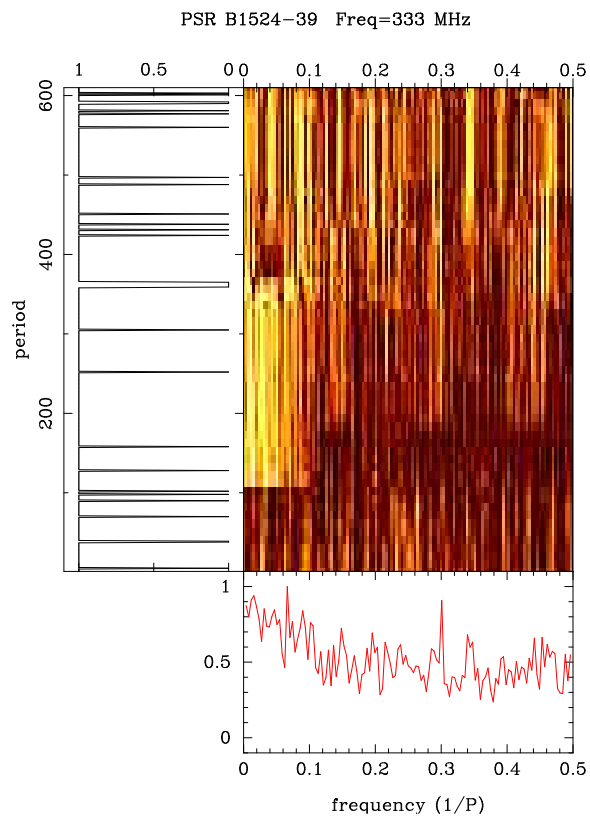


Fig. 43.— The figure shows the time varying Fourier transform of the null/burst time series data at 333 MHz.

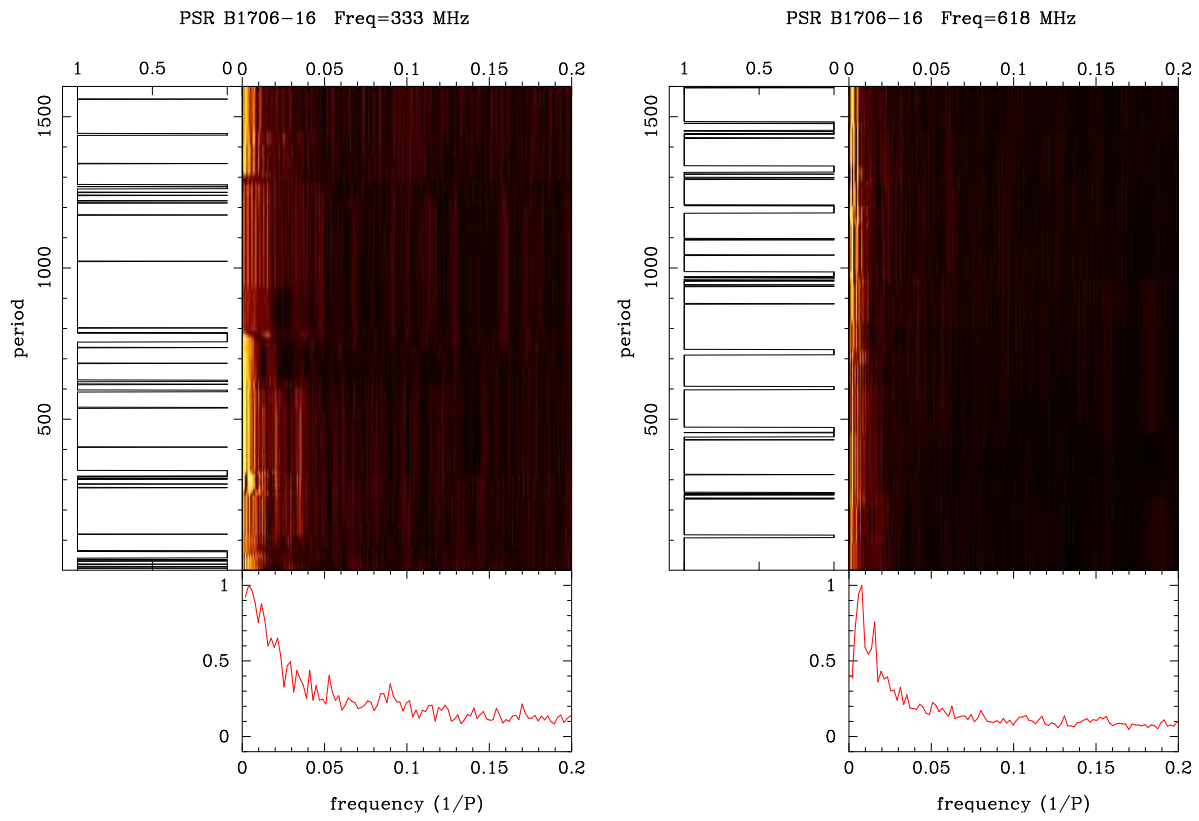


Fig. 44.— The figure shows the time varying Fourier transform of the null/burst time series data at 333 MHz (left panel) and 618 MHz (right panel).

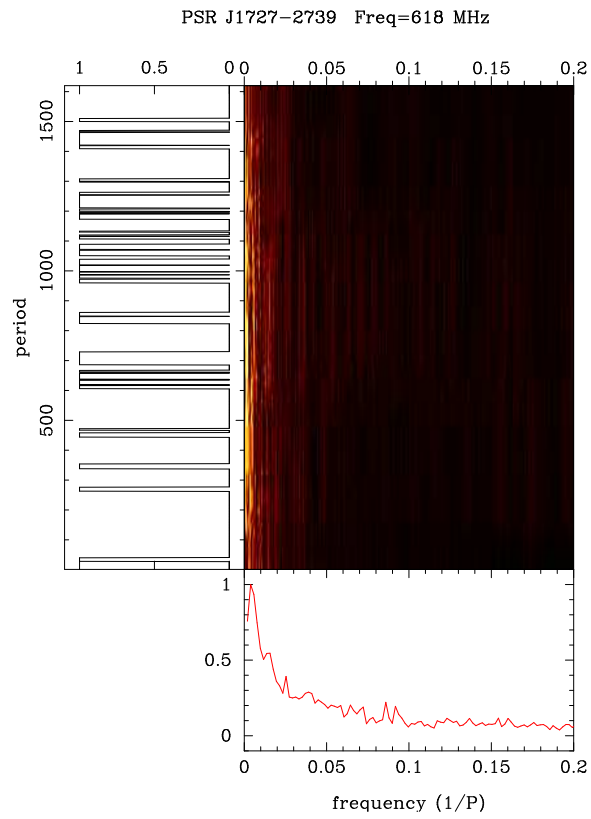


Fig. 45.— The figure shows the time varying Fourier transform of the null/burst time series data at 618 MHz.

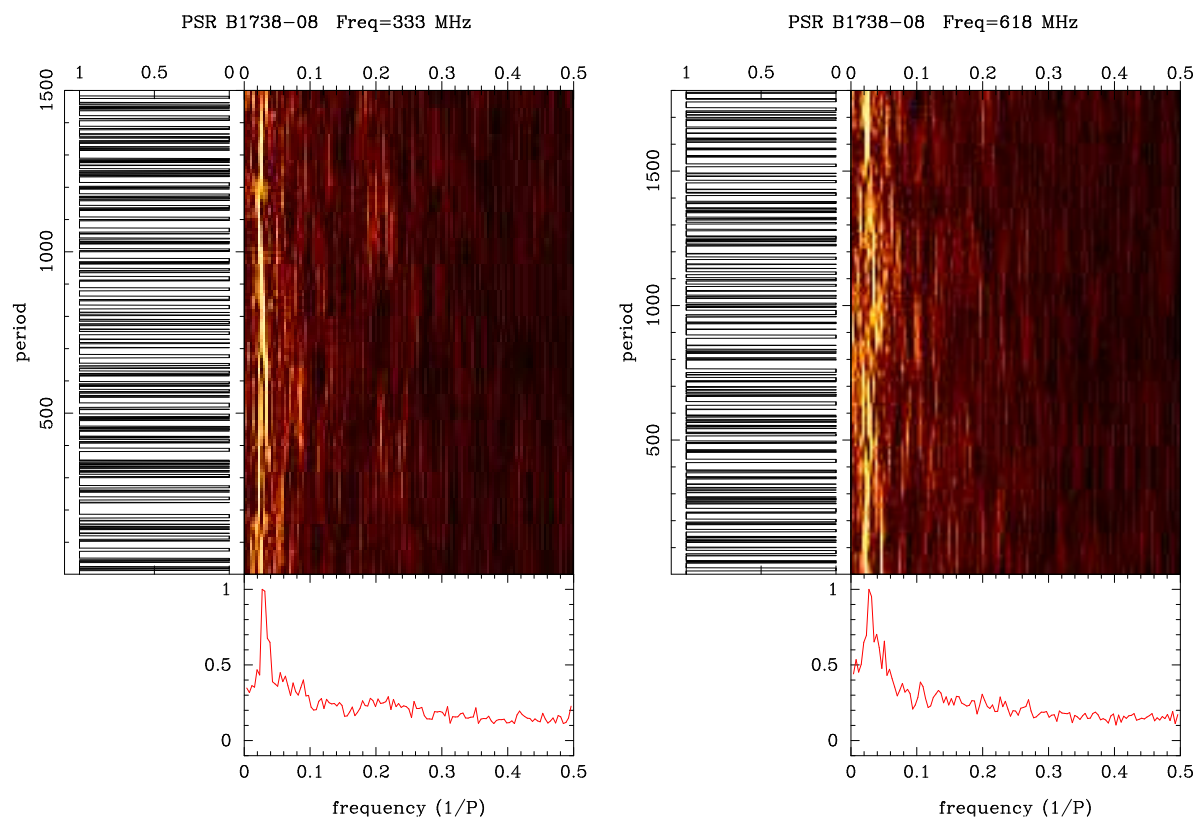


Fig. 46.— The figure shows the time varying Fourier transform of the null/burst time series data at 333 MHz (left panel) and 618 MHz (right panel).

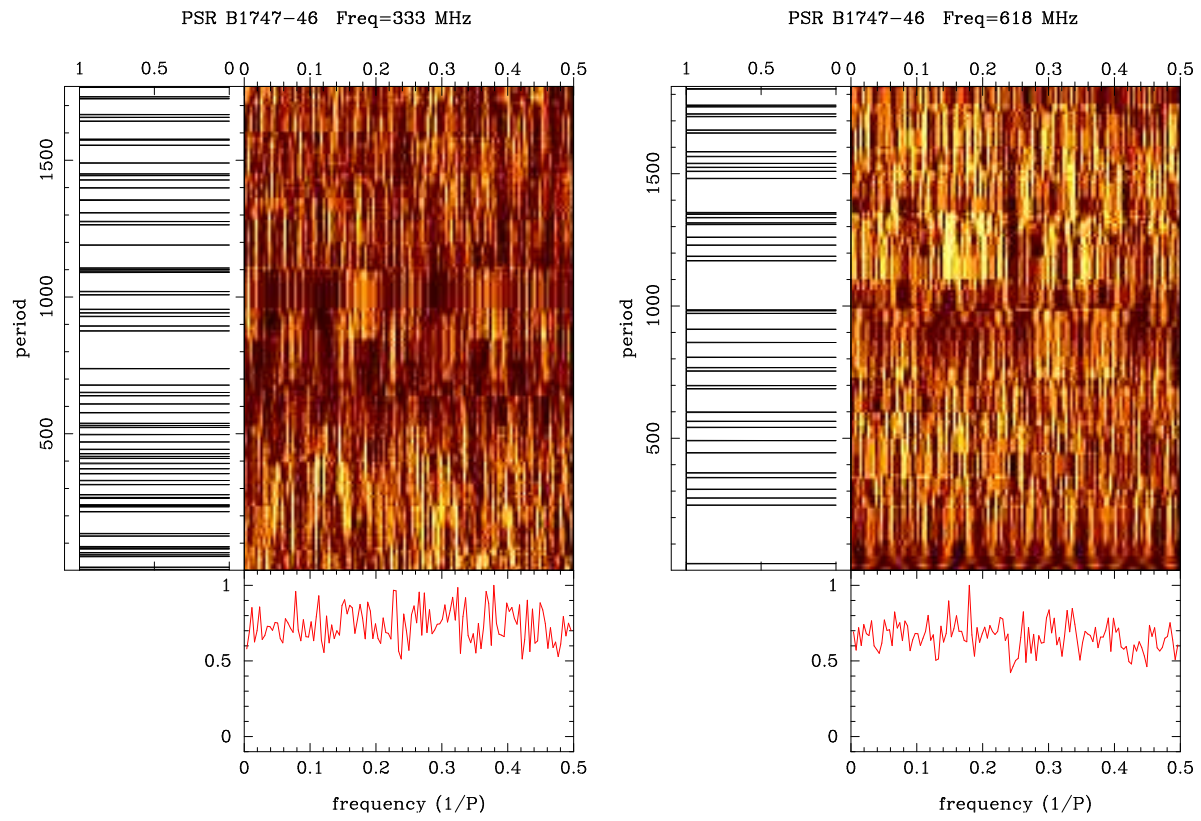


Fig. 47.— The figure shows the time varying Fourier transform of the null/burst time series data at 333 MHz (left panel) and 618 MHz (right panel).

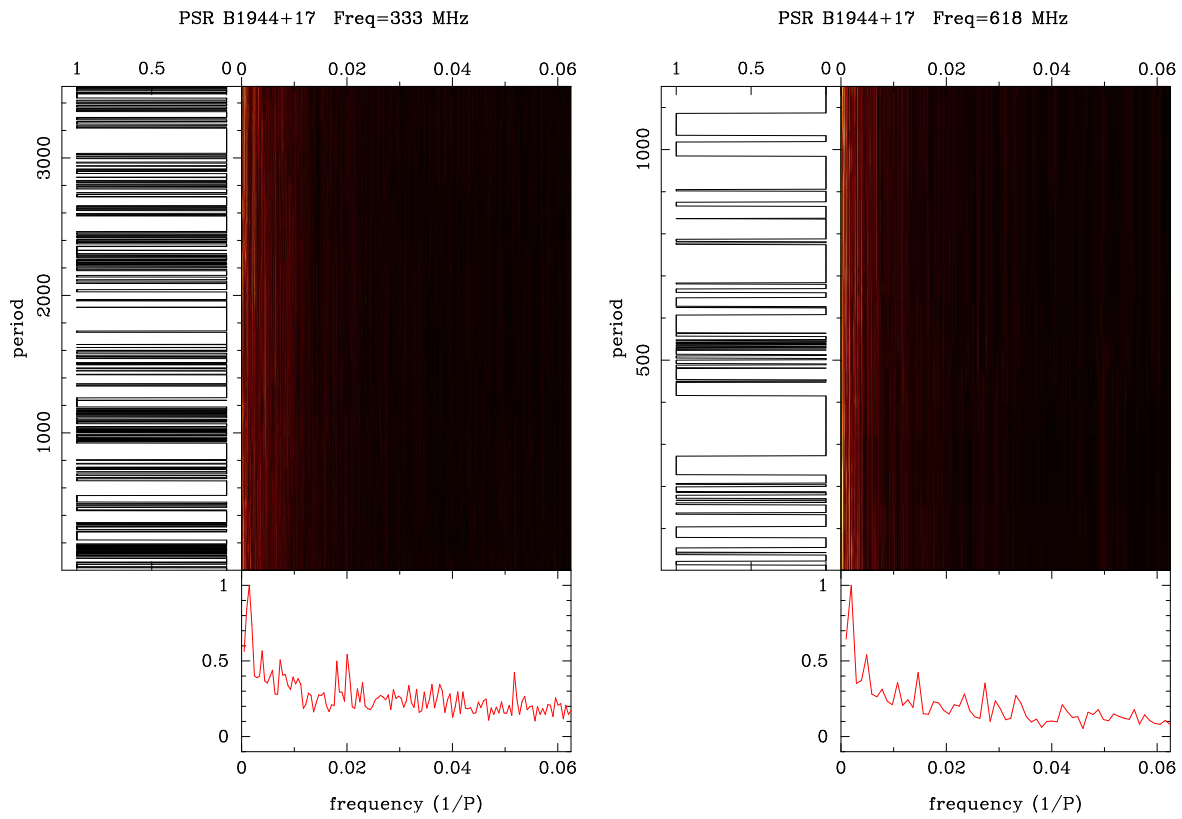


Fig. 48.— The figure shows the time varying Fourier transform of the null/burst time series data at 333 MHz (left panel) and 618 MHz (right panel).

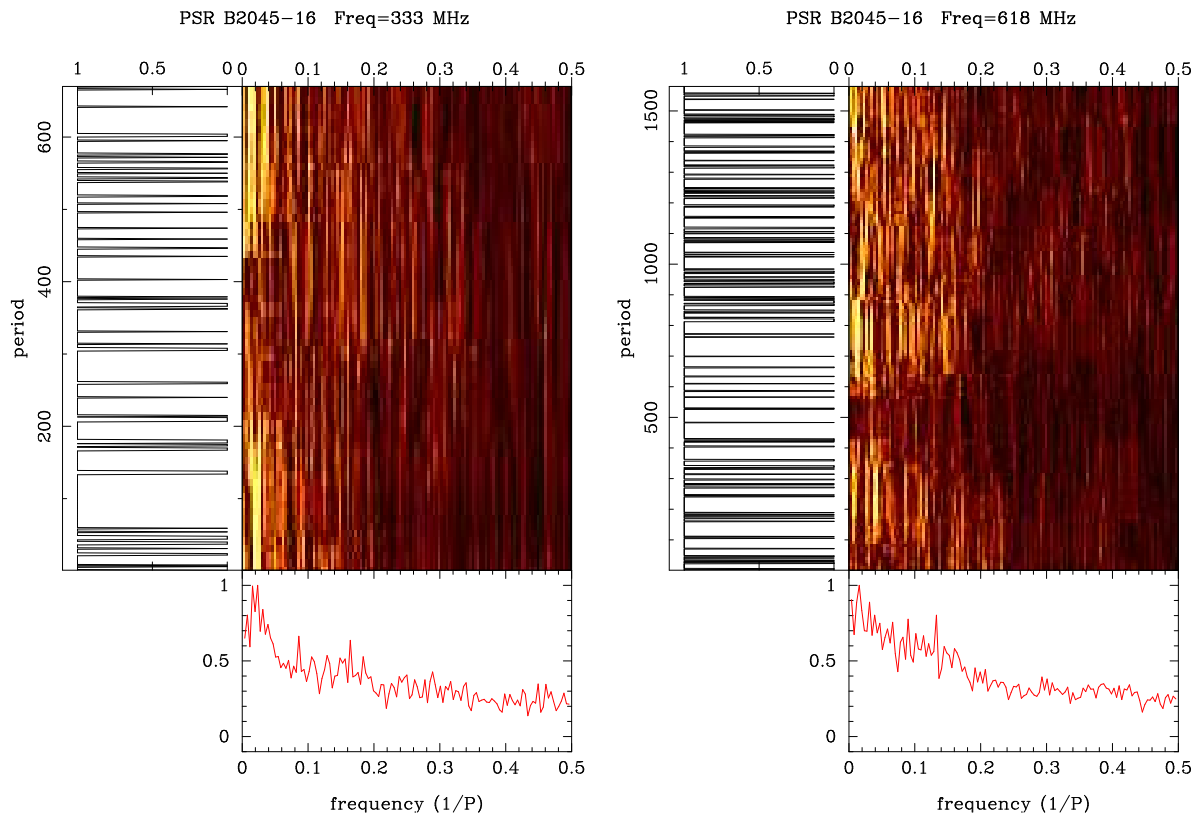


Fig. 49.— The figure shows the time varying Fourier transform of the null/burst time series data at 333 MHz (left panel) and 618 MHz (right panel).

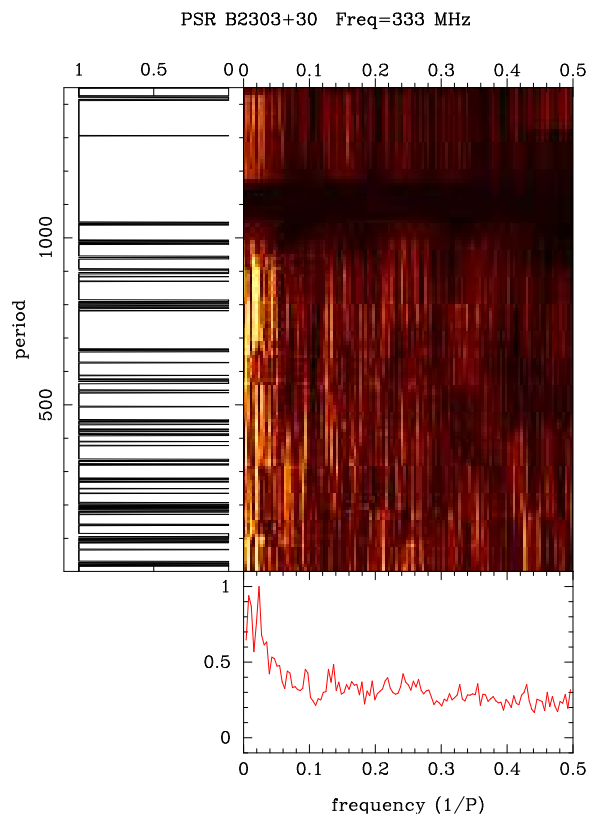


Fig. 50.— The figure shows the time varying Fourier transform of the null/burst time series data at 333 MHz.

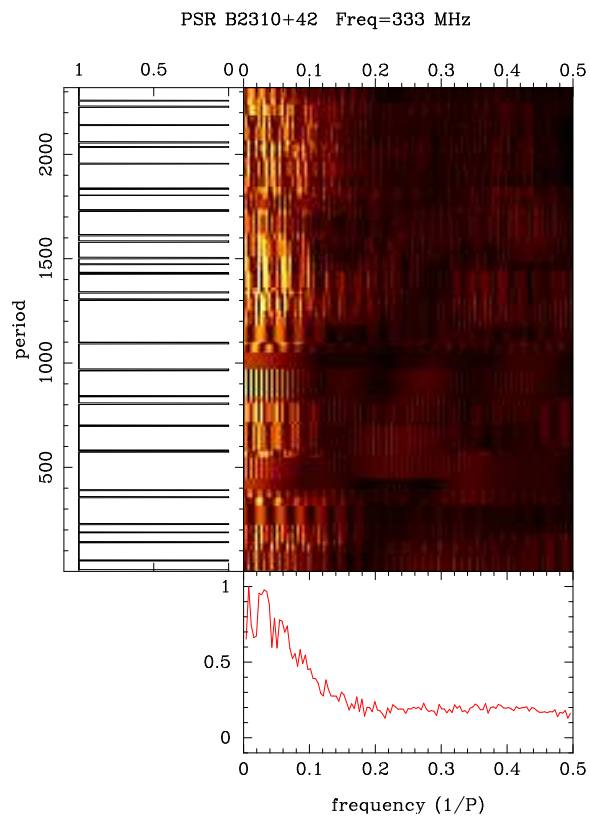


Fig. 51.— The figure shows the time varying Fourier transform of the null/burst time series data at 333 MHz.

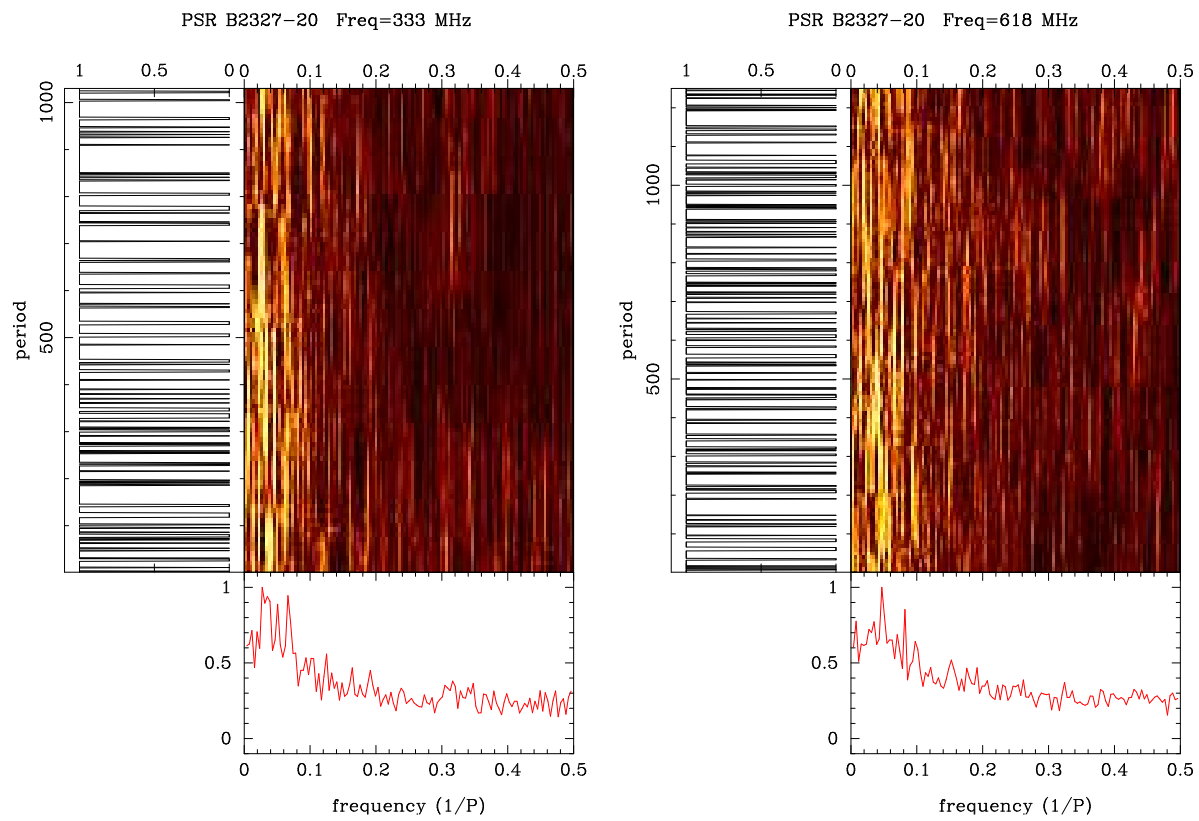


Fig. 52.— The figure shows the time varying Fourier transform of the null/burst time series data at 333 MHz (left panel) and 618 MHz (right panel).